Neural Circuitry Underlying Nociceptive Escape Behavior in Drosophila

Anita Burgos

Submitted in partial fulfillment of the
requirements for the degree of Doctor of Philosophy
under the Executive Committee
of the Graduate School of Arts and Sciences

COLUMBIA UNIVERSITY

2017

Abstract

Neural Circuitry Underlying Nociceptive Escape Behavior in Drosophila

Anita Burgos

Rapid and efficient escape behaviors in response to noxious sensory stimuli are essential for protection and survival. In *Drosophila* larvae, the class III (cIII) and class IV (cIV) dendritic arborization (da) neurons detect low-threshold mechanosensory and noxious stimuli, respectively. Their axons project to modality-specific locations in the neuropil, reminiscent of vertebrate dorsal horn organization. Despite extensive characterization of nociceptors across organisms, how noxious stimuli are transformed to the coordinated behaviors that protect animals from harm remains poorly understood. In larvae, noxious mechanical and thermal stimuli trigger an escape behavior consisting of sequential C-shape body bending followed by corkscrew-like rolling, and finally an increase in forward locomotion (escape crawl). The downstream circuitry controlling the sequential coordination of escape responses is largely unknown. This work identifies a population of interneurons in the nerve cord, Down-and-Back (DnB) neurons, that are activated by noxious heat, promote nociceptive behavior, and are required for robust escape responses to noxious stimuli. Activation of DnB neurons can trigger both rolling, and the initial C-shape body bend independent of rolling, revealing modularity in the initial nociceptive responses. Electron microscopic circuit reconstruction shows that DnBs receive direct input from nociceptive and mechanosensory neurons, are presynaptic to pre-motor circuits, and link indirectly to a population of command-like neurons (Goro) that control rolling. DnB activation promotes activity in Goro neurons, and coincident inactivation of Goro neurons prevents the rolling sequence but leaves

intact body bending motor responses. Thus, activity from nociceptors to DnB interneurons coordinates modular elements of nociceptive escape behavior. The impact of DnB neurons may not be restricted to synaptic partners, as DnB presynaptic sites accumulate dense-core vesicles, suggesting aminergic or peptidergic signaling.

Anatomical analyses show that DnB neurons receive spatially segregated input from cIII mechanosensory and cIV nociceptive neurons. However, DnB neurons do not seem to promote or be required for gentle-touch responses, suggesting a modulatory role for cIII input. Behavioral experiments suggest that cIII input presented prior to cIV input can enhance nociceptive behavior. Moreover, weak co-activation of DnB and cIII neurons can also enhance nociceptive responses, particularly C-shape bending. These results indicate that timing and level of cIII activation might determine its modulatory role. Taken together, these studies describe a novel nociceptive circuit, which integrates nociceptive and mechanosensory inputs, and controls modular motor pathways to promote robust escape behavior. Future work on this circuit could reveal neural mechanisms for sequence transitions, peptidergic modulation of nociception, and developmental mechanisms that control convergence of sensory afferents onto common synaptic partners.

Table of Contents

List of Figures

Acknowledgments

I'll begin by thanking my previous mentors who encouraged me early on. I am greatly indebted to Sarah Woolley for taking me on as an Amgen student in 2009. She showed me that science could be rigorous, but also fun and enjoyable. I would also like to thank my advisors at NYU. Claude Desplan, who was always a constant source of encouragement, and helped me set up a position in Justin Blau's lab. I am so grateful for the excellent training I received in Justin's lab and I attribute a great deal of my presentation and writing style to him. I worked closely with a graduate student in his lab, Afroditi, who initially taught me all that I know about being a scientist.

And of course, the biggest thank you to my current advisor, Wes. I can never express my gratitude for the incredible opportunities and excellent mentorship I have received in this lab. Wes provided a supportive environment for me to follow my research passions, even when it led to a bunch of wild assays with wires sticking out in every direction. Wes put a lot of trust in me early on, which really helped boost my confidence as a scientist. I feel like Wes always knows exactly how to make my presentations, and writing better, and I think we've made a great team over the last few years.

I would like to thank my committee members: Ellen Lumpkin, Richard Mann, and Charles Zuker. I never thought I would use the word "fun" to describe my committee meetings, but I really enjoyed hearing input from a different scientific perspective, and discussing ways to improve my experiments. I would also like to thank Vanessa Ruta for agreeing to be my outside examiner.

The Grueber lab far surpassed any expectations I could have ever had for my lab members. From the constant pranks to late night talks to dressing up as *Drosophila* genes every Halloween. This lab has the perfect combination of intelligent, fun/funny,

and incredibly hardworking people. Jenn, the resident lab “big sister” thank you for always being willing to provide help, a funny anecdote or a detailed account on pretty much any and every topic. (Boy)Sam, thank you for always being willing to let me bounce ideas off of you. You really helped push my project forward in moments when I was feeling really stuck. Taylor, thank you for the emotional support and non-stop laughter. Rebecca, thank you for letting me vent to you when I need help making decisions. Grace, thank you for your kindness, and support. Naureen, thank your thoughtful gifts and coffee walks. Rosa, thank you for doing such a tremendous job of making sure the lab runs smoothly, while having such a positive attitude. And finally, (Girl)Sam, thank you for being my hermana and a constant source of emotional support and wonderfully sarcastic comments. In a very serious way, I do not know how I would have gotten through this process without you. To all of the other wonderful Grueber lab members, and past Grueber lab members, thank you!

To the people who helped keep me sane for the last six years: at Columbia, I was grateful to have strong supportive friends, especially Nancy and Sarah. Our “tea times” of shameless venting are some of my favorite memories from graduate school. Also, thank you Sarah for being especially encouraging and attentive during the last few weeks of writing my thesis. To my longtime “New York City Crew,” a huge thank you for being so supportive, but also providing ample opportunities to step away from the lab a bit to have fun too. Thank you to “OBB” for all the camping trips and late nights of laughter and ridiculousness. To my favorite ladies, thank you for always cheering me on. Thank you Crystal and Marlee for all of the ‘GAB’ dinners, and thank you Polina, for being my number 1 cheerleader. I want to give a special thank you to Jayne for all the love and encouragement over the last 20+ years, and to Aruna, for understanding me like few people can and always picking up the phone to talk at any hour of the day/night.

I have saved my most important “thank you” for last—my family. My family is quite extensive, and I thank them all for all the confidence and encouragement they had for me at such a young age. And, finally, a loving thank you to Mami y Papi. My parents both emigrated from Dominican Republic and had to work full-time jobs during the day to provide for their families, but would still take college classes at night. With your actions, you taught me the importance of both hard work, and getting an education, and because of your sacrifices, I have had the luxury to avidly pursue my academic goals. Mami, your creativity and drive for knowledge are inspiring; thank you for the constant love and support, even when you don’t always agree with my decisions. Papi, you are the hardest working person I know; thank you for being a wonderful friend, always full of loving advice and encouragement. I share my success with everyone who has helped me along the way. Thank you all!

Dedication

I dedicate this work to the loving memory of my Uncle Bob, who was a rock of stability and kindness in our family, and never missed a chance to talk to me about science.

Chapter I: Introduction

Introduction

The origin of behavior has fascinated scientists, philosophers, and medical practitioners for centuries. Sensation and movement, once believed to be rooted in the heart, is now known to be controlled by neural pathways in the brain. Marie-Jean-Pierre Flourens first described a systematic approach for ablating parts of the brain in animals to provide causal evidence for the role of brain function in behavior (Flourens, 1842), a conceptual approach that is still widely used today. How sensory information is encoded and transformed into movement by the nervous system is still a fundamental question in neuroscience. With the increasing availability of genetic tools to manipulate and image neural circuit function, and the push towards mapping the connectivity of the nervous system, a sensory to motor understanding of behavior is an attainable goal.

Sensorimotor processing can be a challenging question to address in a nervous system where neurons are difficult to identify, and neural connectivity from sensory neurons to motor circuits is unknown. However, animals with a relatively simple nervous system can perform impressive feats of sensorimotor transduction on rapid timescales. The efficiency of these circuits should not underestimate their complexity as animals often perform serial behaviors to maximize successful escape, such as a rapid shift away from the predator followed by directed forward locomotion (e.g. Bend-swim sequence in fish, turn-walk escape in cockroach) (Domenici et al., 2008; Sillar, 2009). Work in invertebrates has made significant contributions to our understanding of neural circuit function including the generation of action potentials (Hodgkin and Katz, 1949), central pattern generators for rhythmic movement (Wilson and Wyman, 1965),

redundancy of parallel neural circuits (Card, 2012), and neuromodulation (Marder, 2012).

Drosophila has become a central model for understanding the genes and neural substrates underlying behavior (Bellen et al., 2010). Sensory neural transduction in invertebrates is remarkably similar to vertebrate circuits (Sanes and Zipursky, 2010; Vosshall and Stocker, 2007; Yarmolinsky et al., 2009). For instance, conserved features of the visual circuit organization include parallel layering with cross-talk through radial perpendicular input (Sanes and Zipursky, 2010). Olfactory systems in both vertebrate and invertebrate species consist of unique olfactory receptor expressing neurons converging onto respective glomeruli (Vosshall and Stocker, 2007). However, very little is yet known about somatosensory circuit organization in the fly when compared to well known circuitries for vision and olfaction. Thus, we expect that novel and conserved principles of sensorimotor processing can be learned through our studies of the *Drosophila melanogaster* system. In this chapter, I will introduce sensory to motor processing, with an emphasis on somatosensory-evoked behaviors, beginning with a description of somatosensory detection in vertebrates, sensory transduction and decoding, and then discussing our current understanding of how sensory input elicits behavior. I will end by describing the *Drosophila* larval system as an ideal model for investigating how sensory information is combined, and transformed into appropriate motor outputs.

Somatosensation in vertebrate organisms

Sensory neurons detecting somatosensory stimuli

Our most immediate environment is rich with tactile, thermal, and chemical cues that are detected by an array of somatosensory neurons innervating the skin. Somatosensation allows us to convey changes in our surroundings to our central

nervous system, and adjust our behavior accordingly. Mechanosensation is the detection of tactile stimuli ranging from gentle-touch to potentially damaging, or noxious, harsh touch. Nociception includes the detection of any stimuli that has the potential to cause tissue damage, and includes a polymodal array of cell types that detect chemical, mechanosensory, and thermal stimuli. Somatosensation is evolutionarily conserved across phyla in both form and function (Hall and Treinin, 2011). Both vertebrates and invertebrates (e.g. worms, flies, leech) possess finely, or non-myelinated multi-branched polymodal nociceptors. Behavioral responses to noxious stimuli are conserved as well, as noxious stimuli can elicit aversive withdrawal (termed nocifensive behavior). In fact, most studies investigating nociception in animal models utilize nocifensive behavior as a readout for circuit function, indicating a link between noxious detection and motor activity (Fan et al., 2009). Yet, less is known about the sensory to motor circuitry underlying the range of nocifensive responses. This section will focus on the sensory transduction and coding of somatosensation in vertebrates, highlighting some outstanding questions where simpler invertebrate models might be able to elucidate key mechanisms in somatosensory transduction.

In vertebrates, tactile or low-threshold mechanosensory inputs are encoded by myelinated Aß fibres, whereas noxious stimuli are detected by polymodal lightly myelinated A∂ fibres and unmyelinated C-fibres. A∂- and C-fibres respond to a wide range of temperatures as well as chemical, and high-threshold mechanical stimuli (Lumpkin and Caterina, 2007) (Figure 1.1). Somatosensory cell bodies reside in the dorsal root ganglia, and axons project to modality specific layers in the dorsal horn. There, afferents connect with various interneurons, which locally modulate signals, or transmit sensory information to the brain (Todd, 2010). A∂ nociceptors target lamina I of the dorsal horn, C/ A∂ peptidergic fibres terminate in lamina I and outer lamina II (IIo), whereas C non-peptidergic fibres occupy lamina II (Figure 1.1). While nociceptors

preferentially target the more superficial layers of the dorsal horn, touch-sensing afferents terminate mostly in deeper layers, lamina III to lamina V (Braz et al., 2014). This laminar specific targeting might facilitate modality specific transduction for sensory discrimination (Prescott et al., 2014). Ascending projection neurons deliver nociceptive input to higher brain regions through two tracts: 1) spino-parabrachial tract to medial thalamus and limbic centers for the emotional unpleasantness that is commonly experienced as "pain," and, 2) the lateral spino-thalamic tract which projects to the lateral thalamus and sensory cortex and is responsible for sensory discrimination (i.e. location, intensity of stimulus) (Kuner, 2010). Additionally, GABA-ergic and serotonergic descending inputs play a key modulatory role in nociception (Kuner, 2010). There is evidence that reduction in descending inhibitory input during initial heightened responses to noxious stimuli (hyperalgesia) can lead to chronic hyperalgesic states (Vanegas and Schaible, 2004).

Theories for somatosensory processing

The coding of somatosensory information at the periphery is specialized by neural morphology and ion channel/receptor expression, but this modality-specific tuning is not necessarily a feature of central neurons, which could, in theory, receive inputs from various afferents. Somatosensory coding was the subject of intense debate for many years and can be summarized in the following theories: The intensity theory posits that primary afferents are not specialized, and that coding is based on the intensity of the stimulus (e.g. low stimulation= touch, high stimulation= nociception) (Prescott et al., 2014). Since we know that primary afferents are polymodal, yet mostly specialized, this theory has been refuted (Prescott et al., 2014). The specificity theory proposes that there is a one-to-one labeled line relationship between afferents and central circuits, such that nociceptive information, for instance, would only be processed by interneurons receiving

input exclusively from nociceptive primary afferents (Prescott et al., 2014). However, as early as 1905, Henry Head proposed, based on nerve lesions he performed on his own hand, that there was a degree of interaction between pain-specific information, and non-noxious information, such as temperature or gentle-touch. This led to the to the pattern theory, which states that there is no modality specific tuning of central neurons, and that coding lies in the pattern of primary afferent activation. One prime example of pattern coding is the gate control theory (Melzack and Wall, 1965), suggesting that neurons transducing nociceptive input to higher brain areas receive both low-threshold mechanosensory, and nociceptive input, and can be inhibited by mechanosensory input via local interneurons. Finally, the combinatorial coding theory is a combination of specificity and pattern coding, such that there is some degree of specialization by central circuits in the spinal cord, but afferent input can converge on the same population of neurons (sensory integration), or labeled lines can modulate each other's input indirectly through local circuitry (crosstalk) (Yau et al., 2015). A fascinating example of cross-talk is exhibited with the thermal grill illusion, where activation of cool, and warm-sensing fibres can trigger a feeling of burning pain (Craig and Bushnell, 1994).

Studies have identified circuits that are consistent with the gate control theory. One study found that Aß mechanosensory and C/A∂ nociceptive input converge onto somatostatin (SOM+) neurons, which transduce nociceptive information to the brain (Duan et al., 2014). The activity of SOM+ neurons is additionally regulated by Aß targeted Dynorphin expressing (Dyn+) neurons, which inhibit SOM+ activity in the presence mechanosensory activation. Thus, Dyn+ neurons gate the transduction of SOM+ nociceptive input to the brain. Loss of Dyn+ inhibition allows mechanosensory input to elicit nociceptive behavior, offering a potential mechanism for mechanical allodynia (nociceptive responses to non-noxious tactile stimuli). SOM+ neurons are not involved in thermal nociception, suggesting some degree of specialization that is more in

line with combinatorial coding. Another study found that a subset of A-fiber neurons expressing neuropeptide Y receptor 2 (NPY2R) transmit mechanical nociception, and that the transmission of nociception to other brain areas was gated by low-threshold tactile input. Interestingly, tactile input enhanced the nocifensive paw withdrawal response, suggesting that mechanosensory input might enhance motor outputs while decreasing perception of pain (Arcourt et al., 2017). However, this study did not identify specific central circuits, so we do not know whether their degree of specialization is more consistent with a pattern or combinatorial coding theory. Although there have been recent advances in deciphering the interactions between somatosensory modalities with genetic tools that promise to improve classification of central circuits in the spinal cord (Duan et al., 2017; Prescott et al., 2014), we are only beginning to understand how integration and crosstalk impact somatosensory processing. Studying these questions in simpler models, where wiring diagrams are accessible (Ohyama et al., 2015; Schneider-Mizell et al., 2016; White et al., 1986) could shed light on fundamental mechanisms underlying somatosensory processing and integration.

Sensorimotor processing

Sensorimotor processing is defined as the integration of sensory information by the central nervous system to generate appropriate motor responses. As briefly mentioned in the previous section, information is often combined by neural circuits, which can refine the salience of a sensory event to improve accurate behavior selection. Multisensory integration can result in a response that is greater (multisensory enhancement) or less than (multisensory depression) the sum of its parts (Stein and Stanford, 2008). Multisensory enhancement can be particularly useful when sensory cues are weak, such as an animal collecting sensory information about an approaching predator. This section will describe some of the key questions in understanding how

sensory input is integrated and transformed into motor outputs, and how escape circuits can serve as a simple model to uncover general principles of sensorimotor processing.

Key questions in sensorimotor processing

It is misleading to think of sensorimotor processing as a simple feed-forward system where sensory information is processed by the central nervous system, and then converted into motor patterns. For instance, the same sensory stimulus does not always elicit the same behavioral response, unveiling a high degree of complexity. Central circuits are not only receiving input from sensory cues, but also top-down signaling about behavioral state (i.e. what is the animal currently doing), internal state (hunger, thirst, sleep), time of the day (circadian regulation), and previous experience. Neural circuits also have to distinguish between self-generated movements, and environmental stimuli. On the motor end, postural adjustments can direct the trajectory of movement, and prepare the animal for the initiation of remaining motor sequences. Finally, motor patterns often occur within a specific time frame, and serial order (Huston and Jayaraman, 2011). Thus, how an animal responds to sensory stimuli is a multifaceted problem that can be addressed in simple models to extract conserved circuit features. Even relatively simple brains can execute sensorimotor transformations with remarkable speed and accuracy, such as the gaze-stabilization movements flies perform during flight, or the sequential flexion and extension that allows a locust to jump several feet into the air (Huston and Jayaraman, 2011).

Escape circuits as a model for dissecting sensorimotor transformations

One extraordinary example of sensorimotor processing is when an animal rapidly collects multisensory information about an imminent threat to trigger an escape response. Escape behaviors are, by necessity, accurate and fast; therefore, these neural circuits are often compact with relatively few synapses between sensory and motor

neurons. Three well-studied escape circuit include the C-start startle escape in goldfish, the locust escape jump, and the *C. elegans* touch response.

Perhaps the most widely studied escape circuit is the Mauthner cell circuit underlying the C-start response. Studies of this circuit have made important contributions to our understanding of command neurons, electrical transmission and synaptic plasticity (Sillar, 2009). Initially studied in goldfish (Korn and Faber, 2005; Wilson, 1959), the C-start occurs in response to auditory, mechanosensory and visual stimuli (Eaton and Hackett, 1984). Animals acquire a C-shaped bend to orient themselves away from threatening stimuli and then rapidly straighten out the body and swim away (Sillar, 2009). Mauthner cells are two, relatively large cells (making them amenable for circuit dissection) located in the hindbrain that receive direct auditory input (both chemical and electrical transmission). An auditory stimulus will activate one Mauthner cell more strongly, which then induces muscle contractions towards the center of the animal, initiating the C-shape on the contralateral side. The Mauthner cell concurrently inhibits the ipsilateral motor neuron from firing (which ensures asymmetric bending), and forms connections with excitatory premotor neurons to generate fast swimming. Despite the circuitry indicating a crucial role for Mauthner cells in escape behavior, ectopic activation of these neurons does not induce characteristic escape responses, and ablating this neurons does not abolish startle behavior. Thus, parallel circuits exist that can trigger, with a delayed latency, C-start escape behavior. Additionally, C-bend also takes place during prey capture and feeding (Korn and Faber, 2005), suggesting some modularity in this behavior. Although the C-start is a well-described escape circuit, future work would reveal the similarities between escape circuits in other organisms, particularly in response to additional, non-auditory, stimuli.

The locust escape jump in response a looming object is a fascinating escape response requiring millisecond preparatory movements that result in the locust

catapulting several feet (Simmons et al., 2010). A descending contralateral movement detector (DCMD) neuron receives visual input and projects to motor centers to initiate jump movement. However, ablating these neurons does not eliminate the escape behavior, pointing to parallel circuits that can also trigger jumps (Card, 2012). The incomplete anatomy has precluded identification of additional jump circuits. Moreover, the interneurons controlling the sequential coordination of motor responses have not been characterized (Simmons et al., 2010).

In *C.elegans*, a gentle-touch stimulus to the anterior will induce reverse locomotion with suppressed foraging head movements, while the same touch stimulus to the posterior end will trigger forward locomotion (Chalfie et al., 1985; Pirri and Alkema, 2012). The completed *C.elegans* connectome, along with functional imaging and behavior experiments unveiled the complete sensory to motor circuits responsible for gentle-touch avoidance behaviors. In brief, touch-sensing neurons in the head activate backward locomotion command-neurons, while indirectly inhibiting parallel circuits controlling foraging head movements and forward locomotion (Pirri and Alkema, 2012; Pirri et al., 2009). These results highlight the power of the wiring diagram in dissecting sensorimotor circuitry, particularly in identifying competing parallel neural pathways activated by the same stimuli. Now that the connectome is being reconstructed for *Drosophila* larvae, studies can begin revealing the sensorimotor transformations underlying complex escape behaviors, which are both diverse (i.e. responding to various stimuli) and sequential (Jovanic et al., 2016; Ohyama et al., 2013; Ohyama et al., 2015).

Behavior sequences

Escape circuits provide valuable examples of motor programs activated in series to generate a behavioral response. However, sequential motor patterns are ubiquitous and

evolutionarily conserved, such as grooming sequences, typing and speech patterns, and feeding. Feeding in mammals for instance, may not seem overtly sequential, but involves rhythmic jaw movements that break down food, followed by swallowing, and tongue and jaw movements that aid post meal oral hygiene (Bels et al., 2012). There has been a long-standing interest in the neural circuits that facilitate sequential behavior, but it has been challenging to accumulate experimental evidence for proposed theories. In 1951, Lashley proposed that some behaviors, such as speech generation, which requires sequential motor movements of the tongue and mouth could not be described by neural mechanisms where one element in the series activates the next (response or synaptic chaining). He argued that certain words (tire vs. right) occur with motor movements in reverse, such that response chaining could not explain this pattern. Instead, he proposed a "parallel activation" model where elements were activated at once and sequences were determined by interactions between circuit elements (Lashley, 1951). Although this model makes intuitive sense, and is thoughtfully laid out by Lashley, experimental evidence did not emerge until Long et al. examined these models in the context of sequential bursting in the premotor nucleus (HVC) during bird song. Adult zebra finch male song is produced with stereotyped patterning of syllables, which makes it amenable for studying sequence generation. This study attempted to differentiate between the synaptic chain model and "ramp-to-threshold" model (Lashley's model). The parallel activation, or ramp-to-threshold, model proposes that the first neuron in the series receives the most activation, but also the highest level of inhibition, and as inhibition ramped down, more weakly activated neurons in the series would burst. This ramping down could control the burst timing between HVC neurons underlying sequential syllable generation during singing. However, their findings were consistent with a synaptic chain model with no evidence for slow ramping of action potentials, but rather fast large depolarizations in the HVC.

A study looking at grooming modules in adult *Drosophila* found evidence for a parallel activation model where competing motor programs are activated at once and sequence arises from a winner-take-all competition. The authors identified genetic tools to activate each module separately and tested their hypotheses with various activation patterns. Interestingly, activating one module would allow for previous, but not subsequent modules to take place, arguing against a synaptic chain model. Finally, a recent study in *Drosophila* larvae investigated the neural substrates controlling behavioral transitions, and behavior choice. In response to an air puff, larvae will turn their head (bend) or withdraw their anterior segments (hunch) or perform a sequence of the two (hunch→bend)(Jovanic et al., 2016). The authors used electrophysiological, EM reconstruction, and behavioral approaches to identify the following circuit motifs: 1) to establish initial behavior choice (i.e. hunch vs. bend), competing circuits are activated in parallel and through interactions between reciprocally connected feed forward inhibitory neurons one behavior "wins." 2) To facilitate transitions from one behavior to the next (hunch→bend), there is lateral disinhibitory input from hunch circuits to bend circuits. 3) To prevent reversal back to the first behavioral state (bend→ back to hunch), bend circuits engage in feedforward disinhibition to maintain behavior choice. Thus, in the this circuit, projection neurons controlling bending and hunching are activated in parallel, and downstream inhibitory motifs govern behavior selection, which is in line with the parallel activation model proposed by Lashley. This study highlights how *Drosophila* larval somatosensory circuits can be used as a powerful tool for revealing features of sensorimotor processing from sensory detection to behavior, with synaptic resolution.

Somatosensation in *Drosophila* larvae

Overall, we are beginning to understand more about how sensory inputs are combined, and transformed into complex motor outputs. However, a recurrent issue with work in vertebrates, and even certain invertebrate models, is that much of the underlying circuitry remains elusive. In this section, I will introduce the *Drosophila* larva as a model for dissecting sensorimotor processes, focusing mostly on the escape response evoked by noxious sensory stimuli.

Drosophila larvae use somatosensory dendritic arborization (da) neurons to detect their immediate environment. These cell types have been implicated in modality specific behaviors, and recent efforts are beginning to unveil the surprisingly complex neural circuitry underlying some of these behaviors.

Drosophila larvae as a model for somatosensory circuit dissection

Both vertebrates and invertebrates share many of the same behavioral goals in sensory environments (e.g. locating food and mates, while avoiding predators). Thus, brains could conceivably have come up with similar solutions for achieving these goals, which might explain conserved circuit features such as central pattern generators, neuromodulation, and balanced excitation and inhibition (Marder, 2012; Selverston, 1999). Aside from its rich history in elucidating evolutionarily conserved features of chromosomal inheritance, mutagenesis, embryonic development, and innate immunity, *Drosophila melanogaster* has been instrumental in identifying fundamental mechanisms of neural circuit function (Bellen et al., 2010). Seymour Benzer pioneered the use of *Drosophila* for dissecting the link between genes and behavior, providing seminal contributions to our understanding of learning and memory (Dudai et al., 1976), and circadian rhythms (Konopka and Benzer, 1971).

The *Drosophila* life cycle consists of a larval, pupal, and adult fly stage, lasting around 10 days from egg laying to eclosion at 25˚C. Adult *Drosophila* have ~100,000 neurons which are capable of sophisticated computations underlying learning, visual discrimination, and courtship (Kahsai and Zars, 2011; Sanes and Zipursky, 2010; Yamamoto and Koganezawa, 2013). Neurons in the fly brain are genetically identifiable, and a vast genetic toolkit enables reliable cell-specific manipulations. Yet, *Drosophila* larvae offer additional advantages for somatosensory circuit dissection with only ~10,000 neurons, anatomically and behaviorally defined sensory neurons, and more recently, wiring diagrams based on electron microscopic (EM) circuit reconstruction (Grueber et al., 2002; Ohyama et al., 2015; Schneider-Mizell et al., 2016). Moreover, the larval transparent cuticle and neural organization is easily amenable to electrophysiological and functional imaging techniques (Marley and Baines, 2011; Pulver et al., 2015). Recent efforts have combined these techniques to uncover novel circuit motifs underlying nociception and action selection (Jovanic et al., 2016; Ohyama et al., 2015). Thus, *Drosophila* larvae offer a powerful system in which to study sensorimotor neural mechanisms using functional imaging, comprehensive behavioral analyses, and the synaptic resolution afforded with EM reconstruction.

Tools for manipulating neural circuits

One advantage of using Drosophila to study circuits is the ease with which one can manipulate neural populations with remarkable specificity. This cell-specific targeting is enabled by the Gal4/UAS system (Brand and Perrimon, 1993). Expression of Gal4, transcription activator is dictated by an enhancer fragment, which can then bind to upstream activator sequence UAS to drive expression of a variety of transgenes that allow researchers to label cell morphology, image neural activity, and manipulate neural function (Figure 1.2). Additional binary systems that are conceptually similar to

Gal4/UAS have also been generated, such as QF/QUAS (Potter et al., 2010) and LexA/LexAop (Lai and Lee, 2006), which further expand the number of neural populations that can be manipulated simultaneously. Moreover, expression patterns can be further refined in three ways, 1) suppressing Gal4 activity in subsets of cells by co-expressing an enhancer specific Gal80 (Gal4 inhibitor), 2) utilizing intersectional approaches that label the overlap between Gal4 and LexA or Qf expression, and 3) expressing complementary "split" Gal4 elements in different cell types, manipulating only populations where Gal4 is reconstituted. Laboratories are constantly generating and sharing Gal4 lines, which increases the number of neurons that one can manipulate selectively. Additionally, there are projects that focus on generating thousands of Gal4 lines at once to rapidly progress in *Drosophila* studies. Recently, 7,000 Gal4 lines were generated (Jenett et al., 2012) by fusing defined fragments of the genome to Gal4 sequences. Another group produced the integrase swappable *in vivo* targeting element (InSITE) collection of Gal4 lines (Gohl et al., 2011), which is ideal for circuit analysis because it allows Gal4 to be swapped for the genetic elements of other binary systems (i.e. LexA, Qf, split Gal4), which permits independent manipulation of neural populations. Genetic swapping utilizes recombinase-mediated cassette exchange (RMCE), which allows a sequence cassette (harboring Gal4) to be swapped out for a donor sequence (e.g. LexA) *in vivo;* thus, bypassing time-intensive molecular cloning techniques to recapitulate cell-specific Gal4 expression in other genetic systems. InSITE Gal4 lines were generated by randomly inserting an enhancer trap (*P* element or *piggyBac* transposon with Gal4 sequence) into the *Drosophila* genome, and thus driving the expression of Gal4 by a cell-specific enhancer sequence (Figure 1.2). This technique produced approximately 2,000 isogenic lines that sparsely label neurons in the peripheral and central nervous system providing access to neurons that might have not been identified in other Gal4 collections (Jenett et al., 2012), and do not incur

transvection effects (regulatory region influencing transcription of another region in trans) (Mellert and Truman, 2012).

Dendritic arborization neurons detect various somatosensory stimuli and generate subtype specific behavior

The larval peripheral nervous system consists of sensory neurons with distinct morphologies collectively spanning the entire body wall. The body wall consists of 11 segments, three thoracic (T1-T3), and eight abdominal (A1-A8), each innervated with 44 sensory neurons classified by dendritic morphology: Type I sensory neurons possess single dendritic extensions and include mechanosensory external sensory neurons (es), and vibration-sensing chordotonals (chd) (Bodmer and Jan, 1987). Type II consist of multidendritic (md) neurons with diverse dendritic arborization. The md group is further subdivided into three groups: 1) neurons with bipolar dendrites (bd), 2) neurons with dendrites wrapping around the trachea (tracheal dendritic; td), and 3) the most morphologically complex, dendritic arborization neurons (da).

The larval somatosensory system has become an established model for studying molecular mechanisms underlying dendritic morphogenesis and patterning (Grueber et al., 2003; Matthews et al., 2007), and more recently has emerged as a model for studying neural pathways underlying behavior. Our molecular understanding of these neurons has revealed that each da neuron class expresses a unique profile of ion channels and receptors that enable modality specific detection, and subsequent behavior outputs (Figure 1.3) (Honjo et al., 2016; Turner et al., 2016). da neurons are characterized into four classes (Class I-IV) in order of increasing dendritic branching and expansiveness (Grueber et al., 2002) (Figure 1.3). Class I neurons with the simplest arbors are proprioceptive and important for peristaltic wave progression during larval locomotion (Hughes and Thomas, 2007). Class II dendrites are slightly more complex

than class Is and are likely mechanosensory (Tsubouchi et al., 2012). Class III are mechanosensory with dendritic actin-rich protrusions which are important for their gentle-touch function (Tsubouchi et al., 2012; Zhong et al., 2012) (Figure 1.3), and were also recently shown to be involved in cold nociception (Turner et al., 2016). Class IV neurons have the most complex dendrites. Only three neurons per hemisegment: dorsal ddaC, lateral vdaB, and ventral v'ada (Figure 1.4B-D) tile the entire body wall with their dendrites (Grueber *et al*., 2002). Class IV neurons collectively send their axon terminals to the ventral nerve cord, where they terminate in the ventromedial region of the neuropil (Figure 1.4A,E). Class IV (cIV) neurons are morphologically analogous to C-fibre and A∂ fibres in vertebrates, which also possess multi-branched terminals with free endings lacking accessory receptor cells or glial ensheathment (Hall and Treinin, 2011). Additionally, both cIVs and vertebrate nociceptors detect noxious stimuli using TRP and DEG/ENaC channels, showing evolutionary conservation (Hall and Treinin, 2011; Lumpkin and Caterina, 2007).

Each class of da neurons project their axons to the ventral nerve cord (VNC) and terminate in modality specific locations, analogous to dorsal horn organization (Figure 1.4A) (Grueber et al., 2007). Proprioceptive afferents target the dorsomedial region, nociceptive afferents terminate in the ventromedial region, and mechanosensory neurons target a region adjacent to the nociceptive neuropil (Figure 1.4). This spatial organization seems to suggest that axons could be making modality specific postsynaptic partners, but at least one study suggests that multiple sensory neurons can converge on different locations on a dendritic arbor (Ohyama et al., 2015). There is also a topographical organization in the VNC, which is segmentally organized into bilateral thoracic and abdominal regions such that sensory neurons receiving input from specific hemisegments will project to corresponding regions in the VNC. Furthermore, depending on their morphology, interneurons in the nerve cord can primarily collect input from one

hemisegment, or multiple contra-/ipsi-lateral segments or along the nerve cord. This topographical organization might be important for previously reported directional responses to sensory stimuli (Hwang et al., 2007).

Class-IV neurons are primary nociceptors in Drosophila larvae

Despite *C.elegans* and *Drosophila* being widely used to study molecular and neural mechanisms of nociception today, there was a time when invertebrates were not even thought respond to damaging stimuli. In 1900, Norman zealously argued that attributing "pain sensations" to lower animals, such as worms and leeches, was an anthropomorphic conclusion. To clarify, he was not referring to a conscious or emotional component of pain, but instead denying that invertebrates could detect and react to harmful stimuli. In one section he reasons that the rapid thrashing observed upon throwing leeches into water heated to 40˚ could not be harmful to the leech because blood rushes through the human body at a similar temperature and is not detected as noxious (Norman, 1900). Nevertheless, nociceptive behaviors continued to be catalogued and characterized, notably bending and thrashing responses to noxious stimuli in caterpillars was initially described in 1945 (Frings, 1945) and later found to be subject to sensitization (Walters et al., 2001). The latter study found that a noxious stimulus to one of the prolegs on the larval *Manduca sexta* could induce a generalized sensitization across segments, resulting in nociceptive behavior in response to gentle-touch stimuli. A class of dendritic arborization neurons in *Manduca* was proposed to be nociceptive, potentially driving this effect (Grueber et al., 2001). In *Drosophila*, dendritic arborization neurons were also initially implicated in nociceptive behavior (Tracey et al., 2003). Much like previous studies of nociception, the identification of the nociceptive behavior preceded identification of the nociceptors themselves. Tracey *et al*. discovered that in response to a hot probe or harsh mechanical stimulus, *Drosophila* larvae would

exhibit a peculiar corkscrew-like lateral locomotion, termed rolling, that was unlike the forward contractions observed during crawling. This robust nociceptive behavior has been the basis for many screens aimed at identifying the molecular underpinnings of nociception (e.g. transient potential ion channel, *painless*). (Honjo et al., 2016; Tracey et al., 2003). Tracey and colleagues later identified class IV neurons as being necessary and sufficient for the nociceptive rolling behavior (Hwang et al., 2007). This initial characterization of larval nociceptors has provided the opportunity for studying nociceptive sensitization (Babcock et al., 2009; Babcock et al., 2011; Im et al., 2015), and the neural circuitry driving nociceptive motor responses (see following section).

Functionally similar to C-fibres and A∂ fibres in mammals, Class IV neurons are polymodal nociceptors, sensing chemical, high-threshold mechanosensory, and noxious heat stimuli (>39°C) (Babcock et al., 2009; Terada et al., 2016; Tracey et al., 2003; Zhong et al., 2012). In response to increases in heat (>39°C) or pressure (> 45mN), larvae perform a sequential nocifensive response: C-shape body bending, 360° lateral turns (rolling), and finally a 1.5 fold increase in crawling speed termed, escape crawl (Figure 1.4F) (Ohyama et al., 2013; Tracey et al., 2003). A small fraction of animals exhibit rolling, without escape crawling, or a bend-escape crawl sequence without rolling, suggesting escape response modules can be combined into different sequences (Ohyama et al., 2013). cIVs have been previously shown to be necessary and sufficient for nocifensive escape behavior and seem to be playing a general role in avoidance (Hwang et al, 2007; Xiang *et al*, 2010; Johnson *et al*, 2012). Class IV neurons are also thought to have a proprioceptive role, increasing larval locomotion with minimal turning following loss of *ppk1* (Ainsley et al., 2003). Although the sensory neurons detecting noxious stimuli, and the stereotyped behavior they evoke have been well-characterized, we are only beginning to understand the complex neural circuitry underlying nocifensive escape responses.

Ethological role for nocifensive escape behavior

Nocifensive rolling provides the fastest form of larval locomotion (up to 8mm/s compared to 1m/s during forward locomotion) (Hwang et al., 2007; Ohyama et al., 2013), which might enable an animal to quickly remove itself from a noxious environment. Such rapid locomotion is presumably energetically expensive, and might therefore confer strong fitness advantages. In natural environments, the female parasitoid wasp uses *Drosophila* larvae as a host for development of its offspring. Studies focusing on *Leptopilina boulardi* have revealed that the wasp attack consists of multisensory stimuli: the wasp secretes chemical cues (Ebrahim et al., 2015) as it holds onto larvae (tactile) before injecting its egg through a sharp ovipositor (mechanical noxious stimulus) (Hwang et al., 2007; Robertson et al., 2013). If oviposition and development are successful, the wasp larva consumes the *Drosophila* larvae from within and ecloses from its pupal case. Thus, *Drosophila* are under strong evolutionary pressure to avoid wasp oviposition. Nocifensive escape can offer an effective strategy for evading oviposition as rolling *towards* the wasp, which initially seems counterintuitive, can tangle its ovipositor. If successful, the larva can throw the wasp on its back in extreme cases, and is free to rapidly escape crawl from the dangerous situation (Hwang et al., 2007; Robertson et al., 2013). Thus, the nocifensive escape sequence is crucial for larval survival and must be controlled by neural circuits that produce these behaviors effectively and in coordinated succession.

Neural circuitry underlying nocifensive escape behavior

Neural circuit analysis can be enhanced by electron microscopic (EM) circuit reconstruction to generate wiring maps, uncover novel interactions, and generate testable hypotheses along with behavioral and functional methods. An EM serial section volume has been generated for the 1st instar larva, and dedicated efforts across multiple

labs have so far reconstructed ~60% of the larval CNS (Cardona, personal communication). With the aid of EM reconstruction, a recent study identified a complete microcircuit driving nocifensive rolling via second order Basin interneurons, which receive direct input from nociceptive cIVs and vibration sensing chordotonals (chd) (Ohyama et al., 2015). Among the neurons that have been identified so far are Basin neurons, Goro neurons, and A08 neurons. The Basin population consists of four subtypes, two of which receive chd input exclusively (Basin-1,3), and two of which integrate noxious and chd input (Basin-2,4) (Figure 1.5). Although Basin-1,3 do not receive substantial input from cIV neurons, they synapse onto A08m and A08x neurons, which are lateral interneurons, that can trigger rolling (Figure 1.5) (Wreden et al., 2017). The connectivity downstream of A08m and A08x neurons has not been completed, so connections to known nociceptive interneurons are not yet identified. Co-activating vibration and nociceptive circuits enhances functional responses in Basin-1,4 neurons and probabilistically increases rolling behavior. Additional EM reconstruction revealed that vibration and nociceptive convergence occurs further downstream, including onto Goro rolling command-like neurons, which reside in the motor domain of the nerve cord, but do not directly target premotor neurons. Basins-1,3 indirectly target Goro neurons through a brain pathway (Figure 1.5). Interestingly, chordotonals also express *painless,* a transient receptor potential ion channel, which is required for both mechanical and thermal nociception (Tracey et al., 2003). Notably, neither Goro nor Basin-1,4 silencing completely eliminated rolling behavior pointing to additional circuits promoting rolling. Furthermore, the neural circuitry controlling the C-bending, escape crawling, and sequence progression between escape behavior modules remains unknown. Ohyama *et al.*, highlights the advantage of using EM reconstruction to identify novel circuit motifs that can be relevant to other somatosensory circuits.

The polymodal nature of class IV neurons elicits two interesting circuit questions: 1) how does the same neuronal subtype produce distinct avoidance behaviors?, and 2) does the brain distinguish between sensory stimuli that evoke the same avoidance response (i.e. rolling)? To address the first question, Terada *et al*., recorded from class IV neurons during exposure to blue light or noxious heat stimuli, which generate distinct avoidance behaviors-- head turning/change in crawling direction, and nocifensive rolling, respectively. In response to noxious heat, cIVs produced high frequency firing bursts intermittent with pause periods that led to high Ca^{2+} influx in cIV dendrites. Conversely, low-frequency continuous firing patterns characterized responses to noxious blue light (Terada et al., 2016). Thus, cIV encodes noxious light and heat differently and likely recruits distinct downstream motor circuits to generate modality-specific avoidance behaviors.

As for whether circuit elements distinguish between noxious stimuli that generate the same behavioral response, recent work supports divergent circuits underlying thermal nociception and mechanical nociception (Hu et al., 2017). Although both forms of noxious stimuli can elicit nocifensive escape, mechanical nociception is dependent on mechanosensory class II, and class III neurons, to a lesser extent, which converge with cIV input onto two dorsal insulin-like peptide 7-producing neurons (DP-ilp7). DP-ilp7 activation does not induce escape rolling, but its activity through short neuropeptide F (sNPF) modulates activity in cII-IV neurons. sNPF dependent modulation is required for cII-cIV neurons to promote rolling through A08n ascending projection neurons (Figure 1.5). Although A08n neurons receive direct synaptic input from class IV neurons, the mechanosensory (cII, cIII) and cIV signaling seems to occur primarily through sNFP as reducing sNPF receptor (sNPFR) in A08 neurons abolishes responses to cII-cIV.

Interestingly, A08n, cII-cIII sensory neurons, and the ilp-7 neurons are dispensable for behavioral responses to noxious thermal stimulation, suggesting that these circuit elements are selectively recruited during mechanical nociception.

Taken together, recent work has uncovered the rich circuit complexity underlying the nocifensive escape response. This thesis aims to address how noxious stimuli are transformed into coordinated escape motor outputs by focusing on the following questions: 1) What are the circuit elements driving nocifensive escape, notably, are there microcircuits driving each motor output (e.g. C-shape bending)?, 2) How do nociceptive interneurons interact with downstream premotor/motor circuitry to promote bending and rolling?, and finally, 3) Do nociceptive circuits integrate additional somatosensory input, and if so, how does this affect nocifensive behavior? Thus, we anticipate that a more complete circuit level understanding of nociception in *Drosophila* will uncover novel fundamental features underlying sensorimotor processing.

Figure 1.1: Somatosensory transduction in Vertebrates

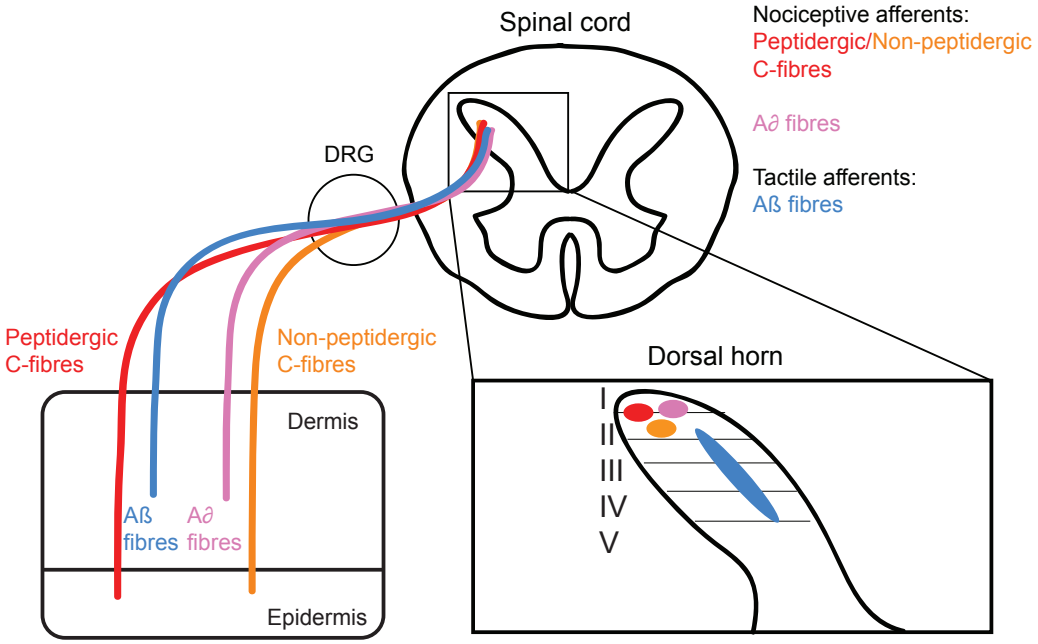

Figure 1.1: Somatosensory transduction in Vertebrates

Schematic representing somatosensory afferent targeting in the periphery and in the spinal cord.

Figure 1.2: InSITE overview

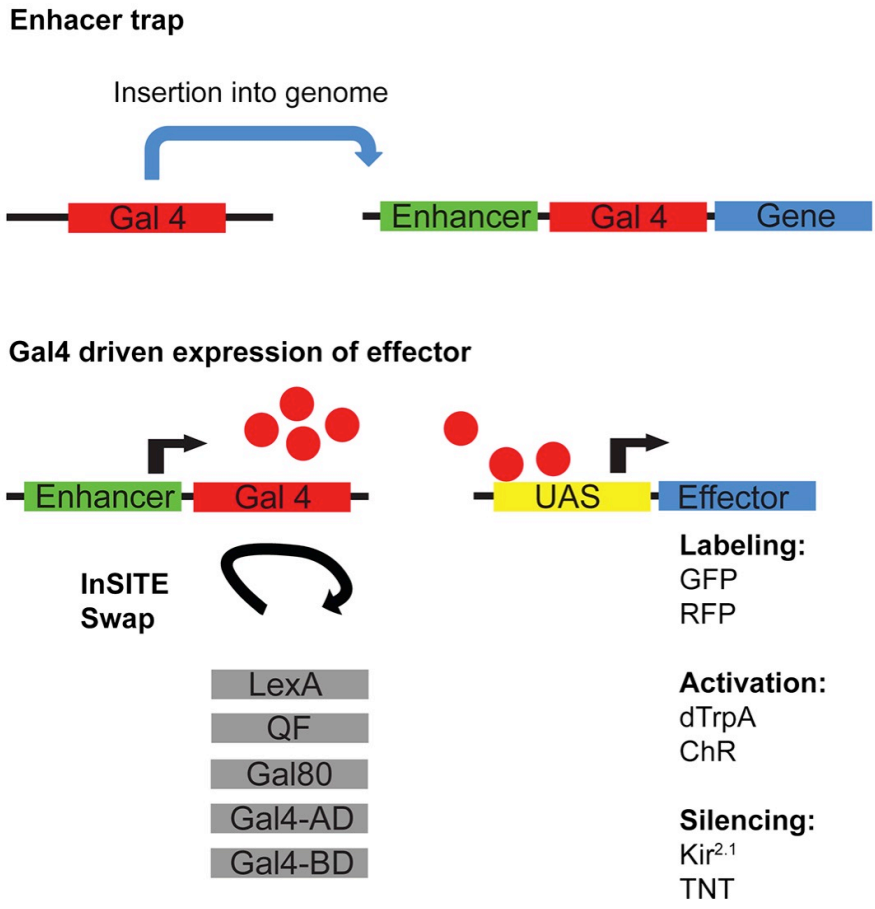

Figure 1.2: InSITE overview

Schematic overview of the InSITE system. Gal4 sequence becomes inserted into the *Drosophila* genome near an enhancer, which will drive expression of Gal4 activator. Gal4 binds to upstream activator sequence (UAS) to express transgene of interest (e.g. to label, activate or silence neurons). InSITE genetic swapping occurs *in vivo* and can replace Gal4 with another genetic element (LexA, QF, Gal80, Gal4-AD, Gal4-BD).

Figure 1.3: Dendritic arborization neurons detect distinct sensory modalities

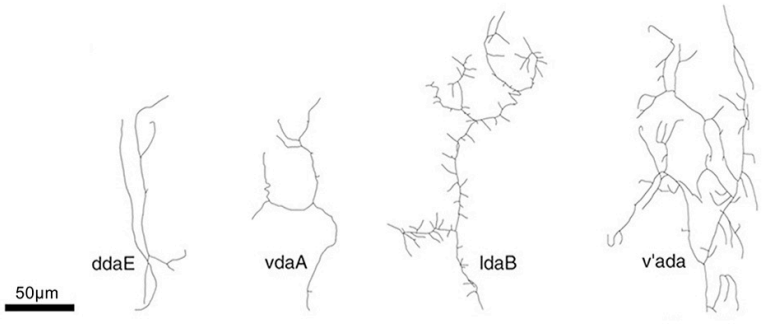

	Class I	Class II	Class III	Class IV
Sensory modality	Proprioception	Putatative mechano-sensory	Low-thrshold Mechanosensory (~1mN) Cold Nociception	Nociception - mechanical (>45mN) - thermal (>39˚C) - chemical (cytokines, AITC) Proprioception Light avoidance
Behavior	Sensory feedback during crawling	?	Mechanosensory -Pause, Anterior withdrawal, Head turn, Reverse locomotion Cold Nociception -head and/or tail raise -full-body contraction	Nociception -nocifensive escape Proprioception -crawling speed, turn/pause frequency Light avoidance -head turn, change in crawling direction

Figure 1.3: Dendritic arborization neurons detect distinct sensory modalities

Dendritic arborization neurons Class I-IV: representative traced neuron showing class morphology (adapted from Grueber et al., 2002), type of sensory stimulus detected, and behavior evoked

Figure 1.4: Class-IV neurons are larval nociceptors

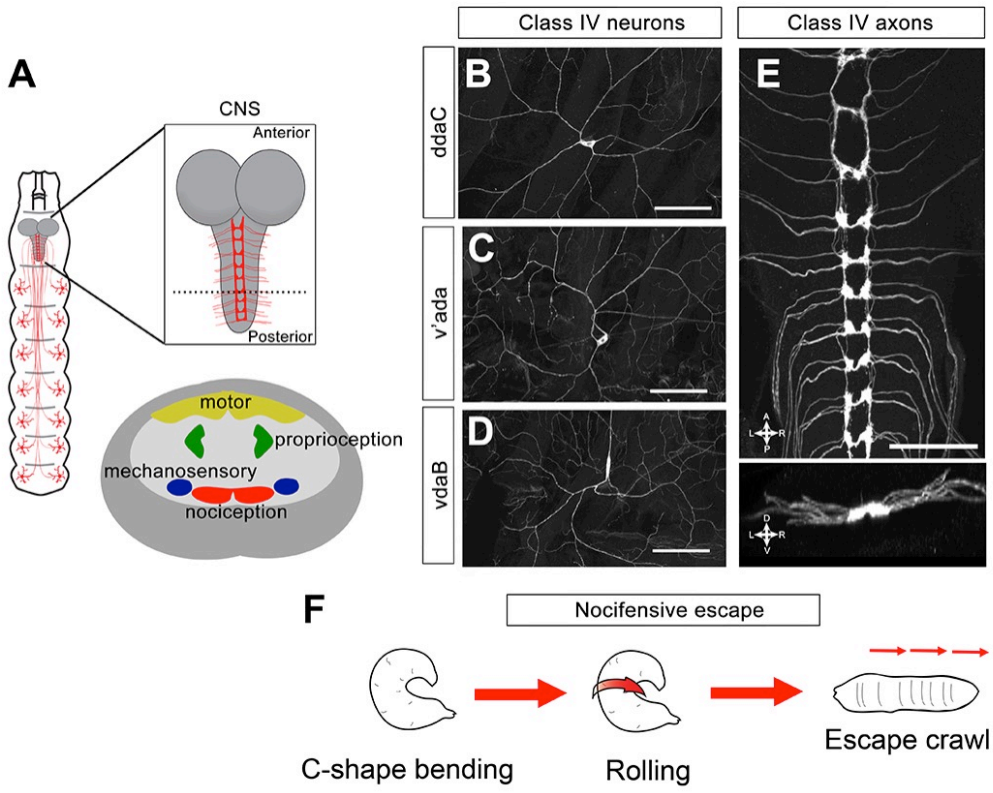

Figure 1.4: Class-IV neurons are larval nociceptors

(A) Schematic showing the *Drosophila* larval CNS. Red neurons on the body wall represent cIV nociceptive neurons, and scaffold in the CNS represents class IV (cIV) axonal projections. Enlarged transverse section through ventral nerve cord (VNC) is shown below. Color-coded regions depict modality specific locations where sensory axons (nociceptive, red; mechanosensory, blue; proprioceptive; green) and motor neurons (yellow) terminate in the neuropil.

(B-E) *ppk-CD4-tdTomato* (anti-dsRed) labeling cIV sensory neurons (B-D) or cIV CNS scaffold (top: anterior-posterior view; bottom: dorsoventral view)

(F) Sequential nocifensive escape behavior consisting of C-shape bend followed by corkscrew-like rolling, and increased forward locomotion, termed escape crawl. Scale bar: 50μm (B-E)

Figure 1.5: Neural circuitry underlying nocifensive behavior in *Drosophila* larvae

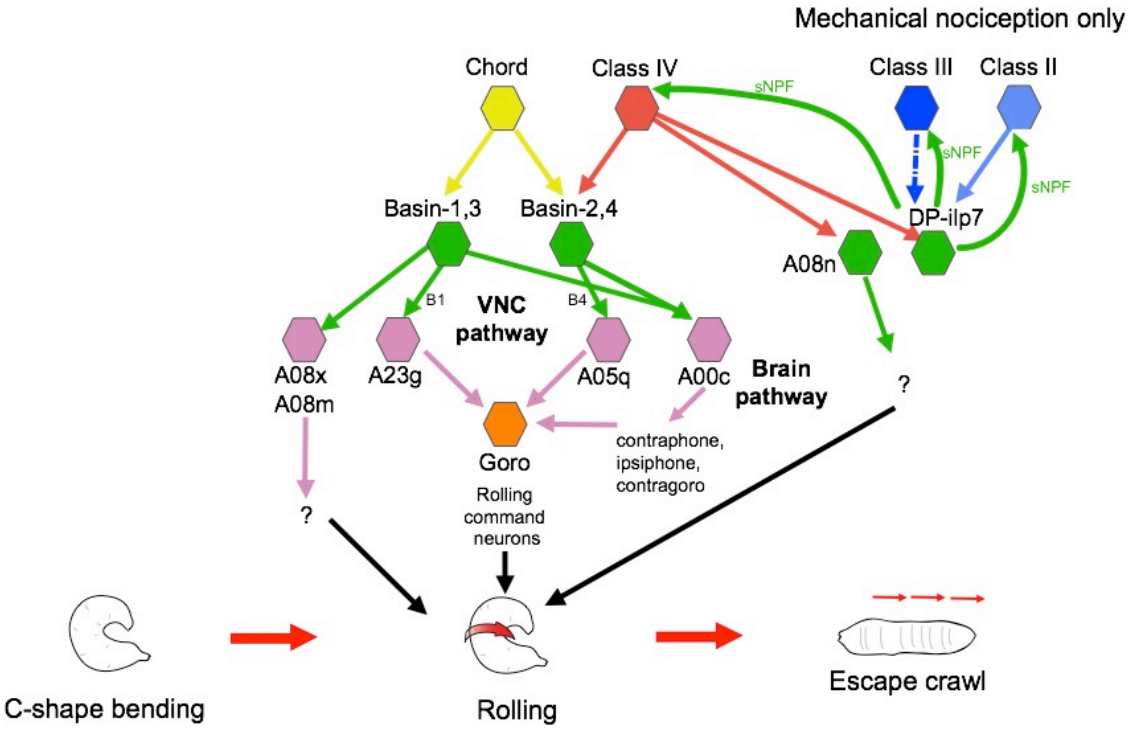

Figure 1.5: Neural circuitry underlying nocifensive behavior in *Drosophila* larvae

Identified neural pathways triggering nocifensive rolling in *Drosophila* larvae. VNC pathways refer to circuits within the ventral nerve cord, and brain pathways refers to pathways that target neurons in the brain lobes. Solid arrow= EM-validated connectivity, dashed arrow= indirect connectivity.

Chapter II:

Down-and-Back nociceptive interneurons promote sequential bending and rolling stages of nocifensive escape behavior[1]

Abstract

Nociception, the detection and avoidance of harmful stimuli, is a fundamental and evolutionarily conserved somatic sense. Although the sensory neurons that detect noxious stimuli are well studied in numerous organisms, how noxious stimuli are transformed into complex coordinated escape behavior remains poorly understood. In response to noxious stimuli, *Drosophila* larvae perform a sequential escape behavior: C-shape bending, and 360˚ turning (rolling), followed by rapid crawling (escape crawl). I have identified a population of interneurons in the CNS of *Drosophila* larvae, termed DnBs, provide anatomical and functional evidence that these neurons are targets of class IV nociceptive dendritic arborization (da) neurons, and show that they are required for nociceptive escape behavior. Activating DnB neurons promotes rolling escape behavior, but can also elicit the initial C-shape bend in the absence of rolling, revealing novel modularity in the neural circuits driving escape behavior. Conversely, silencing DnB activity decreases bending curvature, and reduces rolling probability. These results identify a crucial component of the initial transduction of nociceptive input to the central circuitry underlying escape behavior.

Introduction

[1] I am thankful to my collaborators for their valuable contributions to this work. Ken Honjo performed calcium imaging experiments, Sam (Cheng) Qian performed bending curvature analysis, Lalanti Venkatasubramaniam cloned syb-GRASP, and Wes Grueber, Dan Tracey, Marion Silles, David Gohl, Marta Zlatic, Tomoko Ohyama, and Albert Cardona provided input on data analysis and the main text.

Nociception, the detection and avoidance of harmful stimuli, is fundamental and evolutionarily conserved. Noxious stimuli can elicit aversive withdrawal (termed nocifensive behavior), which is an essential evolutionarily conserved behavior. Nocifensive responses can be diverse within an organism, and occur in serial order. For instance, in response to a local noxious stimulus to the paw, rodents will engage in a sequence of nocifensive behaviors, which can include head and foot movements, posture adjustment, and alternation of foot elevation. The display of nocifensive sequences can vary based on stimulus intensity, revealing a hierarchy of protective motor responses (Blivis et al., 2017; Fan et al., 1995). Although the sensory neurons that detect noxious stimuli have been well studied in numerous organisms, how noxious stimuli are transformed to the complex sequential behaviors that protect animals from harm remains poorly understood.

Drosophila larvae provide an advantageous system in which to dissect neural circuit organization, connectivity and function. Class IV (cIV) dendritic arborization (da) neurons are polymodal nociceptive neurons with receptive territories that together tile the entire larval epidermis (Grueber et al., 2002; Hwang et al., 2007). cIV neurons are both necessary and sufficient for generating defensive withdrawal (nocifensive) behavior in response to noxious stimuli (Hwang et al., 2007). Strong mechanical and high thermal stimulation induce nocifensive C-shaped body bending and rolling behavior, followed by rapid forward locomotion, or escape crawl (Hwang et al., 2007; Ohyama et al., 2015). The behavioral responses of *Drosophila* larvae to noxious stimuli are both diverse and sequential, suggesting significant complexity in the circuits downstream of primary sensory neurons.

In the ventral nerve cord of *Drosophila* larvae, da sensory neurons extend axon terminals to discrete locations in a modality specific manner reminiscent of the organization of the vertebrate dorsal horn (Grueber et al., 2007; Merritt and Whitington,

1995; Todd, 2010). cIV neurons have been characterized both anatomically and functionally, yet the circuit for nociceptive processing is still poorly understood. A recent study identified circuit elements downstream of cIV neurons that integrate vibration and noxious stimuli, but also pointed to extensive circuit divergence at the first somatosensory relay (Ohyama et al., 2015). The stereotypical projections of cIV sensory axons, characterization of cIV function, and accessibility of central neurons afforded by large collections of Gal4 lines facilitate dissection of circuit organization underlying nociceptive escape behavior. In particular, the integrase swappable *in vivo* targeting element (InSITE) collection of Gal4 lines is ideal for circuit analysis because it allows Gal4 to be swapped for other genetic effectors (i.e. LexA, Qf, split Gal4), permitting independent manipulation of neural populations.

Here, I identify a population of second-order somatosensory neurons, termed Down-and-Backs (DnBs), that transduce information from cIV sensory neurons. The activity of DnBs triggers sequential components of the nociceptive escape response: C-shape bending and rolling. Although C-shape bending and rolling normally coincide, DnB activation can trigger bending in the absence of rolling, revealing previously uncharacterized modularity in this escape circuit. Silencing DnB neurons impairs the curvature of C-shape bending, and reduces the probability of rolling.
These findings reveal a novel component of the nociceptive circuit and provide insight into how sensory input is transduced into rapid coordinated escape behavior.

Results

Identification of putative nociceptive interneurons: Down-and-Backs

To gain access to nociceptive circuitry, I examined integrase swappable *in vivo* targeting element (InSITE) Gal4 lines (Gohl et al., 2011) for expression in the ventral region of the ventral nerve cord (VNC) where class IV (cIV) nociceptive axons terminate (Grueber et al., 2007)(Figure 2.1A). I identified *412-Gal4,* which labeled segmental interneurons with processes in the nociceptive ventromedial neuropil (Figure 2.1B). *412-Gal4* also labeled a bilateral population of neurons in the brain lobes, and faintly labeled other cell bodies in the VNC (Figure 2.1B), but did not label primary sensory neurons or motor axons (Figure 2.2B-D'). To characterize the morphology of *412-Gal4* VNC interneurons at single-cell resolution, I used the 'Flip out' technique (Basler and Struhl, 1994; Wong et al., 2002). Primary neurites project to the ventromedial neuropil, where they arborize profusely (Figure 2.1C'). A single process emerged from this dendritic region and projected laterally and dorsally back towards the cell body (Figure 2.1C'). This population of interneurons was also found in the thoracic segments where they exhibited longer medial and lateral processes (Figure 2.2A). Fitting with lineage-based nomenclature, the interneurons labeled by *412-Gal4* were identified as the A09l neurons (Lacin and Truman, 2016). Because these neurons project 'down' to the ventromedial neuropil, arborize, and sent a reverse projection towards the cell body, I refer to them as "Down-and-Back" or DnB neurons.

Single-cell analysis also revealed that *412-Gal4* labels additional interneurons in the nerve cord, including previously characterized serotonergic A26e neurons (Huser et al., 2012; Okusawa et al., 2014) (Figure 2.2E- F''), and GABA-ergic A27j neurons (Fushiki et al., 2016; Schneider-Mizell et al., 2016) (Figure 2.2G-H'').

To characterize the input and output regions of DnB neurons, I examined the distribution of presynaptic and postsynaptic markers. Dendritic marker, or DenMark is a fusion between dendrite-restricted mammalian adhesion molecule ICAM5/Telencephalin and the red fluorescent protein, mCherry. I found that medial processes accumulated the

dendritic marker, DenMark (Nicolai et al., 2010) (Figure 2.3A-A'). The lateral projections accumulated the presynaptic marker bruchpilot.short^{mCherry} (BRP.short^{mCherry}) (Schmid et al., 2008) (Figure 2.3B-B'). I also observed BRP.short^{mCherry} accumulation in medial dendrites, suggesting both presynaptic and postsynaptic functions for these arbors (Figure 2.3B-B'). Next, I investigated the neurotransmitters released by DnB neurons, by immunostaining for glutamate transporter (vGLUT), and inhibitory neurotransmitter, GABA. I did not observe labeling of vGLUT or GABA in DnB cell bodies (Figure 2.3C-D''). I further excluded GABA neurotransmission by introducing *GAD-Gal80* (Sakai et al., 2009), which would inhibit Gal4 activity in GABA expressing neurons, into *412-Gal4, UAS-mCD8:GFP* animals and found no reduction of GFP signal (Figure 2.3E-E'). These data suggest that GABA is not a transmitter for DnB neurons. Next, I examined whether DnB neurons signal via acetylcholine neurotransmission by combining *cha$^{3.3kb}$-Gal80* (Kitamoto, 2002), which inhibits Gal4 activity in cholinergic neurons, with *412-Gal4, UAS-mCD8:GFP.* I found a reduction in GFP signal in both cell bodies and in medial processes of DnB neurons (Figure 2.3F-F'), suggesting that DnB interneurons are cholinergic. To further validate achetylcholine production in DnB neurons, I co-labeled with the protein fusion, ChAT-eGFP, which tags endogenous choline acetyltransferase (ChAT) with eGFP (Nagarkar-Jaiswal et al., 2015). I observed ChAT-eGFP expression in both DnB cell bodies, and axonal processes (Figure 2.3G- G'''). Taken together, these data suggest that DnB interneurons are cholinergic interneurons.

DnB neurons transduce noxious stimuli downstream of cIV neurons

DnB dendrites arborize in the nociceptive neuropil of the VNC, making them

candidate targets of cIV nociceptive sensory neurons. I co-labeled DnB neurons and cIV sensory axons to visualize potential connectivity between these populations. Co-labeling with cIV markers revealed overlap between DnB dendritic processes and cIV axon terminals (Figure 2.4A-A'). A lateral domain of the DnB dendritic field did not overlap with the cIV terminals, raising the possibility of connectivity with additional dendritic arborization (da) somatosensory modalities (Figure 2.4A''; Chapter IV). I next used the GFP reconstitution across synaptic partners (GRASP) technique (Feinberg et al., 2008; Gordon and Scott, 2009) to assess putative connectivity between DnBs and multidendritic (md) sensory neurons, which include cIVs. GRASP consists of complementary non-fluorescent split GFP fragments that exhibit fluorescence when reconstituted across neighboring membranes (~100nM apart), such as the synaptic cleft. We identified an InSITE line, *585-Gal4* that labeled all md neurons, and generated *585-LexA* by standard InSITE swapping methods to perform the GRASP labeling technique (Figure 2.4B). I drove expression of *LexAop-CD4-spGFP*^{11} in md neurons using *585-LexA* and the complementary fragment *UAS-CD4-spGFP*$^{1-10}$ in DnB neurons using *412-Gal4*, and observed GFP reconstitution in a region corresponding to cIV nociceptive axons, but also cIII mechanosensory neurons (Figure 2.4C)(See Chapter IV). Even while amplifying fluorescent signal with an antibody targeting the reconstituted GFP (Gordon and Scott, 2009), I still observed dim fluorescence. To enhance the low signal of reconstituted GRASP, I generated high expressing constructs of spGFP fragments (13XLexAop-spGFP^{11} and 20XUAS-spGFP$^{1-10}$) and repeated the GRASP experiments between md and DnB neurons. High expression GRASP resulted in strong native signal consistent with reconstitution around regions of cIII-cIV axons, but it also resulted in extensive, potentially non-specific, labeling of other parts of the DnB neuron (Figure 2.4D). The GRASP signal detected at sites corresponding to DnB axons (Figure 2.4C-D, arrowhead) might be representative of non-synaptic cell-cell contact due to the diffuse

expression of spGFP fragments along the entire neuron. I sought to eliminate this possibility by restricting spGFP$^{1-10}$ to the presynaptic neuron by tethering it to vesicle-associating membrane protein, synaptobrevin (syb). spGFP$^{1-10}$ is localized to the inside of synaptic vesicles via the C-terminus of synaptobrevin, which leads to increased display of spGFP$^{1-10}$ on the presynaptic membrane following vesicle fusion during neuronal activation (Macpherson et al., 2015). Thus, this version of GRASP reconstitutes in an activity dependent manner. We generated *QUAS-n-syb-GFP$^{1-10}$* (Frank et al., 2015; Karuppudurai et al., 2014; Macpherson et al., 2015) and drove expression exclusively in cIV nociceptive neurons using *TrpA1-QF* and expressed complementary *UAS-CD4-GFP^{11}* in DnB interneurons using *412-Gal4*. I observed GFP reconstitution in a pattern consistent with the cIV axon scaffold (Figure 2.4E). Labeling was not observed in controls when either fragment was expressed alone (Figure 2.4F-G). These results support connectivity between DnB dendrites and cIV sensory neurons.

cIV nociceptive neurons are activated by noxious thermal stimuli above 38˚C (Terada et al., 2016; Tracey et al., 2003; Xiang et al., 2010). To determine whether DnB neurons respond to noxious stimuli, we performed calcium imaging experiments in the presence of noxious heat, in collaboration with Ken Honjo in the lab of Dan Tracey (Indiana University). I provided the Tracey lab with flies expressing GCaMP6m (Chen et al., 2013) in DnB neurons using *412-Gal4.* They performed imaging in a partially dissected preparation and applied a local ramped heat stimulus to abdominal segments. We observed increased GCaMP6m fluorescence in DnB neurons (identified by morphology) beginning at 39˚C and plateauing at approximately 42˚C (Figure 2.5A-C), fitting well with prior studies showing cIV neuron spiking above 38˚C (Terada et al., 2016; Tracey et al., 2003; Xiang et al., 2010). Silencing cIV neurons reduced mean DnB calcium responses by 68% during noxious stimulation and delayed the onset of the calcium response (Figure 2.5D-F). To determine the number of DnB cells responding to

noxious stimulation with or without class IV activity, I used the lowest peak response for DnB neurons in the initial cohort of experiments (Figure 2.5B) to set as a threshold for "noxious responder." Using this classification, the percentage of DnB neurons responding to noxious heat was reduced from 92% to 27% (Figure 2.5G) when cIV neurons were silenced, suggesting that DnB responses to noxious heat are largely cIV dependent. Taken together, these data support a role for DnB neurons in the transmission of noxious heat stimuli from cIV sensory neurons.

DnB neurons trigger nocifensive behavior downstream of nociceptive cIV neurons

Next, I assessed the role of DnB neurons in triggering nocifensive escape behavior using both thermogenetic and optogenetic approaches. Thermogenetic activation of *412-Gal4* neurons elicited rolling behavior (Figure 2.6A-B). I observed similar rolling behavior when I activated *412-Gal4* neurons using red activatable channelrhodopsin (ReaChR) (71% of animals, n=48) in animals raised with all-*trans*-retinal, an essential co-factor for channelrhodopsin (Figure 2.6C). To test whether *412-Gal4* neurons triggered rolling downstream of cIV neurons, I performed a circuit epistasis experiment. Silencing of cIV neurons by driving tetanus toxin light chain (TNT::HA) (Karuppudurai et al., 2014) under the control of a cIV-specific driver *R38A10-LexA* (Jenett et al., 2012) (Figure 2.6D) reduced rolling behavior in response to a local noxious stimulus delivered to segments A4-A6 (Figure 2.6E). Activation of DnBs using *412-Gal4* neurons largely bypassed this inhibition and induced rolling in 82% of animals (n=27) (Figure 2.6F). Thus, DnB neurons likely elicit nocifensive escape behavior downstream cIV neurons.

I identified an additional Gal4 line from the InSITE collection labeling DnB neurons, and tested its ability to induce nocifensive behavior. We generated *412-QF* by

standard InSITE swapping methods (Gohl et al., 2011) (Figure 2.7A-A'') and verified overlapping expression of *4051-Gal4* with *412-QF* in the DnB interneurons (Figure 2.7C-C'''). I also counted the number of overlapping neurons between both drivers, and found that *4051-Gal4* labeled all 22 DnB cell bodies (Figure 2.7D). Thermogenetic activation of *4051-Gal4* induced rolling in 80% of larvae (Figure 2.7E). Among the other overlapping populations between these drivers and *412-QF*, *4051-Gal4* overlapped with 23 non-DnB neurons in the VNC, and 18 neurons in the brain lobes. *412-Gal4* off target A26e and A27j was found occasionally in *4051-Gal4* pattern. To exclude the contribution of A26e and A27j in *412-Gal4* triggered rolling, I activated these populations separately using the pan-serotonergic line driven by the tryptophan hydroxylase (TRH) enhancer, *TRH-Gal4* (Alekseyenko et al., 2010) , and *R38H01-Gal4 (Jenett et al., 2012; Schneider-Mizell et al., 2016)*, respectively (Figure 2.8A-B). I found that activating A27j or A26e neurons did not significantly increase incidence of rolling (Figure 2.8C). Together, these data are consistent with a role for DnB neurons in driving rolling behavior.

DnB neurons promote both bending and rolling modules of nociceptive escape

Our results support a role for DnB neurons in triggering rolling behavior. To refine our manipulations, and exclude the possibility that brain neurons labeled by *412-Gal4* were contributing to rolling, I genetically separated *412-Gal4* brain expression from VNC expression by combining the VNC-specific Gal4 inhibitor *tsh-Gal80* with *412-Gal4* (Figure 2.9B). Rolling was not observed when *412-Gal4* expression was restricted to brain neurons (0% responding, n= 25; Figure 2.9D). Conversely, to determine whether activity in VNC interneurons can trigger nociceptive rolling, I used an intersectional strategy to drive *Gal4* expression at the intersection of *tsh-LexA* and *412-Gal4* (*412-Gal4*

VNC) (Figure 2.9A,C). Compared to control animals that did not roll (0% responding, n=21), activating *412-Gal4* neurons in the VNC, where DnBs reside, probabilistically increased rolling (59% rolling, n=30; Figure 2.9D). I have shown that *412-Gal4* VNC, and *4051-Gal4* neurons are sufficient to trigger rolling. Thus, supporting a role for DnB neurons in generating nocifensive escape behavior.

The behaviors induced by *412-Gal4* VNC neuron activation were similar to the C-shaped body bending and rolling generated by noxious stimuli (Hwang et al., 2007; Ohyama et al., 2013). Since class IV (cIV) da neurons function as primary nociceptors (Hwang et al., 2007), I performed behavioral analyses to determine which subset of the nocifensive escape sequence was being activated by DnB circuits. The escape response consists of 1) C-shape body bending, 2) 360˚ lateral turns (rolling), followed by 3) increased forward locomotion (escape crawl). I initially compared the behavioral consequences of activating primary nociceptors, cIV neurons, versus downstream DnBs neurons labeled with VNC restricted *412-Gal4* (Figure 2.9C). To quantify the motor behaviors that occur during nocifensive escape, I monitored bending behavior that occurs prior to rolling (bend only, B), and bending behavior that occurs during rolling (bending + lateral locomotion, or rolling; R). I also recorded hybrid behaviors, such as bend-crawl (BC) in which crawling larvae were persistently bent (Figure 2.9F). I found that cIV or *412-Gal4* VNC activation led to similar overall time spent in a bent body orientation (B, R, BC) and increases relative to control animals (Figure 2.9G). cIV neuron activation more often led to rolling behavior, whereas *412-Gal4* VNC activation was more likely to induce sustained B or BC behavior (Figure 2.9H-I). For example, activation of *412-Gal4* VNC neurons caused larvae to spend more time performing BC behavior compared to activation of cIV neurons (32% total time; bout mean=7.8s vs. 16% total time; bout mean= 2.7s, respectively; Figure 2.9J). Thus, *412-Gal4* VNC activation can induce body bending both with and without nociceptive rolling, suggesting a degree of

modularity. These data are consistent with a role for *412-Gal4* VNC neurons, including DnBs, in promoting both the body-bending and rolling components of nociceptive behavior.

One possibility is that class IV and Down-and-Back neurons can recruit different motor patterns based on levels of neural activation. To further examine the motor programs induced by cIV and DnB activation, I designed a behavioral paradigm that would allow for improved temporal control of activation at different intensities, along with high-resolution behavior recordings. I chose the light intensity for the "Highest" group based on previously reported measurements for ReaChR activation (Clowney et al., 2015), and scaled down progressively for "Moderate," "Low," and "Lowest" activation (see methods). Again, we monitored bending only (B), rolling (R), and added crawling (C), and pausing (P), which were often observed either before, or immediately following activation. Bend-Crawl (BC) was not observed in this experimental paradigm during activation of either population of neurons, so we did not quantify these responses. I optogenetically activated DnB and cIV neurons at each light intensities for 10 seconds by expressing *UAS-ReaChR*, using *412-Gal4*, and *PPK$^{1.9}$-Gal4*, respectively. Behavioral ethograms show that when cIV neurons are activated, from Low to Highest intensities, animals will only perform rolling within the 1st second of activation (Figure 2.10A). Conversely, *412-Gal4* activation of DnBs, triggered only bending at Low levels of activation, bending followed by rolling (within 10s) at Moderate levels of activation, and mostly rolling (within 5-10s) at the Highest intensity (Figure 2.10B). At the Lowest level of intensity, DnB activation mostly led to crawling, and cIV neurons induced few rolling events and some bending, which did not persist for more than 1s, or result in rolling. These data suggest that cIV activation triggers rolling probabilistically, as an all-or-none response, and DnB activation elicits mostly bending, which depending of levels of activation may or may not lead to rolling events. Since the 1st second of activation

elicited rolling in cIV-activated animals, but only bending in some DnB activation conditions (Figure 2.10C-D), we measured the degree of bending to determine whether there was a relationship between degree of bending, and likelihood to perform rolling. Indeed, we found that the cIV group generally had more values at smaller angles than the *412-Gal4* group within 1s of activation, suggesting that amount of bending might be coupled with probability to execute rolling (Figure 2.10E). Notably, low activation of *412-Gal4* did not result in other somatosensory behaviors, such as gentle-touch responses (i.e. recoil, backward crawling, head turns) (Kernan et al., 1994). These data suggest that whether DnB neurons trigger bending vs rolling modules is intensity dependent, as low levels of activation induce mostly bending, and higher levels of activation trigger mostly rolling (with some delay). Moreover, the bending analysis suggests that rolling appears to coincide with smaller bend angles (i.e. deeper C-shape bends).

DnB interneurons are required for nociceptive rolling and robust body bending

Next, I tested whether Down-and-back neurons were required for robust bending and rolling in response to noxious stimuli. I took an intersectional approach to further refine my manipulations by first performing an *in silico* screen of approximately 7000 enhancer-based Gal4 expression patterns in the Rubin collection (Jenett et al., 2012; Li et al., 2014). I identified several lines with broad expression in the VNC and performed a secondary screen on corresponding LexA versions by crossing them to *412-Gal4, 8X-lexAop2FLPL,* and *10XUAS>stop>myr:GFP* (Shirangi et al., 2013). This approach led to labeling at the intersection of the LexA and Gal4 lines. We identified one line, *R70F01-LexA,* that supported intersectional expression in abdominal DnB neurons, weakly in a small number of other VNC neurons, including A27j, and only rarely in one brain neuron (Figure 2.11 A-B'). I used the *R70F01-LexA∩412-Gal4* (*R70F01∩412*) strategy to drive

expression of Kir$^{2.1}$-GFP (Shirangi et al., 2013), a hyperpolarizing channel (Baines et al., 2001) (Figure 2.11C). Unlike myr:GFP expression where I saw a small percentage of CNS with labeling in the brain lobes (Figure 2.11B'), I did not observe this with intersectional Kir$^{2.1}$-GFP strategy. As has been described (Shirangi et al., 2013), I observed all-or-none expression of Kir$^{2.1}$-GFP so larvae were visualized after experiments to assess *Kir$^{2.1}$-GFP* expression (32%, n=125). Animals were classified as 'non-silenced' (i.e. lacking Kir$^{2.1}$-GFP expression) controls or '*R70F01∩412*-silenced' (i.e. with Kir$^{2.1}$-GFP expression in VNC).

Upon exposure to a noxious surface (40˚C), control animals showed a typical nociceptive sequence of (1) C-shaped body bending and rolling, (2) 'transition,' brief forward crawling with lateral bending and occasional rolling, and (3) 'escape crawl,' rapid forward crawling (Figure 2.12A). Notably, this transition phase consisted of the animal snapping in and out of the lateral bends, which was different that the aforementioned 'bend-crawl' where animals crawled slowly while maintaining a bent posture. During escape crawling, I observed no C-shaped body bending or rolling. Silencing *R70F01∩412* neurons did not abolish rolling, but significantly reduced the absolute number of rolls per trial (rolling median= 0, *R70F01∩412* silencing; median=3, control groups; Figure 2.12B), without affecting the order of the rolling bout in the nociceptive sequence, or the latency to initiate first roll (Figure 2.13C). When I examined the time required to complete an individual roll, I found that *R70F01∩412*-silenced animals took more time to complete a roll (mean=1.54s ±0.976 SD, n=15) compared to control animals (mean=0.84s ±0.652 SD, n=20), indicating that *R70F01∩412* neurons are important for rapid rolling behavior (Figure 2.12D). I also noted that *R70F01∩412* silenced animals appeared to crawl more slowly (data not shown), perhaps signaling a deficit in escape crawl. To determine whether silencing A27j neurons contributed to the

reduced rolling observed upon *R70F01∩412* silencing, I expressed $Kir^{2.1}$ in A27j neurons using *R38H01-Gal4* and found that silencing A27j neurons did not significantly reduce rolling (Figure 2.12E). Together, these data show that reducing activity in DnB neurons both reduces the probability of rolling, and also the rolling speed and efficiency.

Since the DnB activation data suggested that DnBs promote bending and rolling modules of nocifensive escape, I analyzed the amount of time spent bending vs. rolling in *R70F01∩412* animals (Figure 2.12F). I found an increase in the percent of time spent exhibiting bend-crawl behavior, and a significant decrease in time spent rolling. I also found that *R70F01∩412* animals were more likely to engage in bending without rolling compared to control animals (49% vs. 14%) (Figure 2.12G). To exclude non-specific motor defects caused by DnB suppression, I examined crawling behavior while silencing DnB neurons with *412-Gal4* driven TNT (Sweeney et al., 1995). I found that aside from a modest increase in crawling speed, crawling remained intact, suggesting that DnB neurons play a specific role in escape motor circuitry (Figure 2.12H).

My previous results suggested that rolling might be coincident with a high degree of curvature, so next, I considered whether acquisition of the C-shape bending is affected using the *R70F01∩412* silencing strategy. To quantify curvature along the larval body during nocifensive escape, we adapted a technique used to analyze curvature during slime mold migration (Driscoll et al., 2011; Driscoll et al., 2012). Briefly, 300 boundary points were distributed along an outline of the larval body (Figure 2.13A). A curvature index (C.I.) was assigned to each boundary point (see methods), and color-coded to represent higher C.I. values (yellow-red) and lower C.I. values (blue-green). We plotted the curvature indices at each boundary point over the span of a single roll (360˚ rotation), or attempted roll (<360° rotations) as kymographs (i.e. body curvature changes over time). We found that larvae with silenced DnB neurons, using

R70F01∩412, displayed lower curvature indices during either rolling, or attempted rolling events compared to non-silenced animals (Figure 2.13B-C). We plotted the curvature indices (C.I.) for each group as a cumulative distribution plot, and observed a shift to the left, towards lower C.I. values, in the *R70F01∩412*-silenced animals compared to the control (Figure 2.13D). To quantify the difference in C.I. distribution between groups, we defined C.I. values above the median of the control group as "High" and below the median as "Low." To normalize for differences in behavior bout length, and number of C.I. values, we calculated the percent of boundary points per animal that fell into the Low or High category. We found that compared to non-silenced animals, *R70F01∩412*-silenced animals had a significant increase in percent of boundary points in the low curvature range, and decrease in the high curvature range (Figure 2.13E-F). In summary, these data suggest that DnB interneurons function downstream class IV nociceptive sensory neurons promoting both bending and rolling to generate rapid efficient nocifensive escape.

Discussion

Nocifensive behavior in *Drosophila* larvae consists of sequential C-shaped body bending and rolling, followed by rapid forward crawling (Ohyama et al., 2013). Here, I use comprehensive behavioral analyses to characterize the role of nociceptive interneurons, Down-and-Backs (DnB), in generating nocifensive escape behavior. I provide functional and anatomical evidence that DnB neurons are downstream of class IV (cIV) sensory neurons. Our activation and silencing experiments suggests that there is modularity in the escape response, and that DnBs are primarily responsible for promoting high curvature body bending behavior facilitating nocifensive escape rolling. These data highlight a novel behavioral and circuit component of the nociceptive circuit, and

elucidate neural mechanisms underlying the transduction of noxious stimuli into coordinated escape responses.

Nocifensive escape behavior consists of modular components

Whereas body bending and rolling normally co-occur during naturalistic nocifensive responses, activation experiments suggest that circuits that underlie these behaviors are partially separable. Thus, DnB activity can promote rolling, but also C-shape bending independent of rolling. Our dose response activation data suggests that cIV activation triggers probabilistically in an all-or-none fashion, in short bouts, whereas DnB neurons and their downstream components trigger C-shape bending that transitions into *persistent* rolling. One possibility is that there is a degree of inhibition that terminates cIV-triggered rolling that is absent when exclusively activating the DnB microcircuit. The Down-and-Back downstream circuitry will be further explored in Chapter III. It is notable that body bending is a component of reorienting 180˚ from an inverted body position (self-righting), and head turning occurs in response to multiple other environmental cues, including food deprivation and gentle-touch (Kernan et al., 1994; Yang et al., 2000), raising the possibility that DnB mediated bending could be exploited by other sensory evoked behaviors.

It is not yet clear how bending might promote rolling. One possibility is that facilitation occurs at a circuit level such that feedback from shape changes impact neurons that promote rolling motor patterns. Alternatively, but not exclusively, bending might mechanically bias the orientation of the larva and simply allow it to “lean into” a roll, increasing the likelihood of rolling given the participation of appropriate additional motor programs. Our data provides some evidence for the latter hypothesis since we found that cIV animals engaging in rolling displayed more bending (i.e. smaller bend angles), compared to DnB animals that were bending, but not rolling. These results

suggest that perhaps rolling events are associated with highly curved bends. This was consistent with the silencing results where animals that rolled slowly or exhibited bending without rolling had significantly less curvature. Therefore, it seems that a certain degree of body bending is required for larvae to successfully engage in nocifensive rolling. The bend→ roll sequential behavior pattern may be similar to other invertebrate escape behaviors, such as fly escape from a looming object, which consists of sequential preparatory motor modules that cumulatively contribute to an escape behavior (i.e. fly takeoff) (Card, 2012). The obligatory overlap of bending and rolling behaviors appears to contrast with hierarchical sequences in which "higher" components of a behavioral hierarchy suppress "lower" components (Seeds et al., 2014). The neural circuitry that controls sequential bending and rolling is the focus of Chapter III.

Potential significance for C-shape bending during nocifensive escape

Prior data showed that rolling is directional and is advantageous for dislodging attacking parasitoid wasps (Hwang et al., 2007). Efficient rolling occurs coincident with deep C-shaped body bends, but the significance of these body bends for escape behavior had not been determined. In the goldfish startle response, animals perform C-bends away from the auditory stimulus as an initial withdrawal and then swim away, suggesting that C-bending might be a shared strategy for initial defensive responses. Notably, there is modularity in the C-bend, such that it is also triggered during feeding and prey capture (Korn and Faber, 2005). DnB neural circuitry appears to be critically important for evoking body bend behavior prior to and during nocifensive rolling. Bending may provide the initial, most rapid, form of withdrawal from a noxious stimulus, and may subsequently support rolling locomotion by orienting and focusing the energy of muscle contraction into lateral thrusts. Re-orientation of denticle belts, triangle-shaped extensions of the

cuticle that provide substrate traction during crawling, may also aid rapid lateral locomotion. There are genes that have been characterized in denticle belt development (Alexandre et al., 1999), and assessing nociceptive behavior in animals lacking denticles would be a way to test this hypothesis.

Divergent circuits mediate nocifensive escape behavior

Notably, loss of activity in DnBs labeled by our intersectional strategy compromised rolling, but did not inhibit it altogether. Moreover, our data show that DnB silencing does not affect the order of the rolling bout in the nocifensive sequence, but reduces the number of rolls per bout, and the speed of each roll, further suggesting that components of the nocifensive response are still intact upon reduction of activity from most DnB neurons. It might be that residual DnB activity in our manipulations contributes to these partial responses, but also that divergent circuits mediate larval escape behavior. Indeed a recent study identified basin cells as second order targets of cIV neurons that integrate nociceptive and vibration-sensing neurons to probabilistically promote rolling through command-like neurons, Goro (Ohyama et al., 2015). This raises the possibility that bending, and rolling motor programs might be controlled by DnB and Goro neurons, respectively. It is possible that different aspects of rolling behavior, such as timing, preparation, and execution might be initially distributed to different circuit components. Moreover, there seems to be a divergence between thermal and mechanical nociception, where interneurons that have been recently implicated in mechanonociception appear to be dispensable for transduction of noxious heat (Hu et al., 2017). Further analyses will reveal whether these parallel circuits converge further downstream onto command-neurons, or premotor circuits.

Based on our calcium imaging experiments, I expect that DnB neurons can relay input topographically from the periphery to the CNS, which may help to establish the directionality of bending and subsequent rolling. Although our experiments here have necessarily relied on broad activation of DnBs, future experiments might be directed at more localized manipulations to test this scenario.

Methods

Fly stocks

(1) *PB[IT.Gal4]0412* (referred to in the text as *412-Gal4*; (Gohl et al., 2011)), (2) *UAS-mCD8-GFP* (Lee and Luo, 1999), (3) *ppk-CD4-tdTom* (Han et al., 2011), (4) *hsFLP;Sp/CyO;UAS>CD2>CD8-GFP* (Basler and Struhl, 1994; Wong et al., 2002), (5) *UAS-BRP.short*^{mCherry} (Schmid et al., 2008) was provided by Dr. Richard Mann (Columbia University), (6) *UAS-DenMark* (Nicolai et al., 2010), (7) *dTrpA1-QF* (Bloomington Stock Center), (8) *QUAS-syb-spGFP*$^{1-10}$ (Macpherson et al., 2015), (9) *UAS-CD4-spGFP*^{11}(Feinberg et al., 2008; Gordon and Scott, 2009), (10) *20X-UAS-IVS-GCaMP6m* (Chen et al., 2013), (11) *UAS-dTrpA1* (Hamada et al., 2008), (12) *UAS-ReaChR* (Lin et al., 2013). (13) *tub>Gal80>; tsh-LexA, 8X-LexAop2-FLPL/CyO-RFP-tb; UAS-10X-IVS-myr:GFP,* and (14) *tub>Gal80>; tsh-LexA, 8X-LexAop2-FLPL/CyO-RFP-tb; UAS-dTrpA1/TM6b* were a gift from Dr. Marta Zlatic (Janelia Research Campus, Virginia). (15) *UAS-TNT* BL28838 and (16) *UAS-TNTi* BL28840 (Sweeney et al., 1995), (17) *tsh-Gal80* was a gift from Julie Simpson (Janelia Research Campus, Virginia), (18) *R70F01-LexA* (Jenett et al., 2012), (20) *8X-LexAop2FLPL;10X-UAS>Stop>myr:GFP*, and (19) *8X-LexAop2FLPL;10X-UAS >Stop >Kir*$^{2.1}$*-GFP* (Shirangi et al., 2013)were a gift from Dr. James Truman (Janelia Research Campus, Virginia). (20) *13X-LexAop2-IVS-TNT::HA*(Karuppudurai et al., 2014), (21) *R38A10-LexA* (Jenett et al., 2012), (24) *ppk*$^{1.9}$*-Gal4* (Ainsley et al., 2003), (22) *w-; Sp/CyO; 13X-LexAop2-IVS-myr:GFP/ TM3,Sb,e* (23)

cha$^{3.3kb}$*-Gal80* (Kitamoto, 2002) was a gift from Dr. Toshihiro Kitamoto (University of Iowa, Iowa), (24) *PB[IT.Gal4]4051* (Gohl et al., 2011), (25) *[IS.QF]0412*, (26) *20X-UAS-spGFP*$^{1-10}$ and (27) *13X-LexAop-spGFP*^{11} (this study) , (28) *yw; Mi{PT-GFSTF.0}ChAT*$^{MI04508\text{-}GFSTF.0}$ (Nagarkar-Jaiswal et al., 2015), (29) *GAD-Gal80* (Sakai et al., 2009) , (30) *[IS.LexA]0585*, (31) *20XUAS-IVS-mCD8GFP* (32) *TRH-Gal4* (Alekseyenko et al., 2010) , (33) *R38H01-Gal4* (Jenett et al., 2012), (34)*UAS-Kir*$^{2.1}$*-eGFP* (Baines et al., 2001)

Generation of transgenes

pQUAST-attB was generated by replacing the *5XUAS* sequence from pUAST-attB (gift from R Voutev, Columbia University) with an Eco1CR1-EcoR1 fragment from *5XQUAS* (Addgene-24349; (Potter et al., 2010). *QUAS-syb:spGFP*$^{1-10}$ was created by extracting *syb:spGFP*$^{1-10}$ from *UAS-syb:spGFP*$^{1-10}$ (gift from LJ Macpherson, Columbia University) using EcoR1 and Xba1 and ligating into pQUAST-attB. Transgenic lines were generated by integration into attp2. Injections were performed by Best Gene Ltd.

To generate *20X-UAS-SpGFP*$^{1-10}$ and *13X-LexAop-SpGFP*^{11}, *SpGFP*$^{1-10}$, *SpGFP*^{11} (Gifts from K Scott, Berkley), *pJFRC7-20XUAS-IVS-mCD8::GFP* (Addgene 26220) and pJFRC19-13XLexAop2-IVS-myr::GFP (Addgene 26224) were treated with XhoI and XbaI to excise *myr::GFP* and *mCD8::GFP* sequence and re-ligate with appropriate pair (i.e. *20XUAS* with *SpGFP*$^{1-10}$ and *13XLexAop* with *SpGFP*^{11}). Transgenic lines were generated by injection into *M{3xP3-RFP.attP'}ZH-51C* embryos for *13XLexAop-SpGFP*^{11} and *M{3xP3-RFP.attP}ZH-86Fb* embryos for *20X-UAS-SpGFP*$^{1-10}$. Injections were performed by Best Gene Ltd.

Immunohistochemistry

Immunohistochemistry was performed essentially as described (Matthews et al., 2007). Third instar larvae were dissected in 1X PBS, fixed in 4% paraformaldehyde (Electron Microscopy Sciences) in 1X PBS for 15 minutes, rinsed three times in 1X PBS + 0.3% Triton X-100 (PBS-TX), and blocked for 1 hour at 4°C in normal donkey serum (Jackson Immunoresearch). Primary antibodies used were chicken anti-GFP (1:1000; Abcam), mouse anti-GFP (1:100; Sigma), rabbit anti-DsRed (1:250, Clontech), mouse anti-1D4 anti-Fasciclin II (1:10; Developmental Studies Hybridoma Bank), rabbit anti-5HT (1:1000; Sigma), dvGLUT (1:10,000) (Daniels et al., 2004), rabbit anti-GABA (1:100; Sigma). Animals were incubated overnight in primary antibodies at 4°C, rinsed repeatedly in PBS-TX, and incubated overnight at 4°C in species-specific, fluorophore-conjugated secondary antibodies (Jackson ImmunoResearch) at 1:200 in PBS-TX. Tissue was mounted on poly-L-lysine coated coverslips, dehydrated in ethanol series, cleared in xylenes, and mounted in DPX (Fluka).

For GRASP experiments (with the exception of Figure 2.5C), third instar larval brains were dissected in 1X PBS and fixed in fresh 4% paraformaldehyde (Electron Microscopy Sciences) for 15 minutes. Brains were mounted in Vectashield (Vector lab) on poly-L-lysine coated coverslips, and imaged for native reconstituted GFP signal.

Generation of clones

Single-cell FLP-out clones were generated by providing 1 hour heat shock at 38°C in late embryonic and early larval progeny from mating of stocks 1 and 4.

Behavioral analysis

For behavioral analysis, flies were reared at 25˚C and tested as wandering third instar larvae. For each experiment, at least three trials, taken on separate days, were performed for each genotype. Larvae were only tested once unless otherwise noted.

Thermogenetic activation

For *412-Gal4* dTrpA1 experiments, third instar larvae were rinsed briefly in double distilled water and placed on a 1% agarose gel heated to 31-34˚C by a hot plate (Dri-bath type 17600, Barnstead Thermolyne). All other dTrpA1 experiments were performed on 1% agarose gels with 0.6% black ink (Super Black India ink, Speedball) using a peltier device (CP-031, TE technology) and temperature controller (TC-36-25-RS232, TE technology) to heat the gel to 32.5-33.5˚C. Animals displaying 360˚ rotations were classified as 'rollers'. In *412-Gal4* VNC experiments, 'Rolling' was counted as coincident C-shape bending and 360˚ rotation, 'bend-crawl' was counted when animals persistently bent as they crawled and did not perform straight forward crawling, and 'bend-only' behavior, was counted when animals remained in a curved posture without rolling or crawling. Trachea were used as a reference for bending and rolling categorization. Animal behavior was recorded using a Leica M50 camera along with LeicaAcquire or Leica FireCam software with QuickTime screen capture for 60 seconds for *412-Gal4* activation, 29 seconds for *412-Gal4* VNC activation, and 30 seconds for all other activation experiments. Videos were quantified offline with experimenter blind to condition.

Optogenetic activation

For optogenetic experiments, I tested animals in a photostimulation arena (de Vries and Clandinin, 2013). Flies were raised on molasses food with or without 100mM all-*trans*-retinal (ATR). Third instar larvae were rinsed briefly in double distilled water and placed

on a 100 x 15mm petri dish containing double distilled water blended with yeast particles to facilitate nocifensive behavior (S. Mauthner, personal communication). Larvae were recorded using DALSA Falcon 4M30 4 megapixel digital camera and CamStudio screen capture software with 10 seconds blue light off-10 second blue light on (23500 Lux). A dim red light was on for the entirety of the experiment to illuminate larvae during lights off periods (300 Lux). Animals displaying 360˚ rolling were counted as responders. Videos were quantified offline.

Dose optogenetic experiments

For dose optogenetic experiments, I tested animals on the FIM table (Risse et al., 2013) FIM (Frustrated total internal reflection based Imaging Method) table, Basler ACE 4 megapixel near infrared sensitivity enhanced camera equipped with CMOSIS CMV4000 CMOS sensor. Camera lens: LM16HC-SW (Kowa); Filter: BN880-35.5 (Visionlighttech); IR diodes (875nm, Conrad); Image acquisition program: Pylon camera software (Basler). Animals were placed on 0.8% agar surface ~2mm thick (Molecular grade, Fisher Scientific) with a ring of Green (525nm) LED lights (WFLS-G30X3-WHT, SuperBright LEDs) around 5 inches in diameter placed underneath the FIM table, above the camera with a standard barrel connector and LED dimmer (CPS-F2ST; LDK-8A, SuperBrightLEDs). Flies were raised on molasses food with 100mM all-*trans*-retinal (ATR). Third instar larvae were rinsed briefly in double distilled water and tested mostly 3-5 animals at a time. Animals were recorded for at least 1 second before light stimulation, and then for at least 10 seconds following lights ON. Trials were recorded at different light intensities: Lowest (~45 Lux), Low (~200 Lux), Moderate (~850 Lux) and Highest (~1450 Lux). Videos were quantified offline with experimenter blind to the manipulation. Only 11 seconds of behavior were scored per trial (1s pre-stimulus, 10s lights ON). Behaviors quantified: Crawling, segmental waves visible; Pausing, no

movement straightened body; Bending, animal curved or on its side, and Rolling, 360˚ turns using bright trachea as a reference. Bending angles were quantified using the FIMTracker software (Risse et al., 2013)

Global Activation Assay

For the global activation assay, third instar *R70F01∩412* larvae were placed on a 1% agarose 0.6% black ink gel (Super Black India ink, Speedball) heated to 40˚C by a peltier device (CP-031, TE technology) and temperature controller (TC-36-25-RS232, TE technology). Behaviors were recorded for 30 seconds using Leica M50 camera along with Leica FireCam and QuickTime screen capture. After experiments, animals were placed on microscope slide with 70% glycerol and a coverslip, and assessed for GFP expression under a fluorescence microscope. Behavior was quantified offline with experimenter blinded to genotype. Duration of the first rolling event was quantified by using the trachea as a reference to determine the completion of a 360˚ roll (i.e. frame before trachea starts to disappear as beginning of roll and frame where trachea is re-centered as completion of rolling event).

Local Heat Assay

Local heat assay was performed as previously described (Tracey et al., 2003) with slight modifications. Soldering iron (SKU25337, Sinometer) was used as a noxious thermal probe and the temperature was set to 51.6-55.5˚C by adjusting voltage using a variac (3PN1010B, Staco Energy). Digital thermometer (51 II, Fluke) with thermocouple temperature sensor was used to measure the temperature of the thermal probe. Larvae were lightly touched with thermal probe at segments A4-6 for 5 seconds. Animals were characterized as ‘responder’ if they performed 360˚ roll within 5 seconds, and ‘non-responder’ if they did not. Animal behavior was recorded using Leica FireCam and

QuickTime screen capture. Videos were quantified offline with experimenter blind to genotype.

Crawling speed assay

To assess crawling speed, larvae were rinsed in double distilled water and placed on a 1% agarose gel and tested for crawling speed using the Multiworm tracker (Swierczek et al., 2011). Larvae were tested three at a time at 25˚C.

Calcium imaging

DnB neurons

Calcium imaging was performed in a partially dissected larval preparation. Wandering third instar larvae were immersed in ice-cold hemolymph-like saline 3.1 (HL3.1) (70 mM NaCl, 5mM KCl, 1.5 mM $CaCl_2$, 4 mM $MgCl_2$, 10 mM $NaHCO_3$, 5 mM Trehalose, 115 mM Sucrose, and 5 mM HEPES, pH 7.2) (Feng et al., 2014). The body wall of the larva was cut at segment A2 or A3 to expose the central nervous system, leaving the posterior larval body and ventral nerves intact. Dissected larvae were then transferred to an imaging chamber filled with HL3.1 equilibrated to room temperature (23-25 °C). The CNS was covered with a strip of parafilm and gently pressed down onto a coverslip for immobilization during imaging. DnB neurons in the ventral nerve cord were imaged using a Zeiss LSM5 Live confocal microscope with a 20x/0.8 Plan-Apochromat objective equipped with a piezo focus drive (Physik Intrumente). Three-dimensional time-lapse imaging was performed with X-Y dimensions of 256 x 256 pixels, a slice thickness of 7 µm, 8-11 Z slices (covering 49 to 63 µm), a scan speed of 31 µsec per pixel, and 8 bit depth. The acquisition rate of Z stack images with this setting was 4 to 5 Hz. During imaging, a thermal ramp was applied locally to hemisegments A5 to A7 of the dissected larvae using a custom-made thermal probe. The temperature of the thermal probe was

controlled by changing the voltage through a variac transformer (RSA-5E, Tokyo Rikosha). 15V was used to heat the probe and no voltage was applied during cooling. A t-type thermocouple probe wire (0.2mm dia., Sansho) was placed inside of the thermal probe to monitor the temperature of the probe. Temperature data measured by the thermocouple probe were acquired at 4 Hz through a USB-TC01 digitizer (National Instruments) and recorded using the NI Signal Express software (National Instruments). The acquired images and temperature data were analyzed using MATLAB (Mathworks). The average of the lowest 10% fluorescent intensity was used as baseline F (F_0) for each region of interest, and percent fluorescent change from the baseline ($\Delta F/F_0$) was calculated for each time point. Regions of interest (ROIs) were selected as circular areas with a diameter of 6 pixels that contain the cell bodies of the DnB neurons in the maximum intensity projections of the time-series images. Probe temperature for each image frame was estimated by a linear interpolation from the raw probe temperature trace, due to differences in sampling rate and timing across images and probe temperature.

Boundary curvature and kymograph analysis

Larval boundary curvature was determined as previously described (Driscoll et al., 2011; Driscoll et al., 2012) with modifications. Frames were extracted from 30 fps videos and thresholded. A size filter was applied to remove artifacts and debris. Artifacts closely associated with the animal (such as light specks or motion blurs) that would interfere with extraction of boundary curvature were manually removed blind to treatment by painting over the artifact with the background color (black). The boundary shape of the animal was parametrized with 300 boundary points. At each boundary point, we calculated the curvature by fitting a circle to that point and two points that are 10 boundary points away from it. Curvature Index (C.I.) was defined as the reciprocal of the

radius of that circle. If the midpoint of the two points 10 boundary points away is outside the larva, the C.I. was assigned to be positive; otherwise it was assigned to be negative. For visualization, a color scale was generated with warm colors corresponding to positive C.I. (i.e. concave curvature segment) and cool colors corresponding to negative C.I. (i.e. convex curvature segment). Kymographs were generated by plotting curvature index (colored by magnitude) of 300 boundary points across time. Alignment of the 300 points across time in kymographs was achieved by mapping points across frames to minimize the sum of the square distance of points between successive frames. To maintain the relative head and tail positions in the kymographs, I manually corrected for misalignment. Animals from *R70F01∩412*-silenced and non-silenced groups were selected for boundary curvature analysis if they fulfilled one of two criteria (1) completed rolling (360˚ turns), or (2) 'attempted rolling' (i.e. exhibited lateral body turns that were <360˚; trachea was used as a reference to assess lateral turning). Classification was performed blind to genotype. An identical number of animals were analyzed for each treatment, which for the non-silenced animals corresponded to the first 24 animals tested. Custom MATLAB scripts were used for curvature analyses and generation of kymographs.

Quantification of boundary curvature

Quantification was focused on boundary points with positive C.I. values, which reflects concave curvature (i.e. mainly inside C-shape bend). To further refine analyses, curvature indices (C.I.) taken at boundary points along the body were included, with the exception of the head and tail (defined to be within 25 points of the head & tail tip points) as their curvature reflected the animal's shape at the tips, and not the curvature of the animals' body. In order to perform statistical analyses, we had to reorganize the data such that each animal would have one value, as opposed to tens of thousand C.I. values

per trial. Therefore, we calculated percent of boundary points at low curvature (0<C.I.<0.027) and high curvature (C.I.>0.027) for each animal and compared between control and *R70F01∩412*-silenced animals. The C.I. cutoff for low curvature vs. high curvature was defined as the median of the C.I. in the control group. Multivariate analysis of variance (MANOVA) was performed with Bonferroni correction, for multiple testing, followed by post-hoc T-test to determine exact p-value.

Statistical Analysis

For categorical data analysis (i.e. responder vs. nonresponder), I utilized Fisher exact test or Chi square test (if expected value= >5) followed by Bonferroni correction if multiple testing was used. When comparing two groups of quantitative data (e.g. number of rolls), unpaired t-test was performed if data showed a normal distribution (determined using D'Agostino & Pearson omnibus normality test) and Mann-Whitney test if data distribution was non-normal. When comparing three or more groups, data were analyzed using One-way ANOVA or Kruskal-Wallis test with Dunn's correction for multiple testing, followed by post-hoc T-test to determine exact p-value.

Acknowledgments

I am grateful to Drs. Richard Axel, Tom Clandinin, Barry Dickson, Toshiro Kitamoto, Chi-Hon Lee, Troy Shirangi, Julie Simpson, Richard Mann, James Truman, and Charles Zuker for fly stocks. I thank Dr. Lindsey Macpherson for sharing reagents prior to publication. I thank Dr. Roumen Voutev for reagents. I thank Thomas Khan for writing a custom shell script for blinding video files. I am grateful to the Grueber and Clandinin labs for contributing to screening and annotating of the InSITE Gal4 lines. I thank Drs. Peter Soba and Rebecca Yang for communication of unpublished results. The 1D4 anti-

Fasciclin II developed by Dr. Corey Goodman and was obtained from the Developmental Studies Hybridoma Bank, created by the NICHD of the NIH and maintained at The University of Iowa, Department of Biology, Iowa City, IA 52242. This work was supported by a National Science Foundation Graduate Research Fellowship (AB), National Institutes of Health (NIH) Predoctoral Fellowship 1F31NS090909-01 (AB), Columbia University, NIH R01 NS061908 (WBG), NIH R24 NS086564 (T. Clandinin and W.B.G), and NIH R01 GM086458 (WDT)

Figure 2.1: *412-Gal4* labels putative nociceptive interneurons, Down-and-Backs (DnBs)

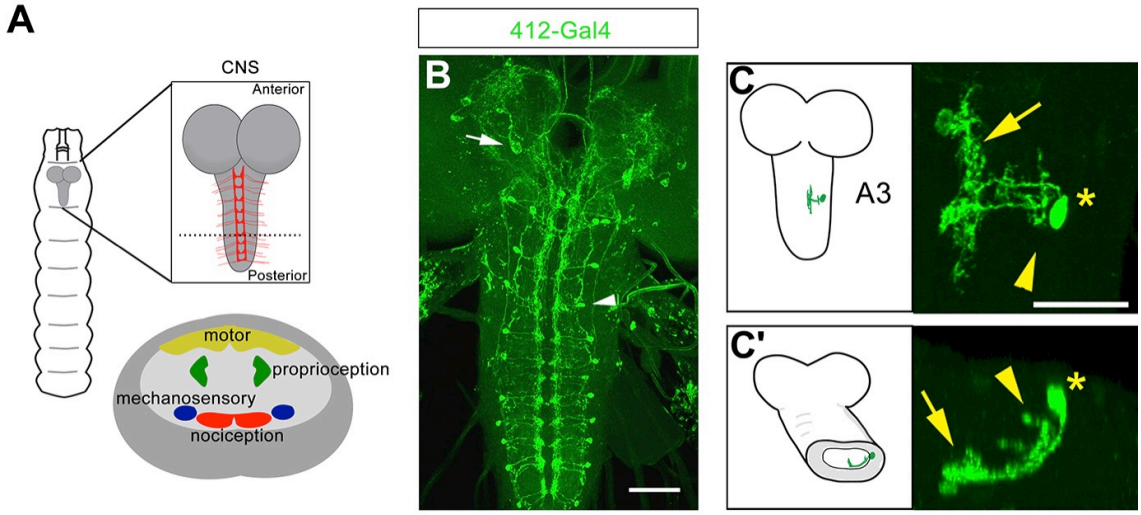

Figure 2.1: *412-Gal4* labels putative nociceptive interneurons, Down-and-Backs (DnBs)

(A) Schematic showing the *Drosophila* larval CNS. Red scaffold represents class IV (cIV) projections. Enlarged transverse section through ventral nerve cord (VNC) is shown below. Color-coded regions depict modality specific locations where sensory axons terminate and the motor neuropil.

(B) *412-Gal4* drives expression in interneurons in the VNC (arrowhead) and neurons in the brain lobes (arrow), anti-dsRed, green.

(C-C') Dorsal view of the morphology of DnB neuron in segment A3. Medial process is indicated by an arrow and lateral projection by an arrowhead. An asterisk marks the cell body. (C') Transverse section of neuron in C.

Scale bars = 50 μm (B), 20μm (C); Genotypes: (B) *412-Gal4,UAS-CD4:tdTomato* (C-C') *hsFLP;Sp or CyO/+;412-Gal4/ UAS>CD2>CD8-GFP*

Figure 2.2: Further characterization of *412-Gal4* expression pattern

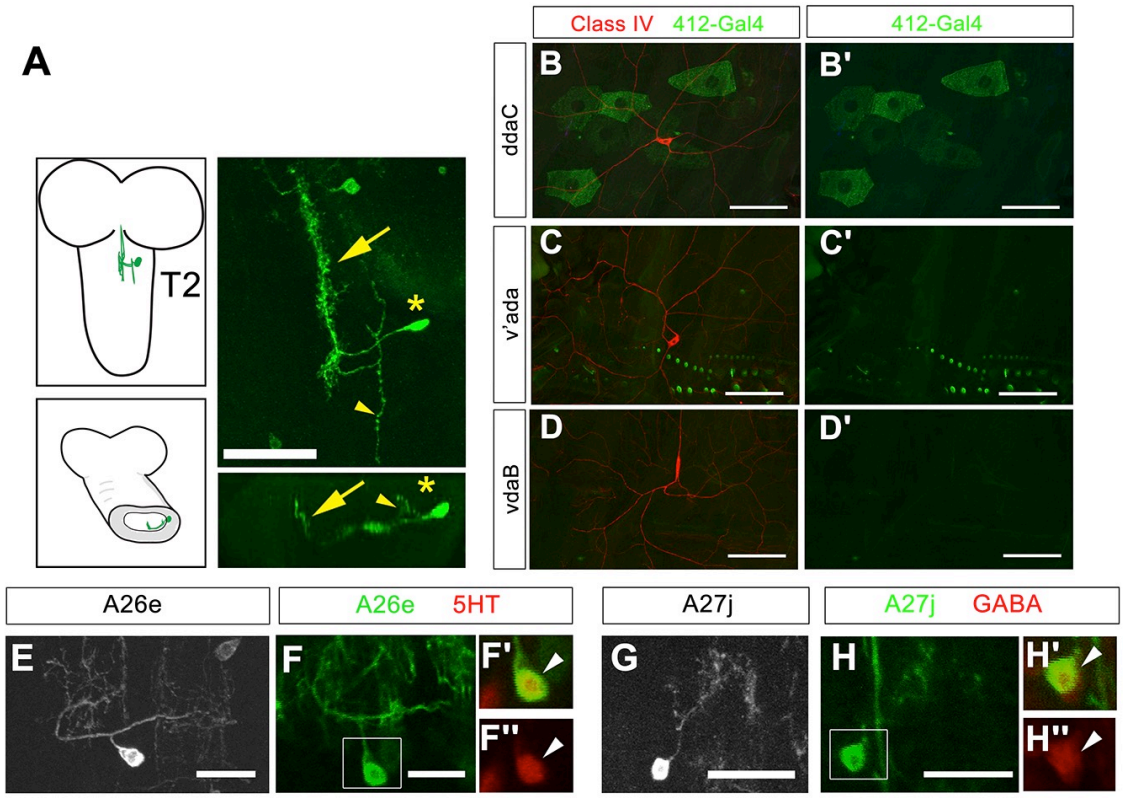

Figure 2.2: Further characterization of *412-Gal4* expression pattern

(A) Single-cell morphology of DnB neuron in segment T2 (top panels). Thoracic segment DnB neurons possess a longer medial process as indicated by an arrow and longer lateral projection indicated by an arrowhead. An asterisk marks the cell body. Top panels: anterior posterior view; Bottom panels: transverse section, dorsoventral view

(B-D') *412-Gal4, UAS-mCD8:GFP* does not label cIV cell bodies or dendrites labeled by *ppk-CD4-tdTomato* (anti-GFP, green; anti-dsRed, red).

(E) Single cell morphology of A26e neuron in *412-Gal4* expression pattern (anti-GFP)

(F) A26e neuron labeled by *412-Gal4* (anti-GFP, green)

(F') Boxed region from (F) centering on A26e soma (arrowhead): Overlap between A26e and serotonin antibody (anti-GFP, green; anti-5HT, red); (F'') 5HT; dsRed channel only

(G) Single cell morphology of A27j neuron in *412-Gal4* expression pattern (anti-GFP)

(H) A27j neuron labeled by *412-Gal4* (anti-GFP, green)

(H') Boxed region from (H) centering on A27j soma (arrowhead): Overlap between A27j cell body and GABA staining, (anti-GFP, green; anti-GABA, red); (H'') GABA; dsRed channel only

Scale bars= 25 μM (A), 50μM (B-D'), 20μM (E,G), 10μM (F,H)

Genotypes: (A,E,G) *hsFLP;Sp or CyO/+;412-Gal4/ UAS>CD2>CD8-GFP* (B-D') *ppk:CD4tdTomato/+; 412-Gal4, UAS-mCD8:GFP* /+ (F-F'', H-H'') *412-Gal4,UAS-CD8GFP/+*

Figure 2.3: DnB neurons are cholinergic interneurons

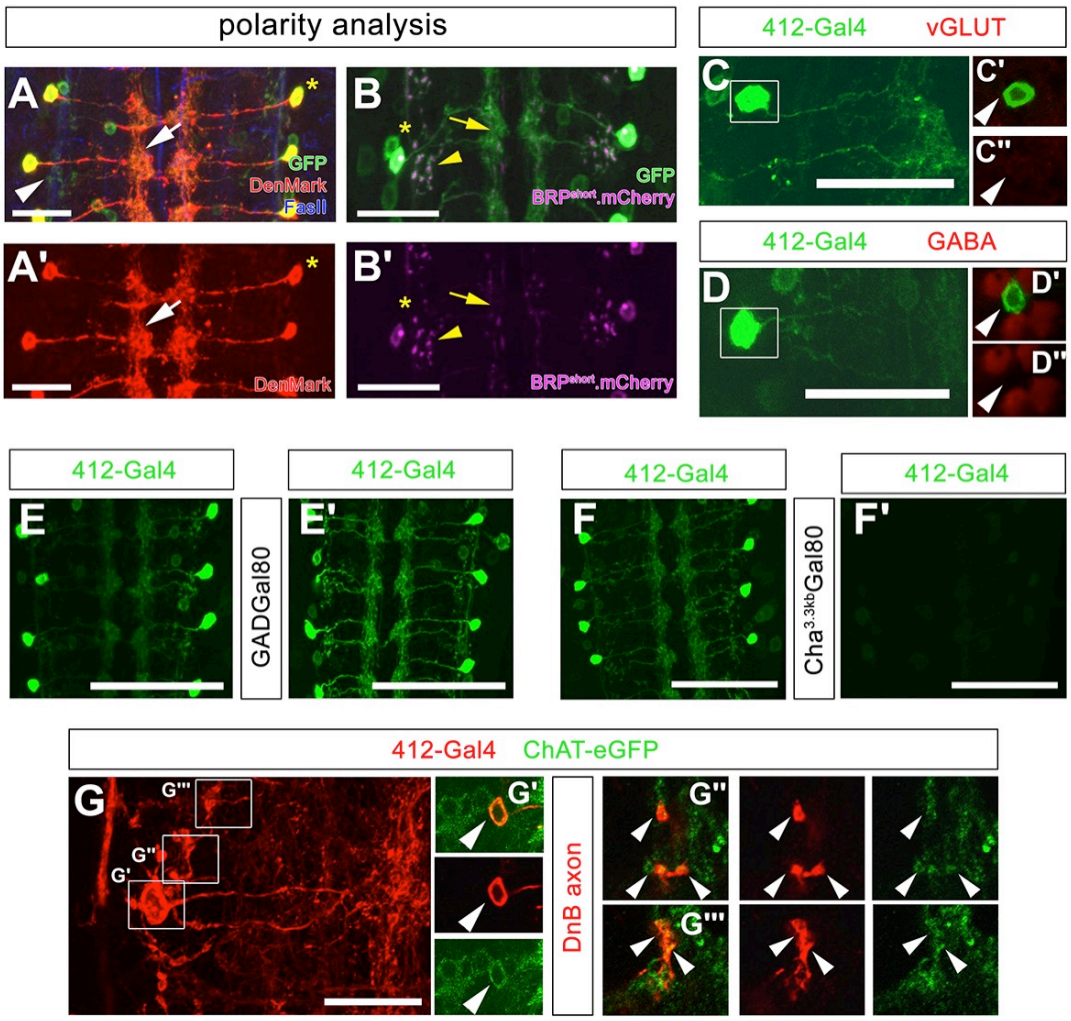

Figure 2.3: DnB neurons are cholinergic interneurons

(A-A') *412-Gal4* driven dendritic marker, DenMark (anti-dsRed, red) localizes to medial-directed projection, and medial arbors (arrow). *UAS-mCD8:GFP* (anti-GFP, green) is abundant throughout all projections. FasII labels axon fascicles. Asterisk marks the cell body. (A') DenMark channel alone.

(B-B') *412-Gal4*-driven BRP.shortmCherry labels putative presynaptic sites sparsely in the medial domain (arrow) and strongly in the lateral domain (arrowhead; anti-dsRed, magenta). *UAS-mCD8:GFP* (anti-GFP, green) labels all processes. Asterisk labels the cell body. (B') BRP.shortmCherry channel alone.

(C) DnB neuron (anti-GFP, green); (C') Boxed region: DnB cell body (arrowhead) shows no overlap with VGLUT (anti-VGLUT; dsRed); (C'') VGLUT; dsRed channel only

(D) DnB neuron (anti-GFP, green); (D') Boxed region: DnB cell body (arrowhead) shows no overlap with GABA (anti-VGLUT; dsRed), (D'') GABA; dsRed channel only

(E) mCD8:GFP driven by *412-Gal4*, labeled with anti-GFP (green) (E') *GAD-Gal80* does not reduce expression of mCD8:GFP (anti-GFP, green) in VNC *412-Gal4* neurons.

(F) mCD8:GFP driven by *412-Gal4*, labeled with anti-GFP (green) (F') *Cha3.3kb-Gal80* reduces expression of mCD8:GFP (anti-GFP, green) in VNC *412- Gal4* neurons.

(G) tdTomato driven by *412-Gal4* labeling DnB neuron (anti-dsRed, red) (G') DnB cell body overlapping with ChAT-eGFP (anti-GFP, green) (top: overlap, middle: tdTomato, red channel only, bottom: ChAT-eGFP cell body) (G''-G''') DnB axons; left panels DnB axon and ChAT-eGFP puncta overlap; middle: DnB axons, tdTomato channel; right panels: ChAT-eGFP puncta, GFP channel only

Scale bars= 20 μm (A-D, G) 50μm (E-F');

Genotypes: A-A') *UAS-DenMark/+; 412-Gal4, UAS-mCD8:GFP/+* (B –B') *UAS-BRP.shortmCherry/+;412-Gal4, UAS-mCD8:GFP/+* (C-D) *412-Gal4, UAS-mCD8:GFP/+* (E) *412-Gal4, UAS-mCD8:GFP/+* (E') *412-Gal4, UAS-mCD8:GFP/GAD-Gal80* (F) *412-Gal4, UAS-mCD8:GFP/+* (F') *412-Gal4, UAS-mCD8:GFP/Cha$^{3.3kb}$-Gal80* (G-G''') *412-Gal4, UAS-mCD8:GFP/Chat-EGFP-Flash-Tev3xFlag*

Figure 2.4: Anatomical evidence for DnB and nociceptive cIV connectivity

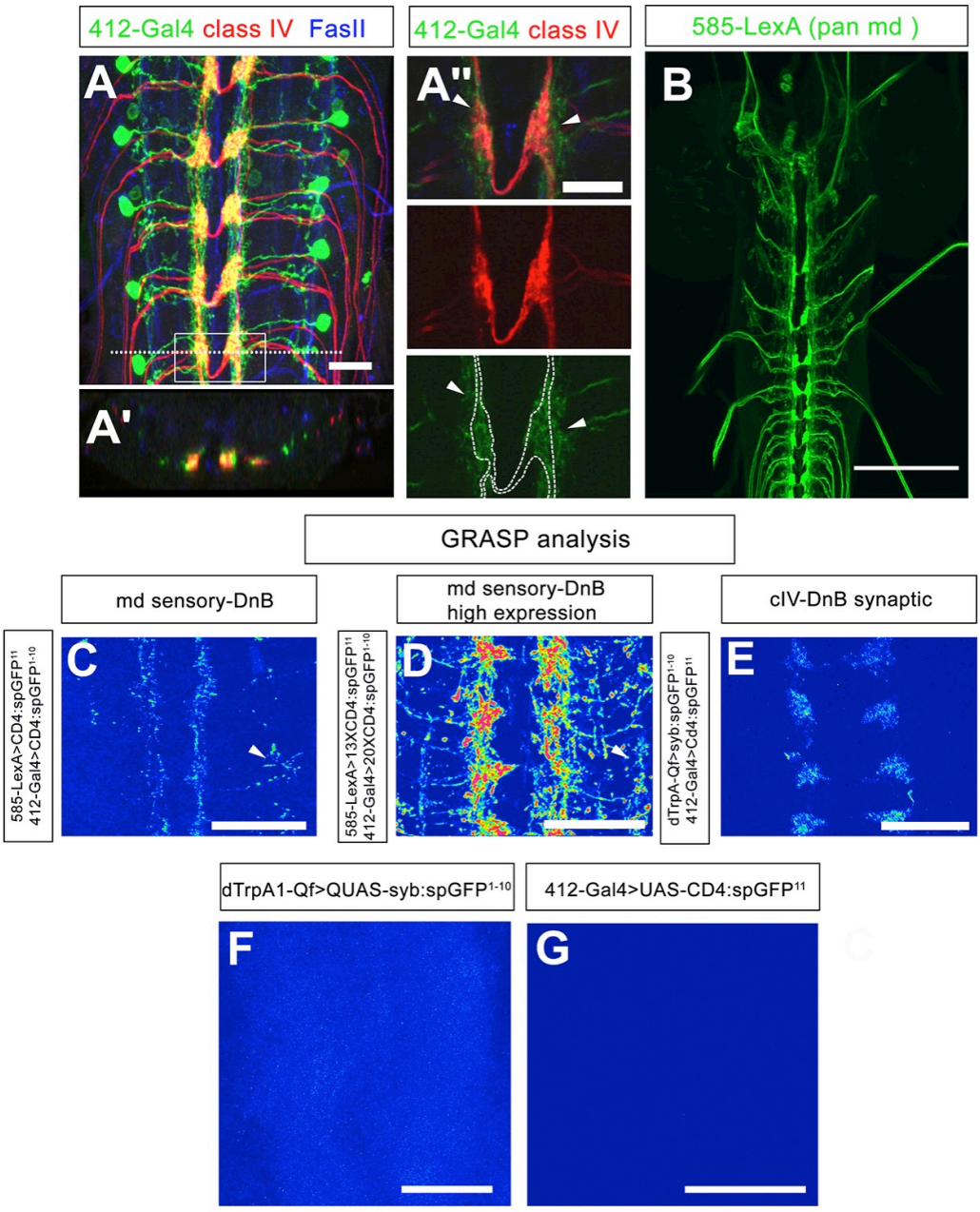

Figure 2.4: Anatomical evidence for DnB and nociceptive cIV connectivity

(A-A'') Overlap of cIV axons labeled by *ppk:CD4tdTom* (anti-dsRed, red), and *412-Gal4, UAS-mCD8:GFP* (anti-GFP, green) neurons. (A) dorsal view, dotted line indicates transverse section represented in A'. Anti-FasII (blue) labels axon fascicles. Boxed

region is enlarged in (A''). A'' shows overlap of processes in single confocal section. Location of nociceptive terminals is outlined in the lower panel to show overlap with DnB dendrites.

(B) *13xlexAop2-IVS-myr::GFP* driven by *585-LexA* labeling multidendritic (md) neurons

(C) Reconstitution of GFP (mouse anti-GFP) when CD4:GFP^{11} was driven in md neurons using *585-LexA* and CD4:spGFP$^{1-10}$ driven by *412-Gal4*. Image shows reconstituted GFP in pseudocolor. Arrowhead points to potentially non-synaptic GRASP signal.

(D) Reconstitution of GFP with high expressing version of GRASP where *13XLexAopCD4:GFP^{11}* was driven in md neurons using *585-LexA* and *20XUASCD4:spGFP$^{1-10}$* driven by *412-Gal4*. Image shows native reconstituted GFP in pseudocolor. Arrowhead points to potentially non-synaptic GRASP signal.

(E) Reconstitution of GFP using synapse-restricted GRASP where synaptobrevin tethered GFP$^{1-10}$ (syb:spGFP$^{1-10}$) was driven in cIV neurons using *dTrpAQF* and CD4:spGFP^{11} driven by *412-Gal4*. Image shows native reconstituted GFP in pseudocolor.

(F) No reconstitution of native GFP was observed with *dTRPA1-QF* driving *QUAS-syb:spGFP1-10.* Image shown in pseudocolor.

(G) No reconstitution of native GFP was observed with *412-Gal4* driving *UAS-CD4:spGFP^{11}.* Image shown in pseudocolor.

Scale bars: 15μm (A), 10μm (A''), 70μm (B), 30μm, (C,D), 40μm (E,F), 50μm (G)

Genotypes: (A- A'') *+/ppk-CD4-TdTom;412-Gal4, UAS-mCD8:GFP/+* (B)*13xLexAop2-IVS-myr::GFP/585-LexA* (C) *LexAopCD4-spGFP^{11}/+ ;585-LexA /412-Gal4, UAS-CD4-SpGFP$^{1-10}$* (D) *13xlexAopSpGFP^{11}/+; 20xUASGFP$^{1-10}$/412-Gal4,585-LexA* (E) *dTrpA1-QF/UAS-CD4-spGFP^{11}; 412-Gal4/QUAS-syb-spGFP$^{1-10}$* (F) *dTrpA1-QF/UAS-CD4-SpGFP^{11}; +/QUAS-syb-spGFP$^{1-10}$* (G)*+/UAS-CD4-SpGFP^{11};412-Gal4/QUAS-syb:spGFP$^{1-10}$*

Figure 2.5: DnB neurons are activated by noxious heat in cIV dependent manner

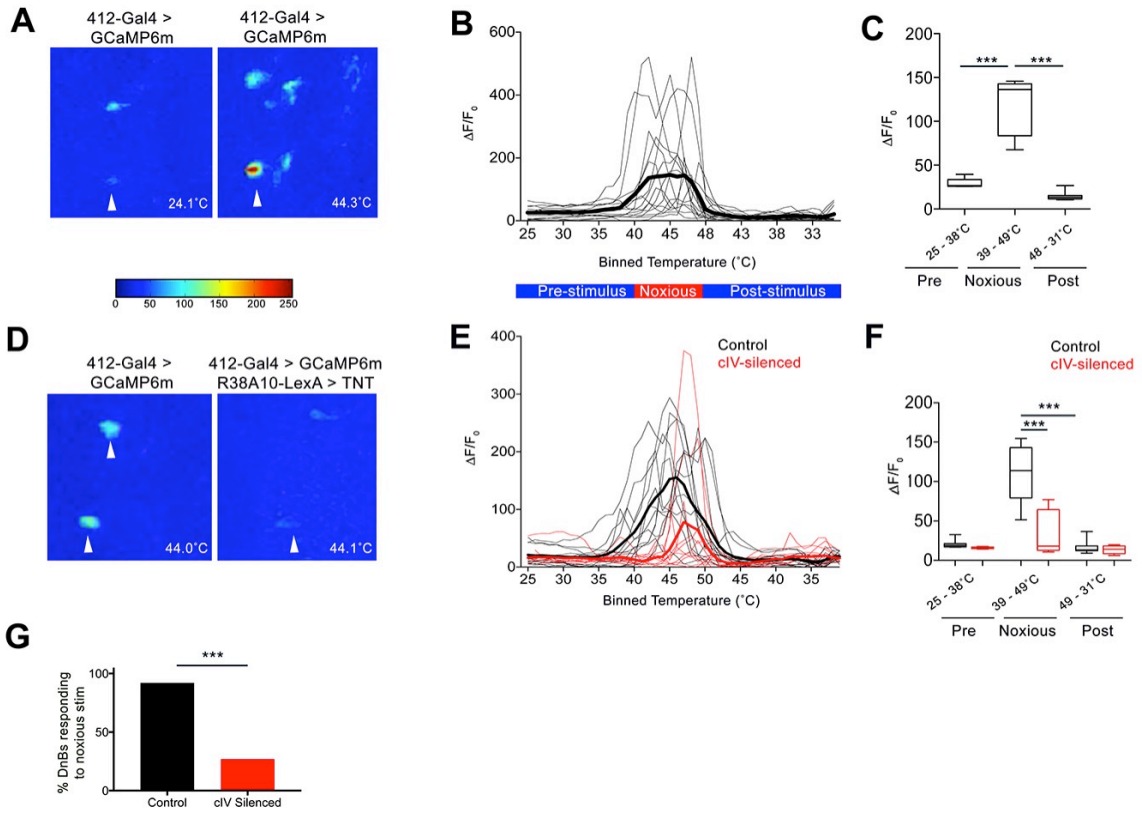

Figure 2.5: DnB neurons are activated by noxious heat in cIV dependent manner

(A) Representative heat maps showing Ca^{2+} responses in DnB cell bodies (arrowhead) before (~24˚C) and during (~44˚C) local noxious heat stimulation of the body wall.

(B) Individual Ca^{2+} responses (thin lines) and average of all trials (bold) represented as $\Delta F/F_0$ in DnB cell bodies (n=15). Larvae received local heat stimulation at segment A7 using a heat probe that was increased from ~24-49˚C, then cooled to ~30˚C.

(C) GCaMP signal binned for 25-38˚C (below noxious threshold), 39-49˚C (above noxious threshold), and 48-31˚C (post-stimulus cool down).

(D) Representative heat maps showing Ca^{2+} responses in DnB cell bodies at ~44˚C (arrowhead) with or without cIVs silenced with *R38A10-LexA* driving TNT.

(E) Individual Ca^{2+} responses (thin lines) and average of all trials (bold) in DnB cell bodies during heating and cooling, Black lines represent control (n=12) and red lines represent cIV silenced trials (n=11).

(F) GCaMP signal binned for 25-38˚C (below noxious threshold), 39-49˚C (above noxious threshold), and 48-31˚C (post-stimulus cooling) for control and cIV silenced trials.

(G) Percent of Down-and-Back neurons responding to noxious stimulus. Threshold of activation set by peak activity in (B). n= 12 control, n=11 cIV silenced

(A-C) *20X-UAS-IVS- GCaMP6m/+;412-Gal4* (D-G) (i) *20X-UAS-IVS-GCaMP6m/+;412-Gal4 /+* (ii) *20X- UAS-IVS-GCaMP6m/R38A10-LexA;412-Gal4 /13X-LexAop2-IVS-TNT::HA*

Box plots show median (middle line) and 25^{th} to 75^{th} percentiles with whiskers representing 10 to 90 percentiles. P values are indicated as ***p<0.001, as determined by Kruskal-Wallis with Dunn's correction for multiple testing (C, F), or Chi squared analysis (G).

Figure 2.6: *412-Gal4* activation triggers nocifensive behavior downstream cIV neurons

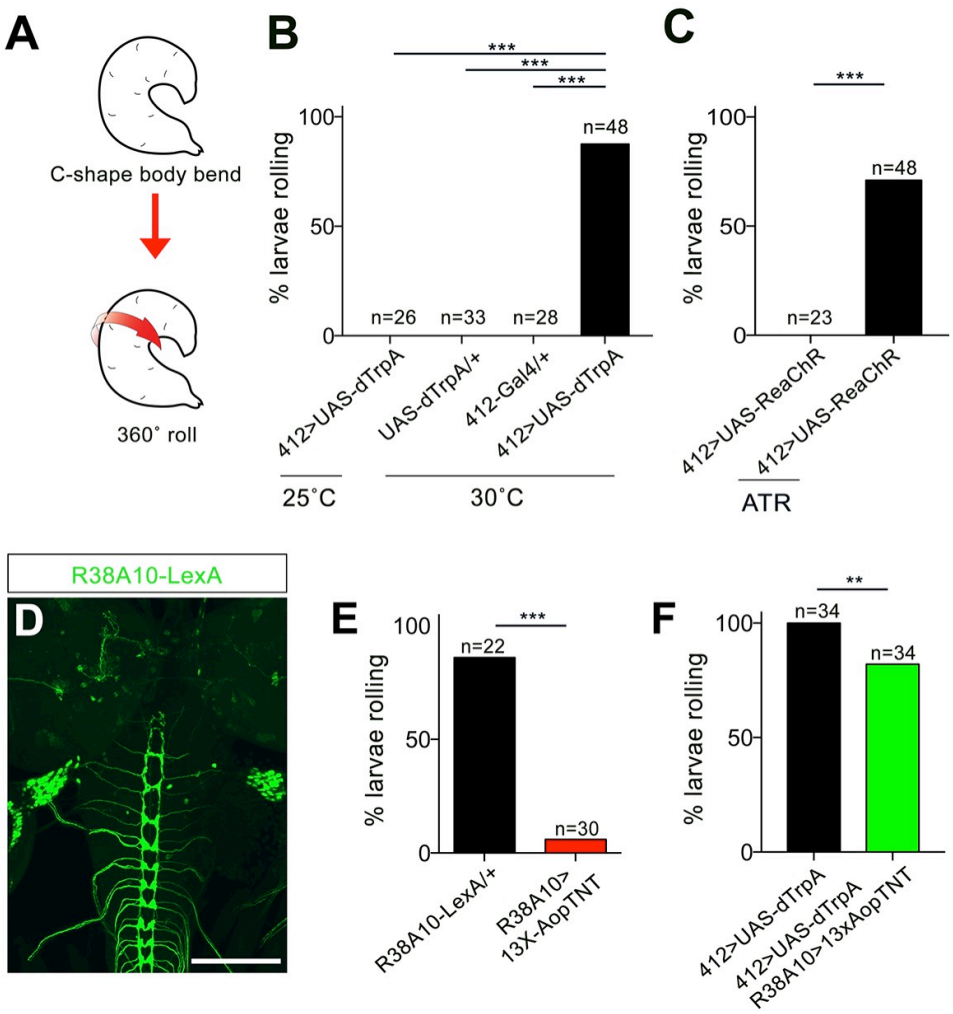

Figure 2.6: *412-Gal4* activation triggers nocifensive behavior downstream cIV neurons

(A) Schematic representation of nocifensive escape behavior, which includes C-shaped body bending and 360˚ rolls.

(B) Percentage of animals exhibiting rolling behavior during dTrpA1 activation driven by *412-Gal4*.

(C) Percentage of animals exhibiting rolling behavior with optogenetic activation of *412-Gal4* neurons using ReaChR with and without all-*trans*-retinal (ATR), which is essential for channelrhodopsin function.

(D) *R38A10-LexA* driven *13XlexAop2-IVS-myr::GFP* labels cIV sensory neurons (anti-GFP, green) and sparse labeling of brain neurons.

(E) Larvae show reduced rolling in response to local noxious stimuli when cIV neurons are silenced using *R38A10-LexA* to drive tetanus toxin light chain (TNT).

(F) Percentage of animals exhibiting rolling responses when *412-Gal4* neurons were induced by dTrpA1 with and without cIV-silencing via *R38A10-LexA* driven tetanus toxin light chain (TNT). **p=0.0056 by Chi squared test.

Scale bar = 50μm (G);

Genotype: (B) (i) *UAS-dTrpA1/+;412-Gal4/+* (ii) *UAS-dTrpA1/+* (iii) *412- Gal4/+* (C) *UAS-ReaChR/412-Gal4* (D) (i) *w-; Sp or Cyo/R38A10-LexA; 13XLexAop2-IVS-myr:GFP/+* (E) (i) *R38A10-LexA/+* (ii) *R38A10- LexA/+;13XLexAop2-IVS-TNT::HA /+* (F) (i) *UAS-dTrpA1/+;412-Gal4/+* (ii) *R38A10- LexA/UAS-dTrpA1;412-Gal4/13X-LexAop2-IVS-TNT::HA*

***p- value < 0.001 by Chi squared test with Bonferroni correction for cases of multiple testing.

Figure 2.7: Additional Gal4 line labeling DnB neurons activates rolling

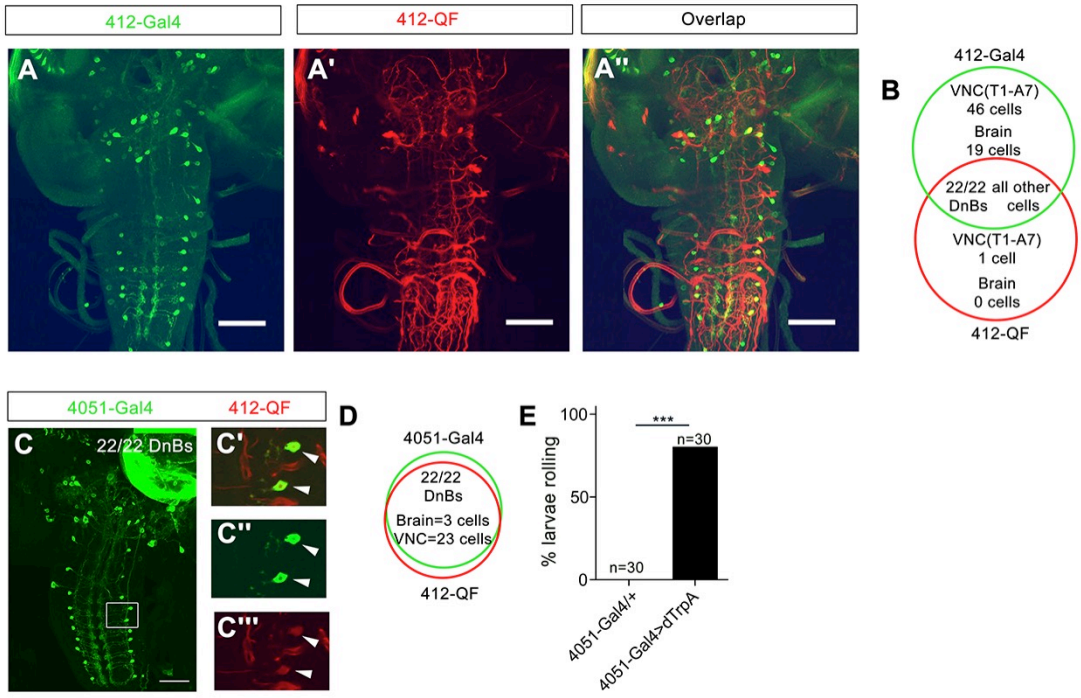

Figure 2.7: Additional Gal4 line labeling DnB neurons activates rolling

(A-A'') Overlap between *412-Gal4* driven mCD8GFP (anti-GFP, green) and *412-QF* driven tdTomato (anti-dsRed, red) expression patterns

(B) Number of overlapping cells between *412-Gal4* and *412-QF*

(C) Expression pattern of *4051-Gal4* (anti-GFP, green)

(D) Number of cells overlapping between *4051-Gal4* and *412-Gal4*

(E) Percentage of larvae rolling upon *4051-Gal4* thermogenetic activation. ***p- value < 0.001 by Chi squared test.

Scale bars: 50µm (A- A'', C)

Genotypes: (A- A'') *20XUAS-mCD8GFP/+;412-Gal4 /412-Qf,QUASTdTomato* (C-C''') *UAS-mCD8GFP/+;4051-Gal4/412-Qf,QUASTdTomato/+* (E) (i) *4051-Gal4/+* (ii) *UAS-dTrpA/+;4051-Gal4/+*

Figure 2.8: Activation of *412-Gal4* off targets does not induce rolling

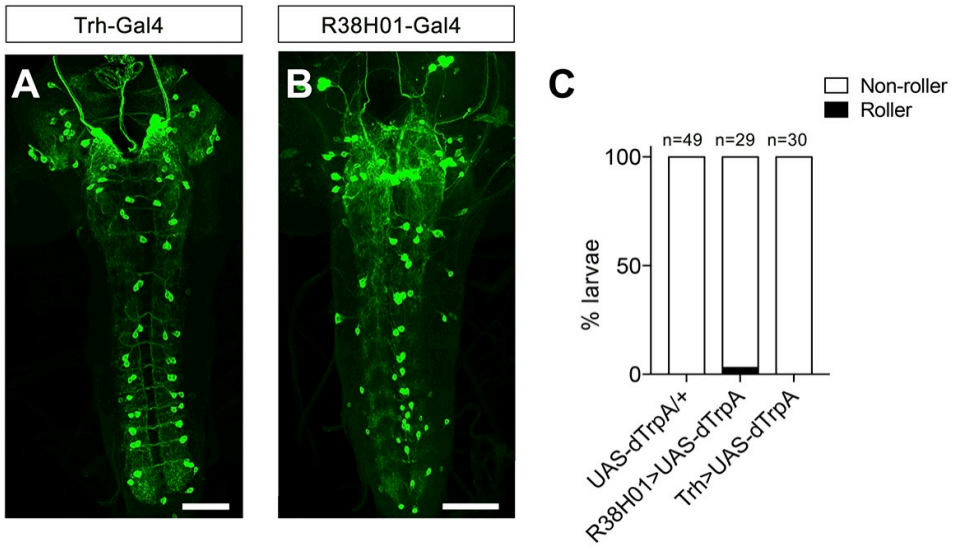

Figure 2.8: Activation of *412-Gal4* off targets does not induce rolling

(A) Expression pattern of *Trh-Gal4* labeling serotonergic neurons

(B) Expression pattern of *R38H01-Gal4* labeling A27j neurons and other interneurons

(C) Percentage of larvae rolling upon *R38H01-Gal4* and *Trh-Gal4* thermogenetic activation

Scale bars: 50μm (A-B); Genotypes: (A) *20X-UAS-mCD8GFP/+;Trh-Gal4/412-Qf,QUASTdTomato* (B) *20X-UAS-mCD8GFP/R38H01-Gal4;412-Qf,QUASTdTomato/+*

(C) (i) *UAS-dTrpA/+* (ii) *UAS-dTrpA/+;R38H01-Gal4/+* (iii) *UAS-dTrpA/+;Trh-Gal4/+*

Figure 2.9: DnB neurons promote both bending and rolling stages of escape behavior

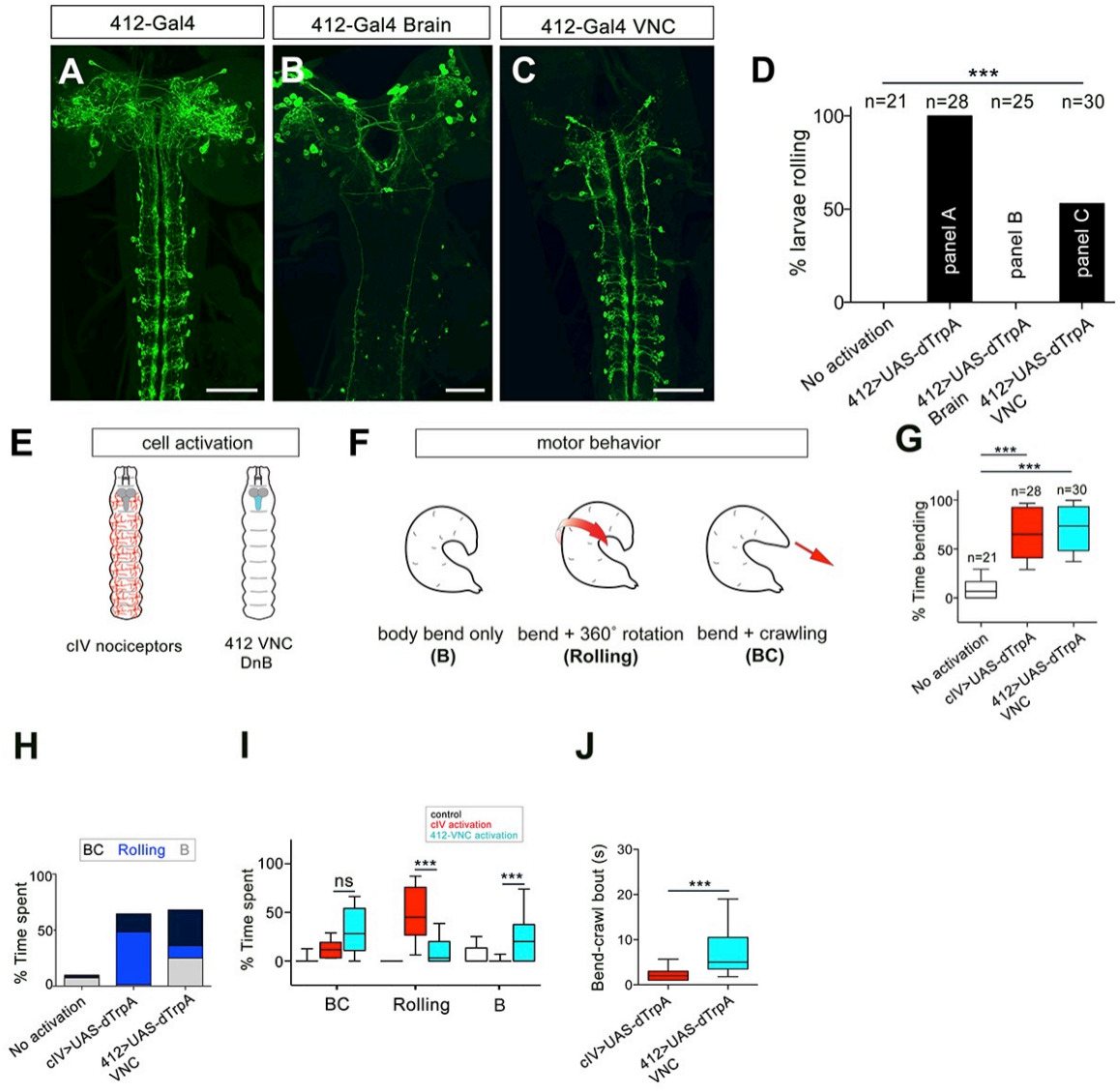

Figure 2.9: DnB neurons promote both bending and rolling stages of escape behavior

(A-C) Intersectional strategy to target GFP either to A) the brain and VNC, B) brain only or C) VNC only. Green channel shows anti-GFP labeling.

(D) Percent exhibiting nocifensive rolling during dTrpA1 activation of subsets of *412-Gal4* neurons corresponding to panels A-C.

(E) Schematic of cIV nociceptors (left) and location of VNC neurons (right)

(F) Schematic of different motor behaviors observed in response to cIV or *412-Gal4* VNC activation. Body bend only, B, larvae entered a curved C-shape but did not roll or crawl; B + 360˚ rotation, animals entered C-shape and performed 360˚ rotations, rolling; bend + crawling, larvae attempted to crawl while remaining in a C-shape. Red arrows show direction of locomotion.

(G) Total amount of time spent in bent-body positions (B, B+360, BC) upon dTrpA1-induced activation of cIV neurons and *412-Gal4* VNC neurons.

(H) Percent of time upon dTrpA1 activation spent in bent-body positions with crawling (black) rolling (blue) or paused (bend-only, gray).

(I) Percent of time spent during 30 second trial in bent-body positions: bend-crawl, rolling, or bend-only. Same data as in (D).

(J) Plot showing length of bend-crawl bouts in seconds upon cIV or *412-Gal4* VNC activation.

Scale bars = 50 μm (A-C)

Genotypes: (A) *+;tsh-LexA,8X-LexAopFLP; 10X-UAS-myr:GFP/412-Gal4* (B) *tsh-Gal80/+;412-Gal4, UAS-mCD8:GFP* (C) *tub>Gal80>;tshLexA,8X-LexAopFLP; 10X-UAS-myr:GFP/412- Gal4* (D) (i) *tsh-LexA,8X-LexAopFLP;412-Gal4/+* (ii) *UAS-dTrpA1/+;412-Gal4/+* (iii) *tsh-Gal80/UAS-dTrpA1;412-Gal4/+* (iv) *tub>Gal80>;tsh-LexA,8X-LexAopFLP; UAS- dTrpA1/412-Gal4* (G-I) (i) *tsh-LexA,8X-LexAopFLP;412-Gal4/+* (ii) *ppk1.9-Gal4/+;UAS-dTrpA1/+*(iii) *tub>Gal80>;tsh-LexA,8X-LexAopFLP; UAS-dTrpA1/412-Gal4* (J) (i) *ppk1.9-Gal4/+;UAS-dTrpA1/+*(ii) *tub>Gal80>;tsh-LexA,8X-LexAopFLP; UAS-dTrpA1/412-Gal4*

Box plots show median (middle line) and 25th to 75th percentiles with whiskers representing 10 to 90 percentiles. P values are indicated as ***p<0.001, as determined by One-way ANOVA with Tukey's multiple comparison's test (G), Kruskal-Wallis with Dunn's correction for multiple testing (I), Mann-Whitney (J), or Chi squared analysis with Bonferroni correction for cases of multiple testing. (D)

Figure 2.10: Dose activation of cIV vs. *412-Gal4* induces distinct motor programs

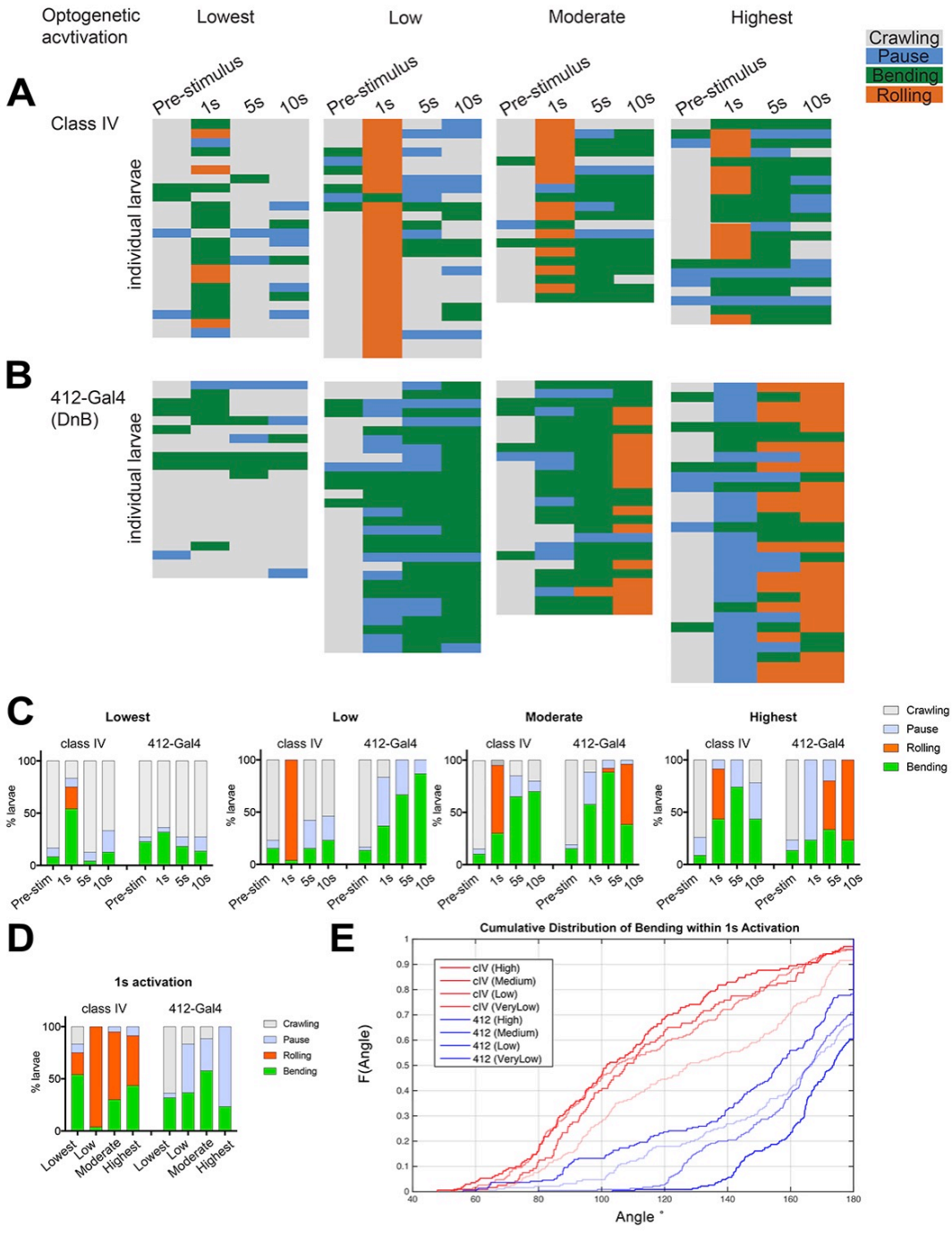

Figure 2.10: Dose activation of cIV vs. 412-Gal4 induces distinct motor programs

(A-B) Behavior ethograms upon optogenetic stimulation of *412-Gal4* or class IV neurons. Groups of animals expressing ReaChR in either population were subjected to different

optogenetic activation at different light intensities for 10s: Lowest (~45 Lux), Low (~200 Lux), Moderate (~850 Lux) and Highest (~1450 Lux). Behavior events are color-coded: crawling (grey), pause (blue), bending (green), and rolling (orange)

(A) Behaviors triggered upon optogenetic activation of Class IV neurons. Lowest, n=24; Low, n=26 Moderate, n=20; Highest, n=23

(B) Behaviors triggered upon optogenetic activation of *412-Gal4* neurons. Lowest, n=22; Low, n=30 Moderate, n=26; Highest, n=30

(C) Percent of larvae exhibiting crawling (grey), pausing (blue), rolling (orange) and bending (green) across different activation intensities

(D) Percent of larvae exhibiting crawling (grey), pausing (blue), rolling (orange) and bending (green) within 1st second of activation

(E) Bending angles observed within 1st second of activation across activation conditions

Genotypes: (A) *UAS-ReaChR/PPK$^{1.9}$-Gal4* (B) *UAS-ReaChR/+:412-Gal4/+* (C-E) (i) *UAS-ReaChR/PPK$^{1.9}$-Gal4* (ii) *UAS-ReaChR/+:412-Gal4/+*

Figure 2.11: Virtual Screen of Rubin collection to identify DnB-labeling LexA drivers

R70F01∩412	sPN1s + one brain neuron	sPN1s + brain	sPN1s	No expression	Total brains
myr:GFP	57%	15%	0%	28%	53
Kir$^{2.1}$-GFP	8%	0%	38%	54%	24

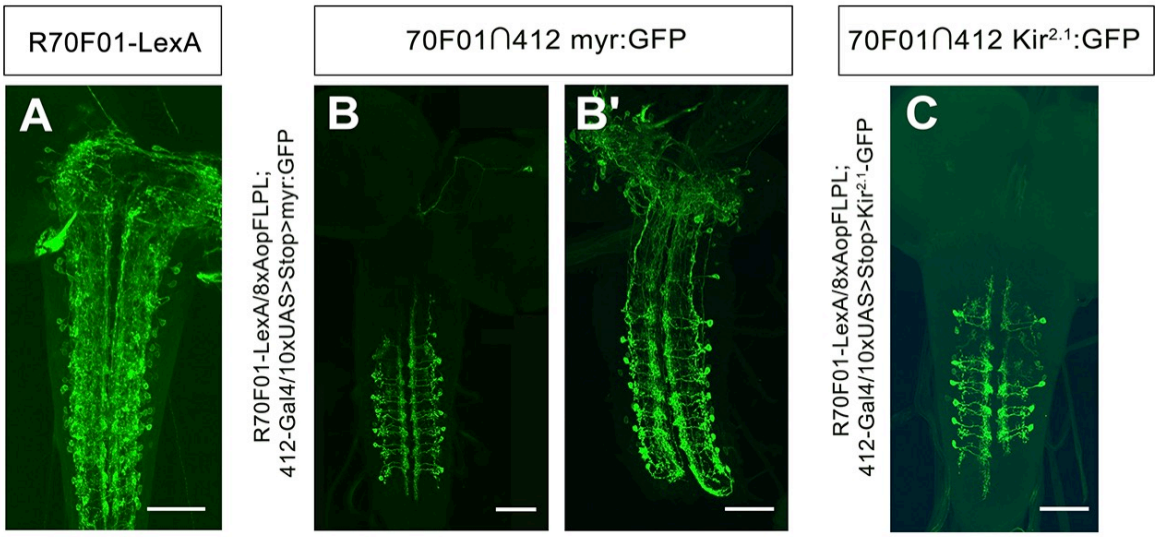

Figure 2.11: Virtual Screen of Rubin collection to identify DnB-labeling LexA drivers

(A) Expression pattern for *R70F01-LexA*

(B-B') Chart showing distribution of expression patterns using *R70F01∩412* to drive either *myr:GFP* or *Kir2.1-GFP*. Representative images showing *R70F01∩412* driving *myr:GFP*: DnB labeling (with one brain neuron) (B) and DnB neurons labeled along with sparse labeling of brain neurons (B').

(C) Labeling DnB neurons using *R70F01-LexA* driving *8X-Aop2-FLPL*, and *412-Gal4* driving *10XUAS>Stop>Kir$^{2.1}$-GFP* (anti-GFP, green).

Scale bars = 50μm (A-C)

Genotypes: (A) *w-; Sp or CyO/R70F01-LexA; 13XLexAop2-IVS-myr:GFP/+* (B-B') *R70F01-LexA/8X- LexAop2FLPL; 412-Gal4/10XUAS>Stop>myr:GFP* (C) *R70F01-LexA/8X- LexAop2FLPL; 412-Gal4/UAS>Stop>Kir2.1-GFP*

Figure 2.12: Silencing DnB neurons reduces rolling probability and duration

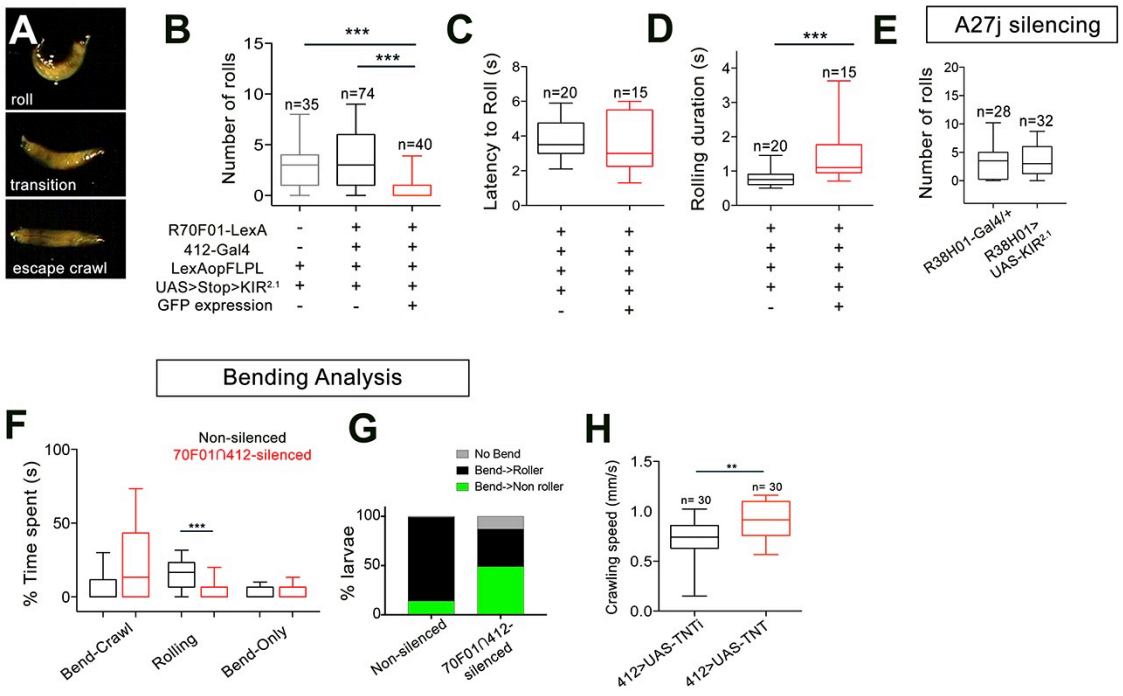

Figure 2.12: **Silencing DnB neurons reduces rolling probability and duration**

(A) Global heat stimulus leads to rolling (top), transition period (middle), and an increase in forward crawling speed (escape crawl; bottom).

(B) Number of rolls per trial. 'Non-silenced' animals lacked *Kir2.1-GFP* expression and '*R70F01∩412*-silenced' animals exhibited GFP expression.

(C) Latency to initiate first roll during global heat stimulus in non-silenced and *R70F01∩412*-silenced animals.

(D) Rolling duration of the 1st roll for animals that completed 360˚ rotations.

(E) Silencing A27j neurons using *R38H01* to drive $Kir^{2.1}$ does not reduce rolling

(F) Percent of time animals spent engaging in bend-crawling, rolling, or bend-only

(G) Percent of larvae exhibiting no bend, bend that leads to rolling (bend→roller), or bending that does not lead to rolling (bend→non-roller)

(H) Crawling speed with *412-Gal4* driving either *UAS-TNT* to silence neurons or *UAS-TNTi* as a control.

Genotypes: (B) (i) *8X-Aop2FLPL/+;10X-UAS>Stop>Kir2.1-GFP/+* (ii) *R70F01-LexA/8X-Aop2FLPL; 412-Gal4/UAS>Stop>Kir2.1-GFP* (C-D,F-G) *R70F01-LexA/8X-Aop2FLPL; 412-Gal4/UAS>Stop>Kir2.1-GFP* (E) (i) *R38H01-Gal4/+* (i) *R38H01-Gal4/UAS-Kir$^{2.1}$-eGFP* (H) (i) *UAS-TNTi/+;412-Gal4/+* (ii) *UAS-TNT/+;412-Gal4/+*

Figure 2.13: DnB neurons are required for robust bending curvature during rolling

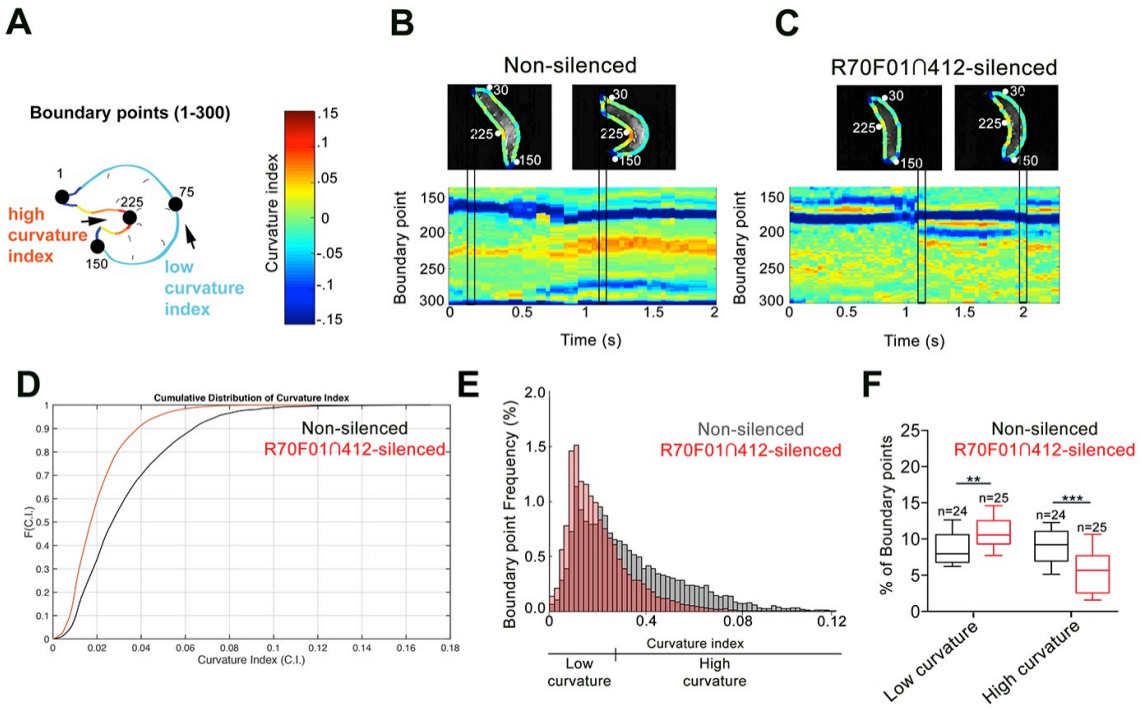

Figure 2.13: DnB neurons are required for robust bending curvature during rolling

(A) Schematic of larva with curvature analysis. Program outlines boundary of larval body and assigns a curvature index value at each of 300 boundary points. Small curvature indices are assigned a cool color (blue-green) and large curvature indices are assigned a warm color (yellow-red).

(B) Representative kymograph showing curvature indices (C.I.) in non-silenced animals during the duration of the first roll. Larval images above kymographs represent C.I. at each boundary point position along the outline of the entire body at time points when the animal acquires a low curvature (left) or high curvature shape (right; indicated in plots as vertical tracks). In this animal, C-bend occurs approximately between boundary points 150 and 300.

(C) Representative kymograph showing curvature indices in *R70F01∩412*-silenced animals. Kymograph is as represented in (B).

(D) Cumulative distribution of all curvature indices for non-silenced and *R70F01∩412*-silenced animals

(E) Distribution of concave curvature indices (C.I.) of all boundary points across the bending duration for animals that rolled (360˚ turn) and 'attempted' rolling (i.e. 0-360˚ rotations) separated into low curvature (C.I.<0.027) and high curvature (C.I.>0.027) values. The C.I. cutoff for low curvature vs. high curvature was defined as the median of the C.I. in the control group.

(F) Percentage of boundary points that fall into the category of low curvature (C.I.<0.027) and high curvature (C.I.>0.027) values

Genotypes: (B-F) *R70F01-LexA/8X-Aop2FLPL; 412-Gal4/UAS>Stop>Kir2.1-GFP*

Box plots show median (middle line) and 25th to 75th percentiles with whiskers representing 10 to 90 percentiles.

P values are indicated as *p<0.05, **p<0.01, ***p<0.001, as tested by MANOVA with bonferroni correction, followed by posthoc unpaired T-test

Chapter III:

Neural circuitry underlying Down-and-Back mediated modular control of escape behavior

Abstract

Rapid and efficient escape behaviors in response to noxious sensory stimuli are essential for protection and survival. Yet, the neural mechanisms underlying sensory evoked sequential motor programs remains largely unknown. In *Drosophila* larvae, noxious stimuli trigger sequential body bending and 360˚ rolling behavior. Down-and-Back (DnB) interneurons promote both bending and rolling modules of escape behavior, but the neural circuitry underlying the sequential activation of these modules remains unknown. This work uses electron microscopic circuit reconstruction to show that DnB interneurons integrate both nociceptive and mechanosensory inputs, are directly presynaptic to pre-motor circuits, and link indirectly to Goro rolling command-like neurons. DnB activation promotes activity in Goro neurons, and coincident inactivation of Goro neurons prevents the rolling sequence but leaves body bending motor responses intact. Thus, activity from nociceptors to DnB interneurons coordinates modular elements of nociceptive escape behavior.

Introduction

Rapid and efficient escape behaviors in response to noxious sensory stimuli are essential for protection and survival. In *Drosophila* larvae, noxious stimuli trigger sequential body bending and 360˚ rolling behavior. A largely unanswered question is how sensory stimuli are transformed into stereotypic sequential motor outputs that allow animals to quickly withdraw from dangerous environments.

Even the simplest behavior requires exquisite coordination across different muscle groups and motor programs; posture and body axis need to be properly oriented, and motor outputs needs be initiated and terminated appropriately to allow sequence progression. Time-locked sequential behaviors are observed across animal phyla, and include grooming, mating, and ingestion. How the nervous system organizes motor modules into a specific sequence remains poorly understood. Two prevailing models for sequential behavior include: 1) response chaining (Long et al., 2010), where one action triggers the activation of the subsequent action in the sequence, and 2) parallel activation coupled with hierarchical suppression (i.e. all actions activated at once, and reciprocal inhibition establishes a 'winner') (Lashley, 1951). Recent studies have begun providing evidence for these models, such that motor sequencing during bird song supports synaptic chaining (Long et al., 2010), whereas hierarchical suppression underlie the larval startle sequence (hunch-bend), and fly grooming (Jovanic et al., 2016; Seeds et al., 2014). Yet, the noxious bend-roll sequence is not explained by these models. C-shape bending might be a feature of non-noxious behaviors (self-righting), and can be activated independently of rolling (Chapter II), arguing against a response chain model. Moreover, the bend both precedes, and co-occurs with rolling, such that the sequence cannot be completely explained by a model of reciprocal inhibition.

One powerful tool for revealing novel circuit dynamics underlying behavior is the use of (EM) reconstruction to generate neural connectivity maps (Takemura, 2015;

White et al., 1986). The Cardona group (Helmstaedter et al., 2011; Schneider-Mizell et al., 2016) has generated serial section transmission electron microscopy (ssTEM) datasets for both the brain hemisphere and ventral nerve cord (VNC) of the 1st instar larva (4840 sections in total). There 1st instar (L1) larval CNS, was chosen because at this stage the CNS contains a similar amount of neurons and synaptic connections as 3rd instar in a more compact region. Collaborative circuit mapping across multiple research labs allows neural circuits in the larva to be described in detail, down to the number of synapses made between identified cell types. Once synaptic partners are mapped, individual microcircuits can be manipulated and imaged using the vastly diverse *Drosophila* genetic toolkit. EM circuit reconstruction using this dataset has already generated novel insights into the inhibitory circuits controlling crawling, behavior choice and sequence progression (Zwart et al., 2016 2016, Jovanic, 2016), as well circuit dynamics underlying feeding and nociception (Ohyama et al.; Schlegel et al., 2016). One study identified circuit elements downstream of class IV (cIV) nociceptive neurons, including Basin and Goro neurons, that integrate vibration and noxious stimuli (Ohyama et al., 2015). Basin cells receive multiple sensory inputs in distinct regions of the arbor, and impinge on the command-like rolling Goro interneurons (Jovanic et al., 2016; Ohyama et al., 2015) (Jovanic et al., 2016). Although previous EM circuit reconstruction suggests complexity in transduction and integration of inputs leading to nociceptive behavior, how microcircuits promote and coordinate the rapid induction of sequential stages of nociceptive behavior remains unknown.

In Chapter II, I provided evidence that Down-and-Back (DnB) interneurons receive direct input from cIV nociceptive neurons, and promote both bending and rolling modules of nocifensive escape (C-bend→roll→escape crawl). Upon DnB activation, animals display persistent bending which can transition into continuous rolling, depending on the degree of DnB activation. I provided anatomical evidence for a direct

connection between cIV and DnBs, but these techniques lack the synaptic resolution required to definitively identify synaptic partners. These findings prompt interesting questions about the neural circuitry underlying DnB-mediated bending and rolling. For instance, whether there might be separate bending and rolling motor pathways that are coordinated to facilitate escape behavior.

Here, we integrate functional, behavioral, and EM circuit reconstruction approaches to provide a comprehensive view of nociceptive circuit function, particularly the generation of sequential motor outputs during escape behavior. EM reconstruction revealed that DnBs receive almost exclusive sensory inputs, integrating from both nociceptive and gentle-touch sensory neurons. Downstream circuit reconstruction uncovered major DnB input to premotor neurons, and indirect input to Goro rolling command-like neurons. We find that DnBs promote the activity of Goro neurons, and that DnB-induced rolling, but not body bending, is dependent on Goro activity. Thus, studies of DnB neurons reveal an essential node in the nociceptive circuit that coordinates modules of nocifensive behavior to enable rapid escape locomotion.

Results

DnB neurons receive synaptic input from nociceptive and mechanosensory neurons

To identify circuit elements upstream and downstream of Down-and-Back neurons, I collaborated with Albert Cardona's lab (Janelia Research Campus), and utilized an electron microscopic (EM) volume of an entire 1st instar larval CNS (Ohyama et al., 2015) to reconstruct DnB connections (Schneider-Mizell et al., 2016) (Figure 3.1). The neural circuit reconstruction software, CATMAID (Saalfeld et al., 2009), is available remotely, allowing a consortium of labs to participate in reconstruction simultaneously. DnB neurons were previously reconstructed as part of an effort to identify all of the

connection downstream cIV neurons (Ohyama et al., 2015). Given the collaborative nature of reconstruction, most circuits are at least partially reconstructed; therefore, I focused on completing the DnB connectome, and reviewing previous reconstructions.

We reconstructed bilaterally symmetric DnB neurons in segment A1 (Figure 3.2A). In addition to inputs from cIV neurons (45.5%, cumulative input to DnB A1), we identified input from cIII neurons (15% cumulative input) and minor input from class II (cII) and external sensory (es) neurons (4%, 3%, respectively) (Figure 3.2B-D). DnB neurons receive class II and es input from A1 segments exclusively, whereas cIII input is also received from thoracic segment T3, and cIV input from T3 and A2 (both ipsi-and contralateral segments). The axons of cIII and cIV provide input onto DnB dendrites (Figure 3.3A-B). However, the input from cII neurons came entirely from their short collateral axon branches (Grueber et al., 2007) onto the lateral-most DnB axons (Figure 3.3A,C), suggesting presynaptic modulation. Es cells provide input to both DnB dendrite, and postsynaptic sites on DnB axons (Figure 3.3A,C). Inputs to DnB neurons were primarily, but not exclusively sensory, with the sole non-sensory input provided by the putative local inhibitory handle-A neurons (Jovanic et al., 2016)(Figure 3.2B). DnB neurons receive the majority of cIV neuron synapses in 1st instar larvae (18%), consistent with an essential role in nociceptive behavior. Together these results indicate that DnB neurons serve as a hub for multisensory integration.

EM reconstruction reveals direct connections to premotor neurons and nociceptive integrators

To gain insights into circuit mechanisms of nociceptive motor behaviors, we performed EM reconstruction of downstream partners of DnB neurons. We identified the complete set of neurons that receive DnB synaptic input. The neurons with the highest

numerical connection with DnB neurons (>3 synapses on each A1 segment; Figure 3.4B), or the 'top hits,' could be broadly divided into two groups: premotor neurons, and 'nociceptive integrators'. Premotor neurons are upstream motor neurons, and nociceptive integrators are interneurons that receive input from multiple types of nociceptive neurons. Notably, DnB output synapses to these different groups of downstream neurons are anatomically segregated (Figure 3.4A,D). Based on the localization of presynaptic and postsynaptic markers, DnB medial processes were characterized as dendrites, and lateral projections as axons (Chapter II). Nociceptive integrator circuit components receive input from DnB presynaptic sites located on the DnB dendrite. By contrast, premotor neurons receive synaptic inputs from DnB axons. Neurites with dual input/output function have been previously observed in EM reconstructed neurons (Schneider-Mizell et al., 2016)

One major group of DnB downstream targets neurons receives nociceptive information from several different second-order nociceptive interneurons, and thus appear to function as nociceptive integrators. This group includes three neuron types: A10f-like, A09e, and TePn05; Figure 3.5A-C). A10f-like projects its axon to the brain, and integrates input from DnBs, along with additional nociceptive interneurons— Basins, and Goro neurons (Figure 3.5A). A09e in segments A4 and A5 extend a short ipsilateral projection, and an ascending contralateral projection, terminating around T1, that receives multi-segmental input from DnBs, cIII and cIV sensory neurons (3.5B-C). TePn05 makes ascending projections along the nerve cord that are postsynaptic to DnBs and cIV sensory neurons, and that are presynaptic to Basin-2, 4 nociceptive interneurons (Figure 3.5D) (Ohyama et al., 2015). TePn05 thus provides a path for communication between DnB and Basin circuits, which have been previously implicated in rolling behavior (Ohyama et al., 2015). Interestingly, all of the nociceptive integrators possess ascending projections with output sites that terminate in the SEZ or the brain

lobes, suggesting processing by higher order brain regions, and potential integration with chemosensory or memory centers.

The majority of top downstream hits (68%) are between DnBs and premotor neurons (synapsing directly onto motor neurons; exception A07c4) (Figure 3.4B,E; Figure 3.5E-N), providing a potential route to drive escape behavior, particularly the robust C-shape bending. DnBs form the most synapses with segmentally repeating premotor neurons A27k, A01d-3, A02g and A02e (6-18 synapses/hemisegment) (Figure 3.4D-E; Figure 3.5E,M,I,K). With one exception, synapses are made on the ipsilateral side of the nerve cord, which implies that DnB neurons might help coordinate muscle activity within individual segments. (Figure 3.4E). A01d-3 interneurons receive input from contralateral DnB neurons, and project to interneurons in contralateral posterior segments. DnB neurons also make direct connections with *412-Gal4* off-target A27j, and are two synapses away from A26e (downstream A27k neurons) (Figure 3.4E). Some premotor neurons downstream of DnB have been implicated in the duration and propagation of segmental waves during larval forward locomotion, including A02g and A02e (part of PMSI inhibitory interneurons)(Kohsaka et al., 2014), and A27k (Fushiki et al., 2016; Zwart et al., 2016). DnBs also make modest connections with motor neurons innervating muscle LT1 (Zwart et al., 2016)(Figure 3.5E; Figure 3.5L). The strong input of DnB to multiple premotor neurons could enable the rapid motor responses during nociceptive escape behavior.

DnB presynaptic sites accumulate dense core vesicles

I noted in EM sections that in addition to small clear vesicles characteristic of acetylcholine release, large dense core vesicles accumulate at many DnB presynaptic sites (both on dendrites and axons), which is indicative of aminergic or peptidergic signaling (Zhu et al., 1986) (Figure 3.6A). In line with previous descriptions (Park et al.,

2014; Zhu et al., 1986), I observed dense core vesicles as large dark spheres located further away from the presynaptic T-bar than small clear vesicles. Thus, in addition to affecting nociceptive circuitry by direct synaptic connections, DnB neurons may modulate circuitry through neuropeptidergic or aminergic signaling. Consistent with this possibility, I found that PreproANF fused with emerald GFP, which accumulates at peptidergic output sites (Rao et al., 2001), overlaps with DnB axons, suggesting that DnBs posses the machinery to package and release neuropeptides (Figure 3.6B). However, I did not observe co-localization between neuropeptide specific synaptotagmin (SYT)-α and β (labeled with antibodies against SYT isoforms) and DnB neurons (Figure 3.6C-D). SYT−α and β isoforms label a large subset of peptidergic neurons, but not all (Park et al., 2014). SYT−α and β isoforms largely overlap with DIMMED, transcription factor regulating expression of genes involved in peptidergic release machinery, which labels ~90% of peptidegic neurons in larvae (Hewes et al., 2003). Taken together, these data suggest that DnB neurons are potentially modulating downstream circuits via aminergic or peptidergic signaling.

DnB neurons activate the rolling pathway via Goro command-like interneurons

EM reconstruction revealed that Down-and-Back neurons had the highest number of synapses with premotor neurons. I was not able to identify reagents to selectively manipulate downstream pre-motor neurons; however, A02e and A02g belong to the *period*-positive median segmental interneuron group (PMSIs) (Kohsaka et al., 2014), which include A02a-j neurons (Kohsaka et al., 2016). Silencing PMSI neurons with *period-Gal4* (Figure 3.7A) significantly reduced the number of rolls per trial on the global activation assay without significantly affecting the time spent rolling (Figure 3.7B-C). I observed a slight increase in bend only behavior and modest shift towards bending without rolling (Figure 3.7C-D). Notably, animals did retain some degree of rolling.

Although these manipulations are not specific to A02e and A02g neurons, they are consistent with premotor neurons downstream DnBs playing a role in nocifensive behavior.

The direct pathways from DnB neurons to nociceptive integrators (Figure 3.4C) provide a possible functional link with Goro neurons, command-like neurons for rolling. Goros receive indirect input from Basin nociceptive interneurons to promote rolling behavior (Ohyama et al., 2015). We first asked whether DnBs are functionally connected to Goro rolling command-like neurons. In collaboration with Tomoko Ohyama in the lab of Marta Zlatic (Janelia Research Campus), we activated DnB neurons using a red-shifted channelrhodopsin, Chrimson (Klapoetke et al., 2014), and monitored calcium responses in Goro using GCaMP6s (Figure 3.8A). We targeted Chrimson activation to the entire *412-Gal4* CNS pattern using 630nm LED or to 1-2 segments (A4-A6) of DnB neurons in the nerve cord, using a phaser module (3i INC) to target the multiphoton laser. Both whole CNS and DnB targeted activation generated calcium increases in Goro axons (Figures 3.8B and 3.8D). Activating *412-Gal4* brain neurons, which do not include DnBs, did not alter Goro responses (Figure 3.8C). These results support a functional link between DnB neurons and Goro rolling command-like neurons.

EM reconstruction identified multiple pathways between DnB and Goro (Figure 3.9), through A09e and TePn05 neurons. Goro is a projection neuron located in segment T2 that spans the entire nerve cord, gathering input from various segments (Ohyama et al., 2015). Thus, Goro is poised to modulate its neural activity based on the valence and strength of input received along the nerve cord. DnB neurons target segmentally repeating interneurons presynaptic to Goro (Figure 3.9A-B). The DnB-A09e pathway (Figure 3.9B) consists of a connection between DnB and A09e neurons, which receive bilateral input from DnBs in multiple segments. A09e connects with Goro via A02o ‘Wave’ and A05q neurons. The DnB-TePn05 pathway (Figure 3.9B) consists of a

connection between DnBs and TePn05, which synapses with both Basin-2,4, and Basin-3 populations. Basins make extensive connections with A23g, and A05q, which synapse onto Goro (both directly and indirectly through Wave) (Ohyama et al., 2015). A05q links to Goro have been functionally validated (Ohyama et al., 2015). We note that since the EM reconstruction of the larval nerve cord is still incomplete, we are underreporting the number of synapses segmentally repeating neurons are contributing to projection neurons such as TePn05 and Goro. Taken together, these data indicate that A09e and TePn05 networks may underlie DnB-Goro communication.

The EM circuit reconstruction suggests that DnB activity might coordinate swift C-body bending through premotor networks, and rolling through Goro downstream circuitry to produce effective escape behavior. To test this hypothesis, we activated DnBs while selectively silencing Goro activity (*412-Gal4*$^{+}$Goro^{-}) using *16E11-LexA* (Ohyama et al., 2015) (Figure 3.10A-B). As expected, control animals (*412-Gal4*$^{+}$) showed nociceptive behavior consisting of C-shaped bending and rolling (61% bend→roll, 39% bend→no roll)(Figure 3.9C). By contrast, *412-Gal4*$^{+}$Goro^{-} larvae showed bending behavior without rolling upon thermogenetic activation (12% bend→roll, 88% bend→no roll) (Figure 3.10C). Correspondingly, we observed a significant decrease in total number of rolls exhibited by *412-Gal4*$^{+}$Goro^{-} larvae (Figure 3.10D). These data suggest that C-shape body bending and rolling are modular motor behaviors that are coordinated by DnB activity to divergent motor pathways to generate rapid escape locomotion.

Discussion

The nocifensive escape sequence consists of rapid acquisition of C-shape body curvature, essential for subsequent 360˚ rolling escape behavior. Relatively little is

known about the circuit basis for the rapid lateral locomotion phase that underlies nociceptive escape behavior. Here, we use electron microscopic (EM) reconstruction to identify upstream and downstream DnB partners in order to determine how DnB activity promotes sequential bending and rolling. We find that DnB neurons are dually innervated by nociceptive and mechanosensory neurons, providing potential modulation of nociceptive outputs by mechanosensory neurons. The connectivity data also revealed that DnB neurons target two motor pathways: 1) direct connections to premotor neurons, which could account for swift formation of C-shape bend, and 2) indirect connections to Goro command-like neurons. Our functional imaging results supported an indirect connection between DnB and Goro. Furthermore, silencing Goro activity while activating DnB neurons selectively inhibits rolling, while leaving bending intact. Together, these data support DnB neurons as an essential functional node in the nociceptive circuit, potentially converging multisensory input to drive the bending and rolling modular motor pathways underlying escape behavior.

Down-and-backs provide a node for gentle-touch and nociceptive integration

We found that DnB neurons are direct targets of nociceptive cIV neurons and multiple mechanosensory cell types, including cII and cIII gentle touch da neurons and es neurons. Thus, DnBs provide a node for multisensory integration of tactile and noxious stimuli. Furthermore, these sensory inputs are spatially segregated on the DnB arbor, with cII neurons forming synapses via axonal collaterals to postsynaptic sites on the DnB axon. Thus, cII, and to some extent es input, may modulate DnB presynaptic activity as opposed to contributing to dendritic integration. Based on these studies nociceptive inputs appear to be integrated with multiple mechanosensory submodalities by Basin and DnB interneurons. The potential implications of gentle-touch and nociceptive integration will be discussed in Chapter IV. Notably, DnBs received the most

input from nociceptive sensory neurons (45.5%). cIV neurons provide ipsi- and contralateral input from neighboring segments to A1 DnB neurons. This might ensure activation of multiple DnB neurons upon local noxious insult, increasing the likelihood of an escape response. An interesting feature of DnB neurons is that they receive sensory input almost exclusively, with the exception of the putative inhibitory neuron, Handle-A. Given the important role DnBs play in coordinating bending and rolling motor outputs, inhibition at this early point in the circuit might serve as a way to rapidly terminate bending and rolling in order to progress through the remaining nociceptive sequence (i.e. escape crawl). Lack of Handle-A inhibition might explain the continuous rolling observed during DnB activation with *412-Gal4* that is not observed upon cIV activation (Chapter II). Identifying tools to silence Handle-A are essential for testing this hypothesis, and identifying mechanisms for nociceptive escape sequence progression.

Down-and-Back neurons target divergent motor pathways

EM reconstruction of DnB targets identified divergent major downstream circuitry. Output synapses on DnB axons converge on premotor neurons, at least some of which promote peristaltic wave propagation during locomotion (Fushiki et al., 2016; Kohsaka et al., 2014). Another prominent downstream network receives input from presynaptic sites on the DnB dendrite, and leads to Goro rolling command-like neurons (Ohyama et al., 2015). The spatial segregation of DnB output sites appears to mirror a functional segregation of downstream circuitry into bending and rolling modules. It is still unclear what muscle groups are recruited and how segments coordinate during body bending and rolling. Although silencing DnB neurons slightly increased the speed of forward locomotion, overall, forward crawling remained intact. Given that peristaltic waves and bending consist of segmental contractions, links to premotor neurons provide candidate

neurons for dual control of C-shape bending behavior and crawling. DnB neurons provide an opportunity to study how the same premotor circuit can be used to achieve both forward and lateral locomotion patterns. Selectively silencing premotor neurons during rolling escape behavior would reveal whether A02g/e and A27k also regulate speed and propagation of lateral locomotion. I provide some evidence that silencing the PMSI cohort, which includes A02g and A02e, reduces rolling behavior. PMSIs are glutamatergic inhibitory premotor neurons that terminate motor neuron bursting to regulate the timing of segmental wave propagation during crawling (Kohsaka et al., 2016; Kohsaka et al., 2014). Silencing the PMSI neurons reduced the number or rolls, but did not eliminate it altogether or significantly affect the amount of time spent rolling, suggesting that PMSI neurons might selectively impair some components of rolling, but leave others intact. Identifying tools with which to manipulate premotor neurons will be important for determining how they facilitate bending and rolling motor patterns. Notably, DnB neurons target motor neurons innervating LT1 muscles, which have been implicated in larval self-righting behaviors (Picao-Osorio et al., 2015). Self-righting consists of a C-shape-like body bend, and 180˚ turn, so it is possible that LT1 muscles facilitate curved body bends that underlie both self-righting and rolling behavior. Understanding the coordination of premotor circuits that promote bending downstream of DnB neurons, and the muscle activities and physical mechanisms that underlie rolling behavior are important future aims.

Down-and-Back neurons provide a potential avenue for peptidergic/aminergic modulation of nociception

We note that the impact of DnB neurons on nociceptive circuits is likely to be broader than indicated by synaptic connections, since EM sections indicate that DnB neurons accumulate dense core vesicles on presynaptic sites in both dendrites and

axons. Our prepro:ANF labeling suggested that DnB neurons posses the machinery to process neuropeptides, yet we did not find overlap with peptidergic-specific synaptotagmin (Park et al., 2014). These results suggest either that DnB neurons are aminergic, or that they produce a neuropeptide whose expression does not overlap with synaptotagmin (SYT)-α and β (Park et al., 2014). It is unclear what percentage of peptidergic neurons overlap with SYT isoforms. There is a high degree of overlap with DIMMED (transcription factor involved in peptidergic processing), which overlaps with 90% of peptidergic neurons, so DnB could express a neuropeptide that has been uncharacterized, or that does not overlap with DIMMED/SYT (e.g. proctolin or tackykinin) (Hewes et al., 2003). There is evidence that nociceptive circuitry in larvae is subject to peptidergic control (Hu et al., 2017). Two insulin-like peptide 7-expressing neurons (ilp7) signal to mechanosensory class II, class III and nociceptive class IV neurons through sNPF to modulate mechanical nociception. However, ilp7, cII, and cIII neurons are not involved in thermal nociception (Hu et al., 2017), so the extent of peptidergic modulation on nociceptive circuitry requires further investigation. Identification of the putative neuropeptide expressed by DnB neurons, and physiological effects, will be an important future direction, particularly given the important role of neuropeptides in vertebrate pain pathways. (Faris et al., 1983; Mantyh et al., 1997; Ribeiro-da-Silva and De Koninck, 2008; Sun et al., 2004) and their potential for therapeutic targets (Inui, 2003).

Modular control of nociceptive escape behavior via Down-and-Back neurons

We previously showed, that when DnB neurons were ectopically activated, we observed C-shaped body bending that was often, but not always, associated with rolling (Chapter II). These observations provided initial evidence that C-shaped bending is separable from rolling, and that C-bending could be combined with other behaviors, like

pausing or crawling. Our loss of function data supported bending as a primary motor output of DnB activity, with probabilistic activation of rolling motor programs. The concurrent reduction in bending and rolling upon DnB silencing could be explained by two, non mutually exclusive, possibilities, 1) these behaviors could conceivably be linked, such that reduction in bending compromises rolling ability, or, 2) could arise from parallel influence of DnB activity on bending and rolling. Consistent with the former possibility, our previous data (Chapter II) provides some evidence that a certain amount of curvature might be required to facilitate rolling behavior. Here, we also provide evidence for DnB activation of both bending and rolling motor pathways. We found that silencing rolling command neurons Goro while activating DnB neurons promoted persistent bending without rolling. These results indicate that C-bending itself is not sufficient to induce rolling, and the bend-roll sequence must be tightly regulated by interactions between the parallel bend-roll premotor circuits, such that bending occurs first to facilitate rolling, which occurs second. Since the majority of DnB output is targeting premotor neurons, this might explain why weakly activating DnB neurons (Chapter II) might selectively induce bending over rolling. Such independent, but sequentially regulated behavioral modules are consistent with hierarchical models of sequence generation as in fly grooming (Seeds et al., 2014), human speech (Lashley, 1951), roll-crawl sequence (Ohyama et al., 2013), and hunch-bend sequence (Jovanic et al., 2016). We note however, that although bending and rolling are sequential, they co-occur for much of the defensive behavior sequence, in contrast to such sequential and non-overlapping behavioral sequences. Elucidating the mechanisms of timing and interaction between the different circuit modules (bend vs roll) identified therefore promises to shed light on the general mechanisms of circuit implementation of sequence generation and co-ordination between different motor modules.

Methods

Fly stocks

(1) *PB[IT.Gal4]0412* (referred to in the text as *412-Gal4*; (Gohl et al., 2011)), (2) *UAS-mCD8-GFP* (Lee and Luo, 1999), *13X-LexAop2-IVS-myr:GFP/ TM3,Sb,e* (3) *Sp/CyO;nompC-LexA, 10X-LexAop2-myr-GFP/TM6B* (Shearin et al., 2013), (4) *R16E11-LexA* (5) *R69E06-LexA*, (Jenett et al., 2012), (6) *LexAop-Kir2.1* (Feng et al., 2014) was a gift drom Dr. Barry Dickson (Janelia Research Campus, Virginia), (7) 20x*UAS-CsChrimson-mCherry* (Jovanic et al., 2016), (8) *13xLexAop2-IVS-GCaMP6s* (Chen et al., 2013), (9) preproANF:EMD (Rao et al., 2001), (10) *UAS-TdTomato,* (11) *Per-Gal4* (Kaneko and Hall, 2000)

Immunohistochemistry

Immunohistochemistry was performed essentially as described (Matthews et al., 2007). Third instar larvae were dissected in 1X PBS, fixed in 4% paraformaldehyde (Electron Microscopy Sciences) in 1X PBS for 15 minutes, rinsed three times in 1X PBS + 0.3% Triton X-100 (PBS-TX), and blocked for 1 hour at 4°C in normal donkey serum (Jackson Immunoresearch). Primary antibodies used were chicken anti-GFP (1:1000; Abcam), rabbit anti-DsRed (1:250, Clontech), rabbit anti-SYT−α and anti-SYT-β (1:500, gift from T. Littleton, MIT) (Adolfsen et al., 2004). Animals were incubated overnight in primary antibodies at 4°C, rinsed repeatedly in PBS-TX, and incubated overnight at 4°C in species-specific, fluorophore-conjugated secondary antibodies (Jackson ImmunoResearch) at 1:200 in PBS-TX. Tissue was mounted on poly-L-lysine coated coverslips, dehydrated in ethanol series, cleared in xylenes, and mounted in DPX (Fluka).

Behavioral analysis

For behavioral analysis, flies were reared at 25˚C and tested as wandering third instar larvae. For each experiment, at least three trials, taken on separate days, were performed for each genotype. Larvae were only tested once.

Thermogenetic activation

dTrpA1 experiments were performed on 1% agarose gels with 0.6% black ink (Super Black India ink, Speedball) using a peltier device (CP-031, TE technology) and temperature controller (TC-36-25-RS232, TE technology) to heat the gel to ~32.5˚C. Animals displaying coincident C-shape bending and 360˚ rotations were classified as ‘ Bend→Roller’. ‘Bend→No Roller’ was counted when animals remained in a curved posture while crawling or pausing. Trachea were used as a reference for bending and rolling categorization. Animal behavior was recorded using a Leica M50 camera along with Leica FireCam software and QuickTime screen capture for 30 seconds. Videos were quantified offline with experimenter blind to condition.

Global Activation Assay

For the global activation assay, third instar larvae were placed on a 1% agarose 0.6% black ink gel (Super Black India ink, Speedball) heated to 40˚C by a peltier device (CP-031, TE technology) and temperature controller (TC-36-25-RS232, TE technology). Behaviors were recorded for 30 seconds using Leica M50 camera along with Leica FireCam and QuickTime screen capture. Behavior was quantified offline with experimenter blinded to genotype. Rolling events (360˚ turns) were quantified using the trachea as a reference.

Calcium imaging

Goro neurons

For activation of presynaptic neurons (Down-and-Back) with CsChrimson and imaging in postsynaptic neurons (Goro), the central nervous system of wandering third instar larvae were dissected out in cold physiological saline, Baines solution (Baines et al., 2001) containing (in mM) 103 NaCl, 5 KCl, 5 HEPES, 26 $NaHCO_3$, 1 NaH2PO_4, 5 Trehalose, 6 Sucrose, 2 $CaCl_2$ 2H2O, 8 $MgCl_2$ $6H_2O$, and kept stable by sticking CNS on poly-L-lysine (SIGMA, P1524) coated cover glass placed in small Sylgard (Dow Corning) plates. 620 nm LED (Mightex Systems Inc.) was used for whole CNS CsChrimson activation and 1040 nm laser using Phaser module (Intelligent Imaging Innovations, Inc.) for localized CsChrimson activation. We imaged the axon of Goro neurons. Image data were processed by ImageJ software (NIH) and analyzed using custom code written in MATLAB (Mathworks). Regions of interest (ROIs) were determined by averaging the 10 frames before stimulation and segmenting this data by the function MEAN83 in ImageJ. The mean intensity of ROI was measured by ImageJ. In all cases, changes in fluorescence were calculated relative to baseline fluorescence levels (F_0) as determined by averaging over a period of at least 3 seconds just before CsChrimson activation. $\Delta F/F_0$ values were calculated as $\Delta F/F_0 = (Ft - F_0) / F_0$, where Ft is calculated by subtracting the background fluorescence from the fluorescence mean value of a ROI in a given frame.

EM Reconstruction of DnB Circuits

EM reconstruction was performed using CATMAID as previously described (Ohyama et al., 2015; Schneider-Mizell et al., 2016). A09l (DnB) neurons in A1 were identified during circuit reconstruction downstream class IV sensory neurons (Ohyama et al., 2015), and were verified as *412-Gal4* labeled neurons based on morphology and cell body position.

DnB annotated synapses then served as starting points to reconstruct the pre- and post-synaptic connectome.

Statistical Analysis

When comparing two groups of quantitative data (e.g. number of rolls), unpaired t-test was performed if data showed a normal distribution (determined using D'Agostino & Pearson omnibus normality test) and Mann-Whitney test if data distribution was non-normal.

Acknowledgments

We thank Rick D. Fetter and the Fly EM Project Team at HHMI Janelia for the gift of the EM volume, and HHMI Janelia for funding. We thank Hiroshi Kohsaka, Akinao Nose, Ingrid Andrade, Javier Valdes-Aleman, Akira Fushiki, Aref Arzan Zarin, Maartin Zwart and Casey Schneider-Mizell for neuron reconstructions. We additionally thank Javier Valdes-Aleman for neuron reconstruction training, and Casey Schneider-Mizell for useful feedback. This work was supported by a National Science Foundation Graduate Research Fellowship (AB), National Institutes of Health (NIH) Predoctoral Fellowship 1F31NS090909-01 (AB), Columbia University, NIH R01 NS061908 (WBG), NIH R24 NS086564 (T. Clandinin and W.B.G), and NIH R01 GM086458 (WDT).

Figure 3.1: Reconstructing neural circuits using electron microscopy

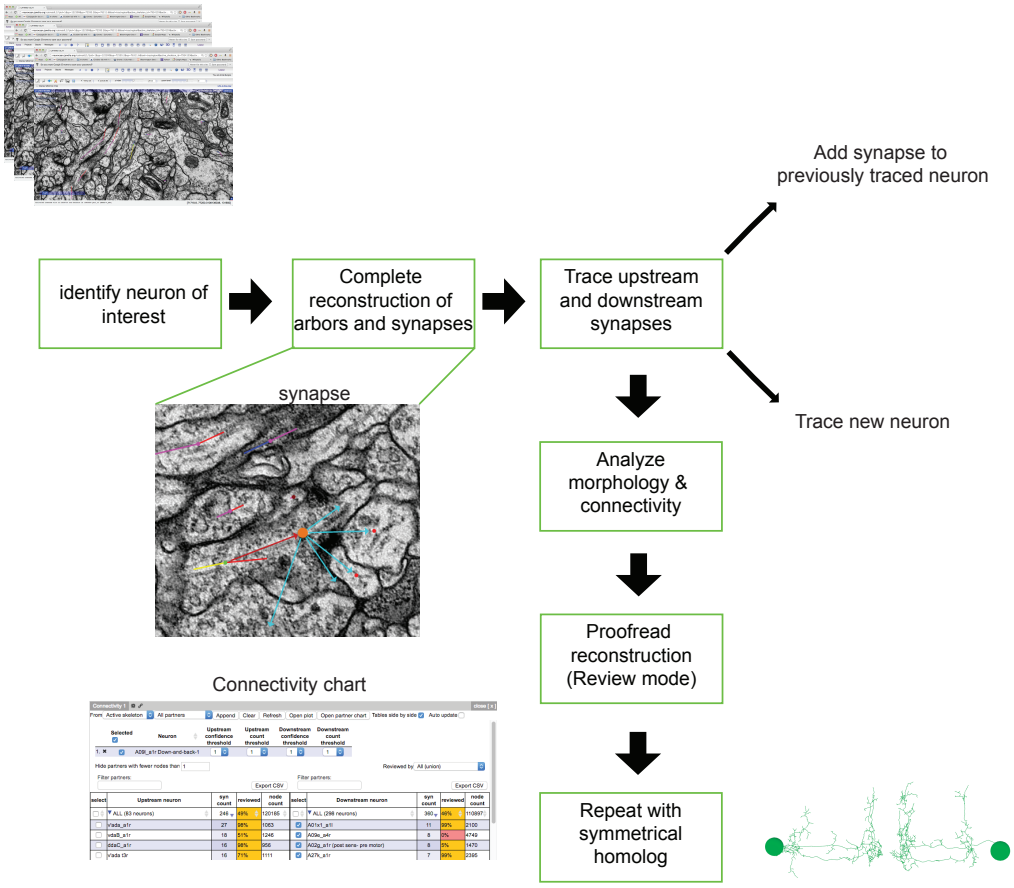

Figure 3.1: Reconstructing neural circuits using electron microscopy

Flow chart showing steps for neural reconstruction using the CATMAID software

Figure 3.2: Connectome of sensory and interneuron inputs to DnB neurons

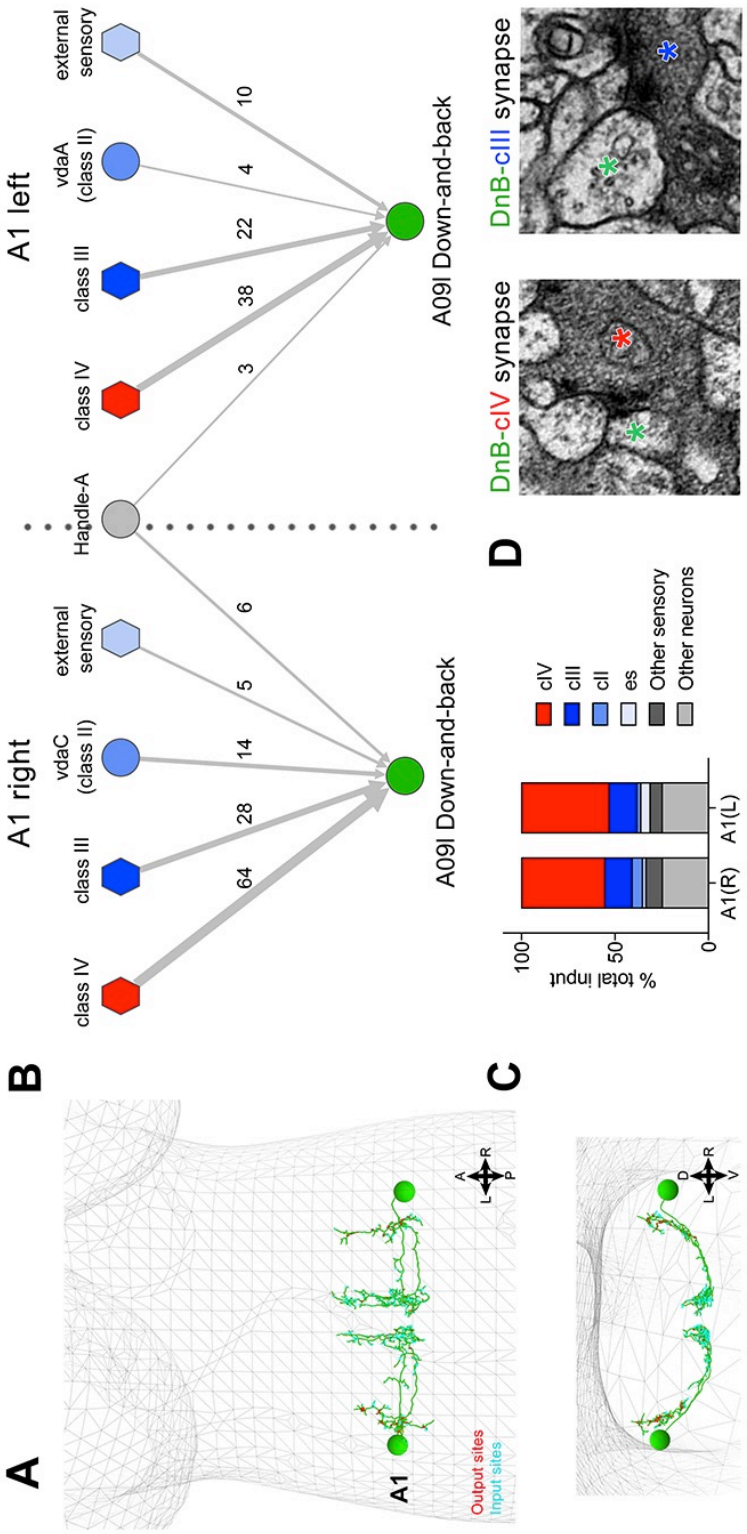

Figure 3.2: Connectome of sensory and interneuron inputs to DnB neurons

(A) First instar larva brain with bilateral reconstruction of DnB neuron morphology in segment A1. Cyan and red dots indicate input and output synapses, respectively. Top, dorsal view; bottom, transverse view.
(B) Connectome of input synapse onto DnB neurons in right and left A1 hemisegments. Numbers of synaptic connections between segment A1 neurons in top row and DnB neurons are shown. Width of arrow corresponds to degree of synaptic connectivity. Circles represent individual neurons, and hexagons represent groups of neurons.
(C) Percent of input provided to total postsynaptic sites on right and left A1 DnB as a function of cell class (not restricted to segment A1). cIV nociceptors provide dominant input to DnBs.
(D) Electron micrographs of DnB-cIV and DnB-cIII synapses.

Figure 3.3: DnB neurons received polarized input from sensory neurons

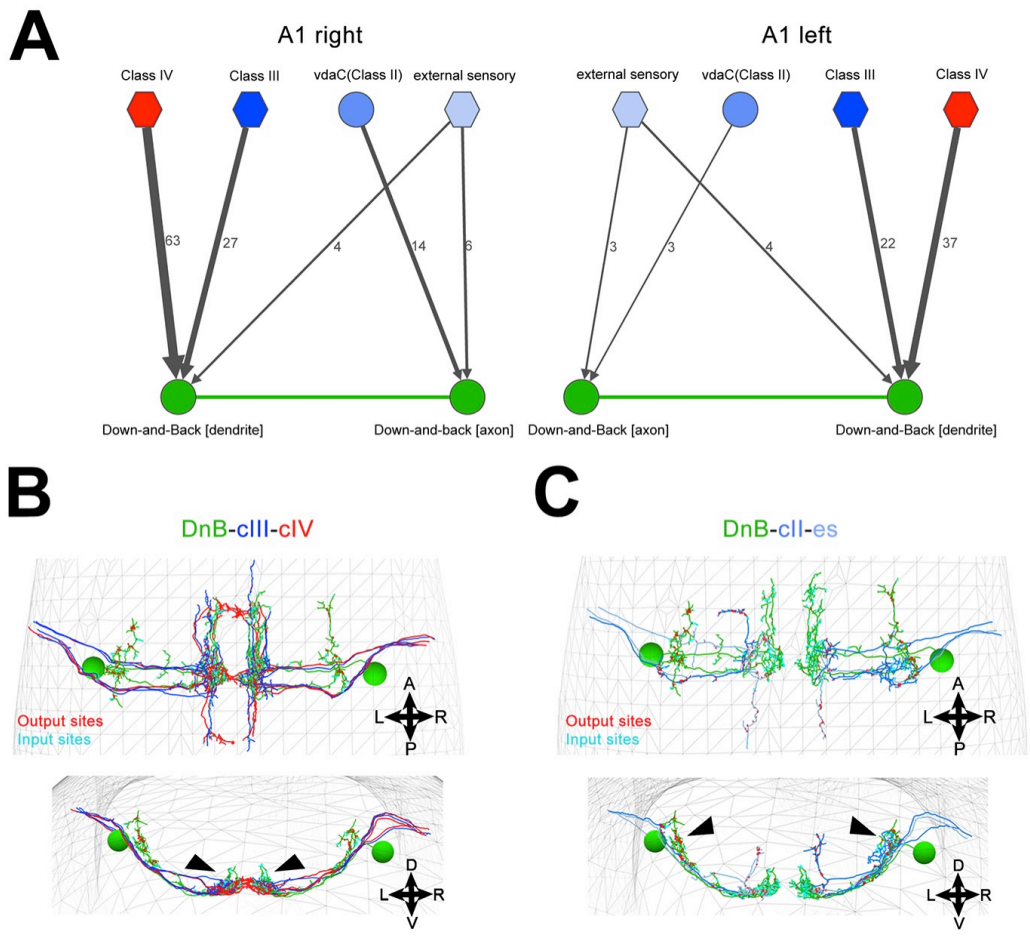

Figure 3.3: DnB neurons receive polarized input from sensory neurons

(A) Connectome of sensory input onto DnB axon vs. dendrite in right and left A1 hemisegments. Numbers of synaptic connections between sensory neurons in top row and DnB neurons are shown. Width of arrow corresponds to degree of synaptic connectivity. Circles and hexagons represent individual neurons, and groups of neurons, respectively.

(B) Reconstruction of DnB neurons synapsing with cIII (blue) and cIV (red) axons. Arrowheads indicate region of synaptic connections between DnB dendrites and cIII, cIV axons. Presynaptic sites in red, postsynaptic sites in cyan.

(C) Reconstruction of DnB neurons synapsing with cII (blue) and es (light blue) axons. Arrowheads point to connectivity between postsynaptic sites on DnB axon and cII, es axons. Presynaptic sites in red, postsynaptic sites in cyan.

Figure 3.4: DnB neurons target premotor and nociceptive outputs

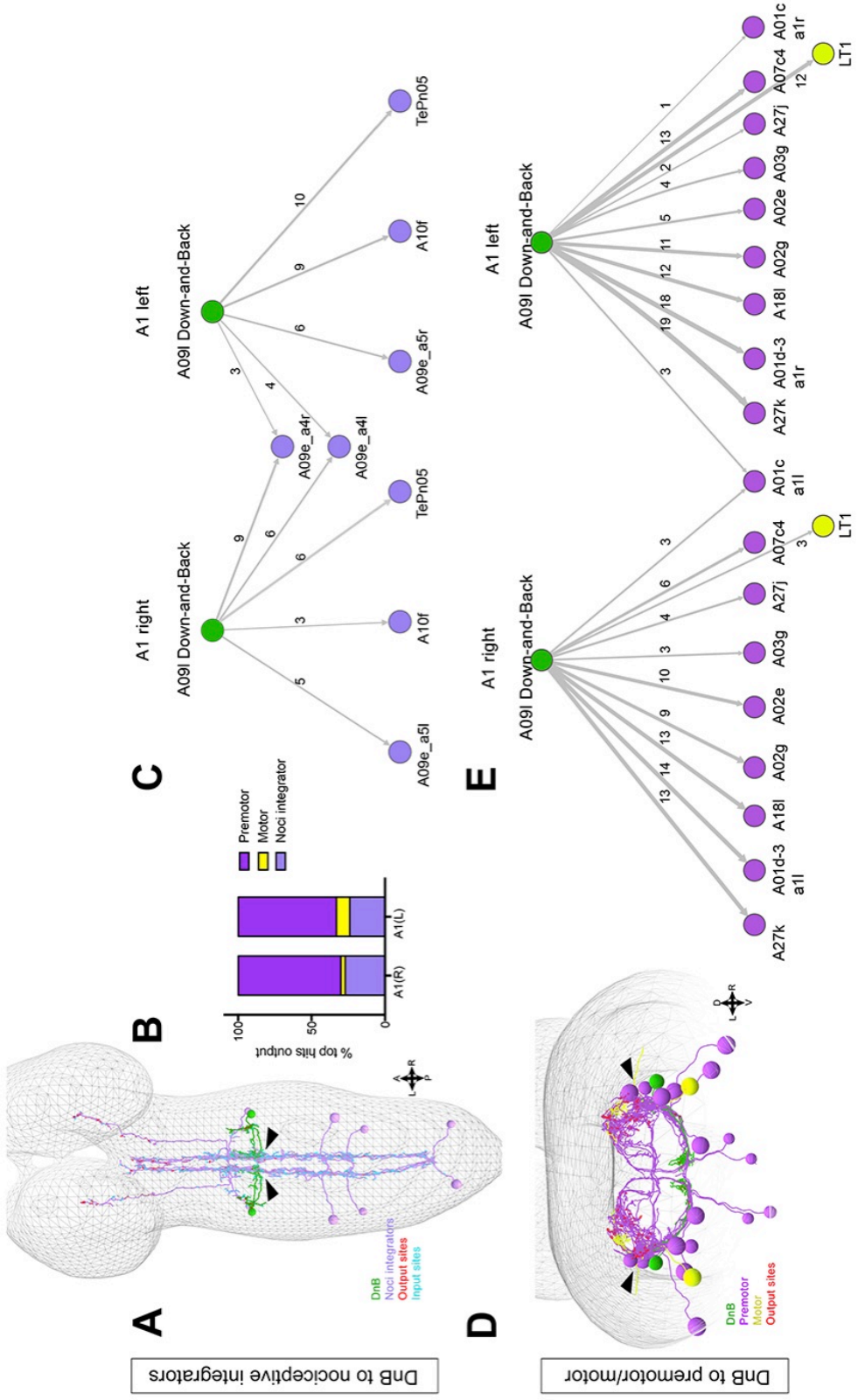

Figure 3.4: DnB neurons target premotor and nociceptive outputs

(A) First instar larval CNS showing reconstruction of DnB neurons (green), and nociceptive integrating interneurons (purple). Output synapses are indicated in red and input synapses in cyan. Nociceptive interneurons primarily receive input from output sites on DnB dendrites.

(B) Percent of top hits' (>3 synapses) output from right (DnB a1r) and left (DnB a1l) A1 DnB neurons as a function of cell type. Premotor circuits and nociceptive integrators are dominant outputs of DnB neurons.

(C) Identities of nociceptive integrating targets for right and left DnB neurons in A1. Numbers of synapses reconstructed are indicated. Width of arrow corresponds to degree of synaptic connectivity.

(D) First instar larval CNS showing reconstruction of DnB neurons (green), premotor (purple), and motor targets (yellow). Premotor neuron output synapses (red dots) located primarily in motor domain (arrowhead).

(E) Identities of premotor targets for right and left DnB neurons in A1. Numbers of synapses reconstructed are indicated. Dominant outputs are A27k and A01d-3 premotor neurons. Width of arrow corresponds to degree of synaptic connectivity.

Figure 3.5: EM reconstruction of downstream neurons

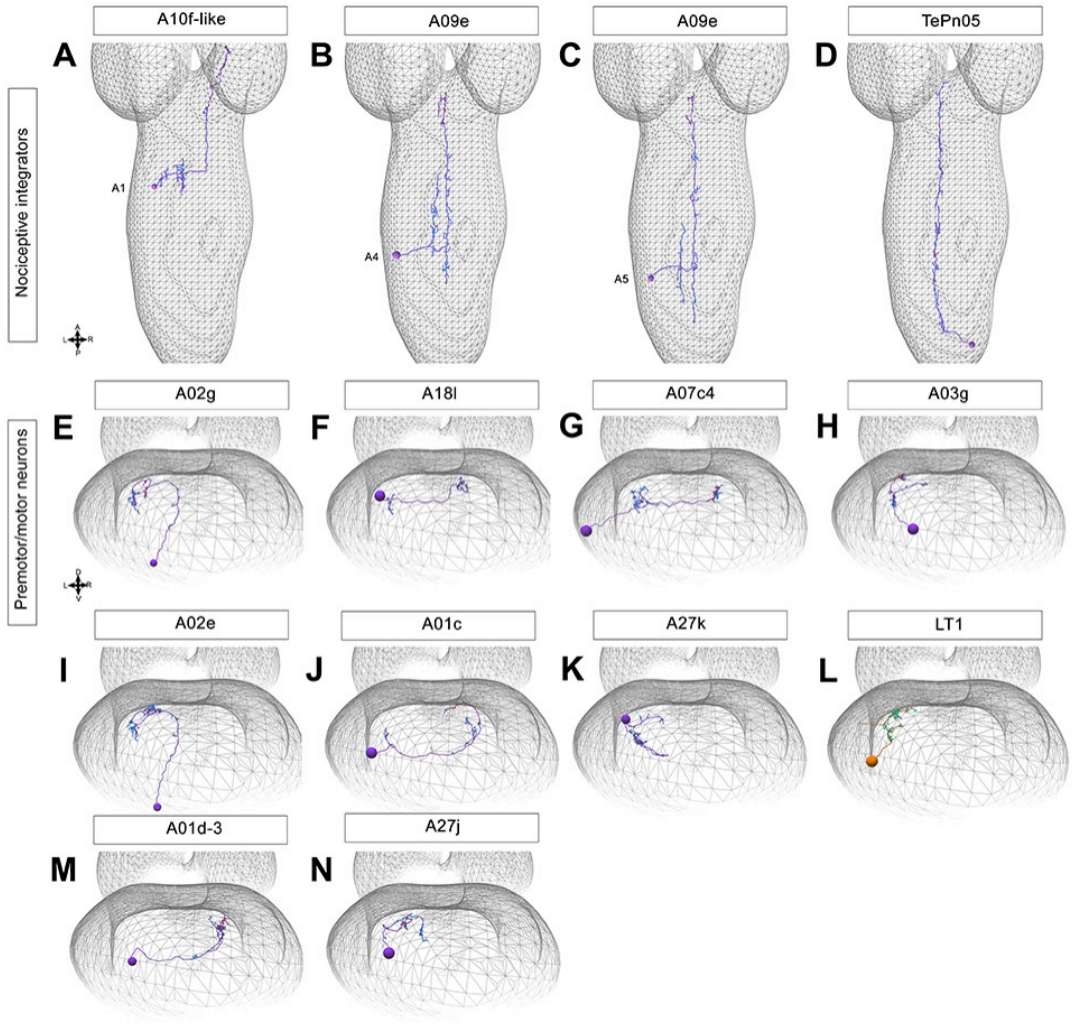

Figure 3.5: EM reconstruction of downstream neurons

(A-D) Neural reconstructions of 'nociceptive integrator' neurons downstream DnB neurons

(E-N) Neural reconstructions of premotor neurons (purple) located in segment A1 and one motor neuron class (orange) downstream DnB neurons. Presynaptic sites labeled in red, and postsynaptic sites in cyan. CNS mesh provided by Philipp Schlegel.

Figure 3.6: DnB synapses accumulate dense core vesicles

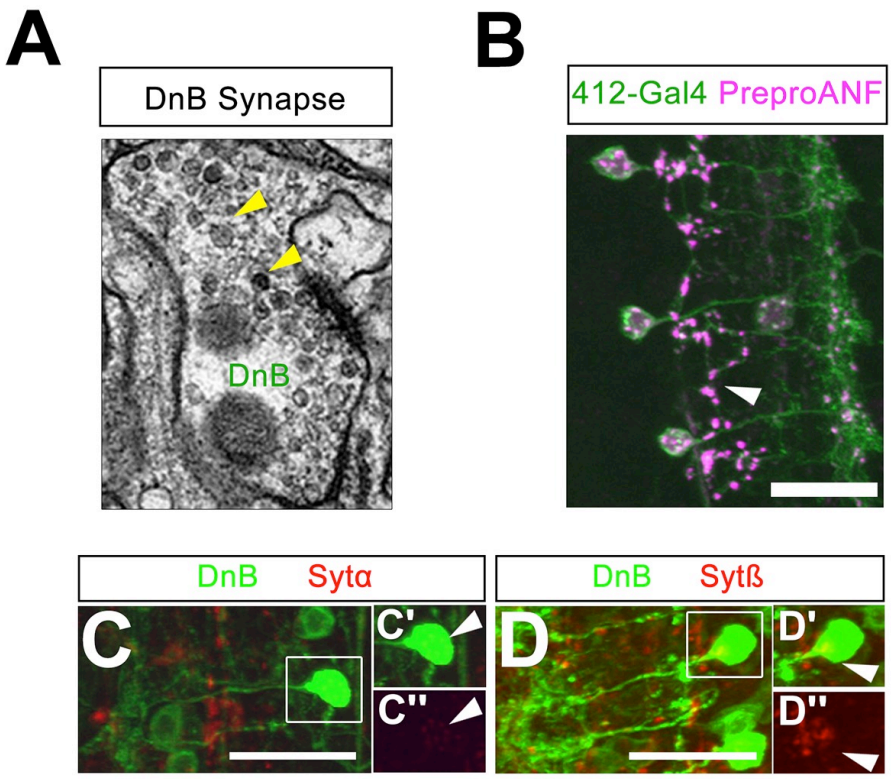

Figure 3.6: DnB synapses accumulate dense core vesicles

(A) Electron micrograph of DnB synapse showing dense core vesicles (arrowheads) indicative of peptidergic or aminergic release

(B) Neuropeptide precursor, PreproANF fused with emerald GFP (anti-GFP, magenta) is processed and expressed in DnB axons (arrowhead; anti-dsRed, green), suggesting that DnBs are peptidergic.

(C) DnB neurons labeled with GFP (anti-GFP, green) do not overlap with synaptotagmin−α (anti-SYT-α, red) Boxed region around DnB soma shown in (C') (arrowhead) GFP and SYT-α channels and (C'') SYT-α channel only

(D) DnB neurons labeled with GFP (anti-GFP, green) do not overlap with synaptotagmin-ß (anti-SYT-ß, red) Boxed region around DnB soma shown in (D') (arrowhead) GFP and SYT-ß channels and (D'') SYT- ß channel only
Scale bar: 20 µm (B-D)

Genotypes: (B) *UAS-Prepro:ANF-EMD;;412-Gal4,UAS-TdTomato/+* (C-D) *412-Gal4,UAS-CD8-GFP/+*

Figure 3.7: Silencing PMSI premotor neurons reduces rolling

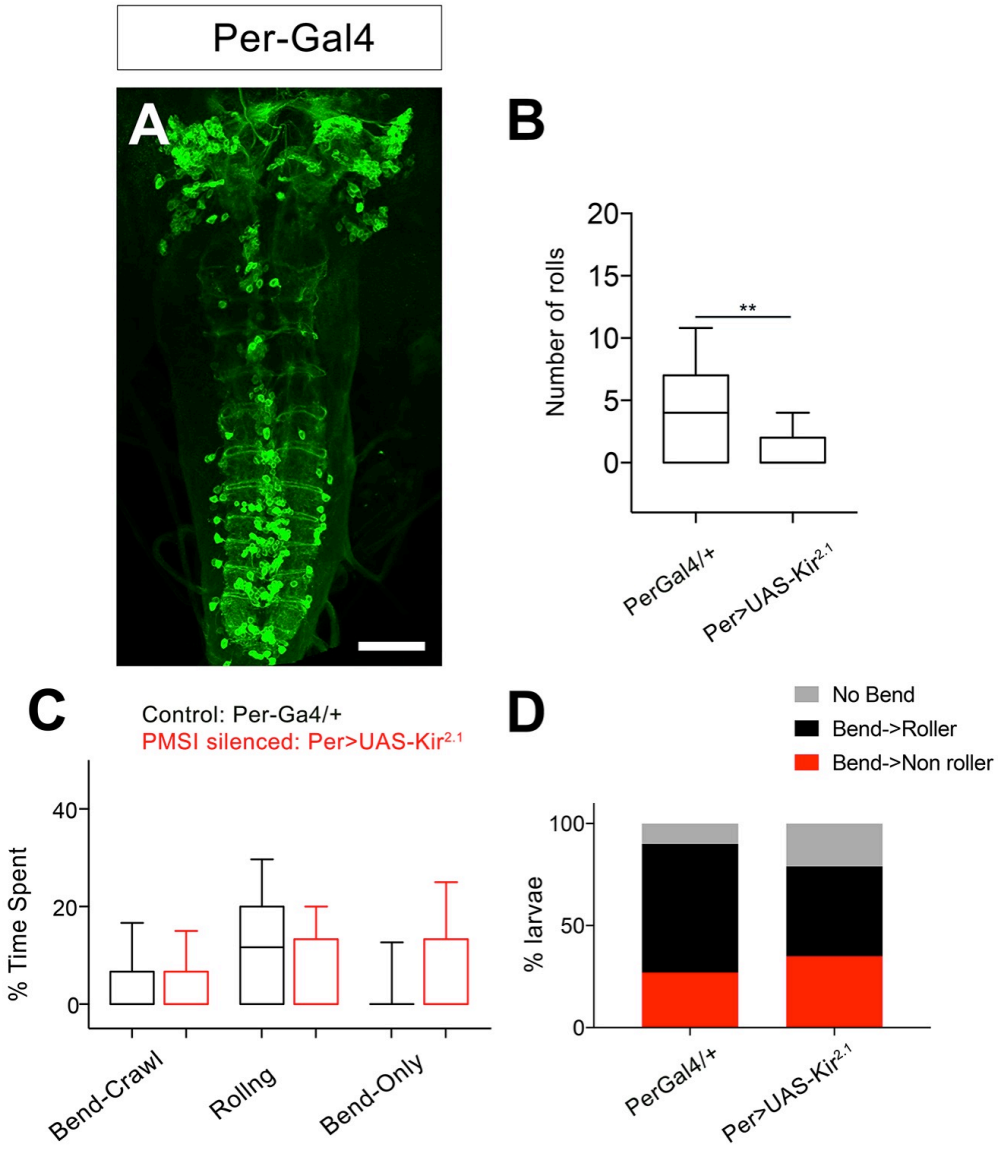

Figure 3.7: Silencing PMSI premotor neurons reduces rolling

(A) Expression pattern of *Per-Gal4*, which includes PMSI premotor neurons in the VNC

(B) Number of rolls decreases upon *Per-Gal4* silencing during global heat assay

(C) Percent of time spent engaged in Bend-crawl, Rolling, or Bend-only behavior upon *Per-Gal4* silencing

(D) Percent of larvae engaged in No-bend, bending followed by rolling: Bend→Roller, or bending without rolling: Bend→ Non Roller

Scale bar: 50μm (A)

Genotypes: (A) *Per-Gal4/20x-UAS-CD8-GFP; 412-QF, QUAS-TdTomato/+* (B-D) (i) *PerGal4/+* (ii) *PerGal4/+; UAS-Kir$^{2.1}$-eGFP*

Box plots show median (middle line) and 25th to 75th percentiles with whiskers representing 10 to 90 percentiles. P values are indicated as **p=0.0027, as determined by Mann Whitney test

Figure 3.8: DnB neurons are functionally connected to Goro circuits

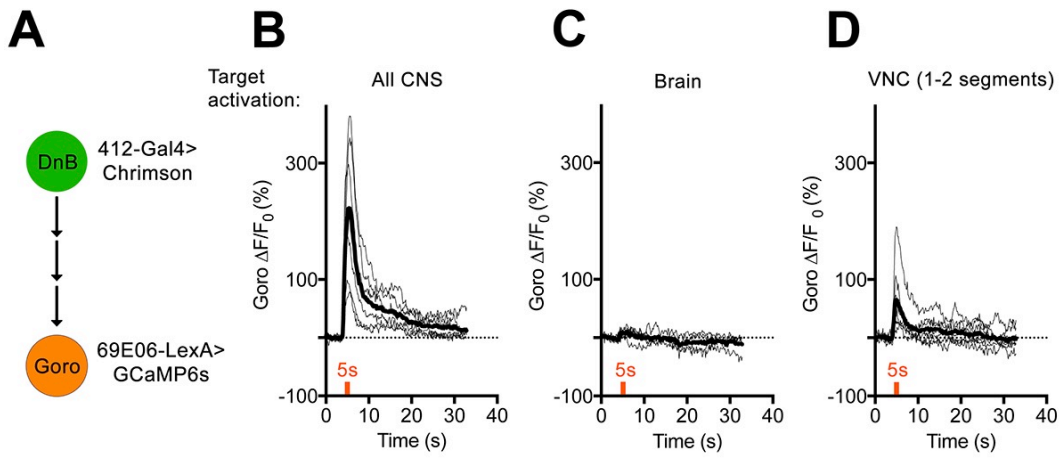

Figure 3.8: DnB neurons are functionally connected to Goro circuits

(A) Experimental setup for Goro imaging experiments. Activity in DnB neurons is driven by *UAS-Chrimson* expression optogenetic stimulation across the entire CNS (A), brain only (B) or 1-2 segments of DnB neurons in segment A4-6 VNC (C). GCaMP6s was targeted to Goro neurons using *69E06-LexA* to monitor calcium responses.

(B) dF/F_0 measured in Goro axons (n=6) upon full CNS optogenetic activation of *412-Gal4* neurons.

(C) dF/F_0 measured in Goro axons (n=4) upon brain only (lacking DnBs) optogenetic activation of *412-Gal4* neurons.

(D) dF/F_0 measured in Goro axons (n=7) upon optogenetic activation of 1-2 segments (includes DnB neurons)

Genotypes: (B-D) *R69E06-LexAp65/+;20xUAS-CsChrimson-mCherry,13xLexAop2-IVS-GCaMP6s- p10/412-Gal4*

Figure 3.9: Connectivity between DnB and Goro circuits

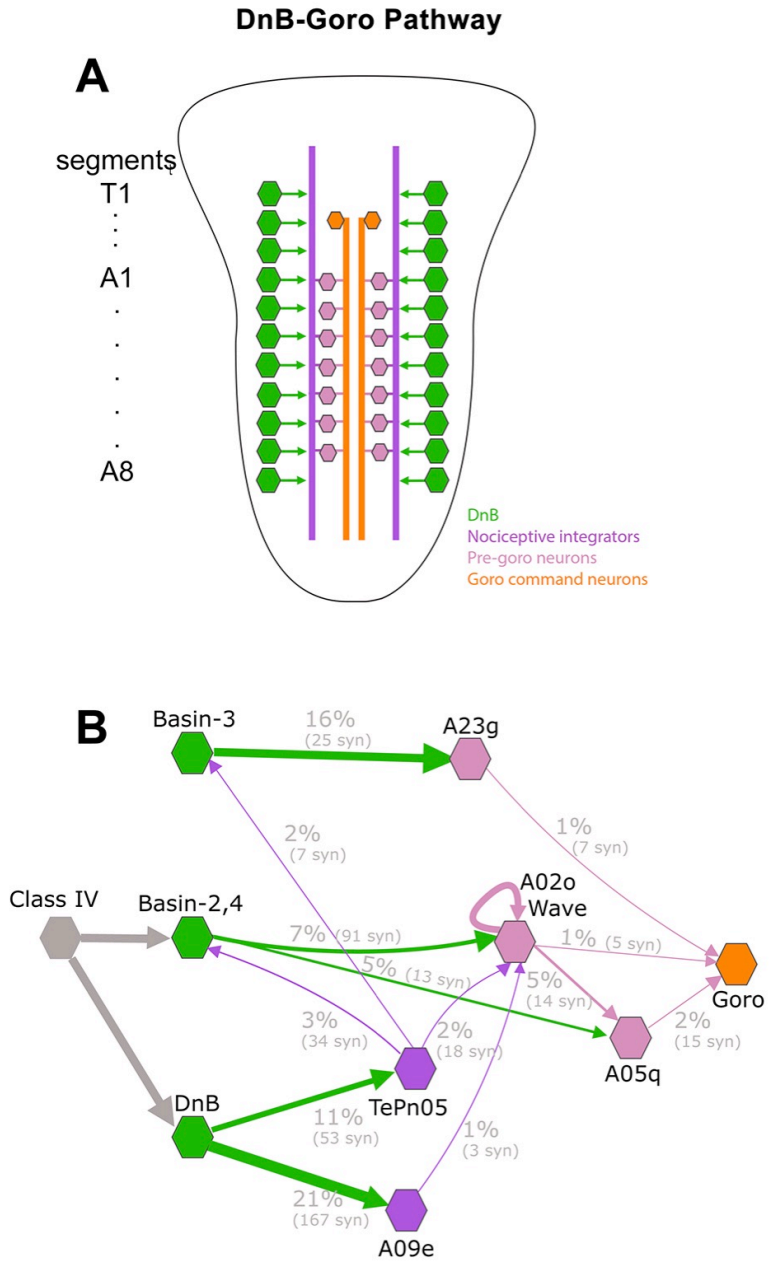

Figure 3.9: Connectivity between DnB and Goro circuits

(A) Schematic representation of DnB to Goro pathway. DnB neurons (green) synapse with neurons traversing the nerve cord (purple), which provide input to segmentally repeated neurons (pink) presynaptic to Goro (orange).

(B) Wiring diagram of DnB neurons to Goro rolling command-like neuron. Percentage represents fraction of total dendritic inputs provided by upstream neuron class. Percentages may underestimate contribution of neuron class due to lack of data from all segments. Number of reconstructed synapses is indicated in parentheses.

Circuit diagram: DnB group; A09l Down-and-Back (T3 A1 A2 A3 A4 A5 right/left); Basin-2,4 group: A09a Basin-2 (A1 left, A2 right, A3 right, A4 right/left), A09c Basin-4 (A1 left/right, A3 left, A4 left); Basin-3 group: A09g Basin-3 (A1 right/left, A4 right); A09e group: A09e (A4 right/left, A5 right/left); TePn05 group: TePn05 class-IV related projection C (Right/Left); A02o Wave (T3 A1 A2 A3 A5 right/left, A4 A6 Left); A23g group: A23g (A1 right/left, A2 right/left); A05q group: A05q (A1 right/left); Goro group: Goro (T2 right/left)

Figure 3.10: DnBs promote rolling, but not body bending, through Goro network

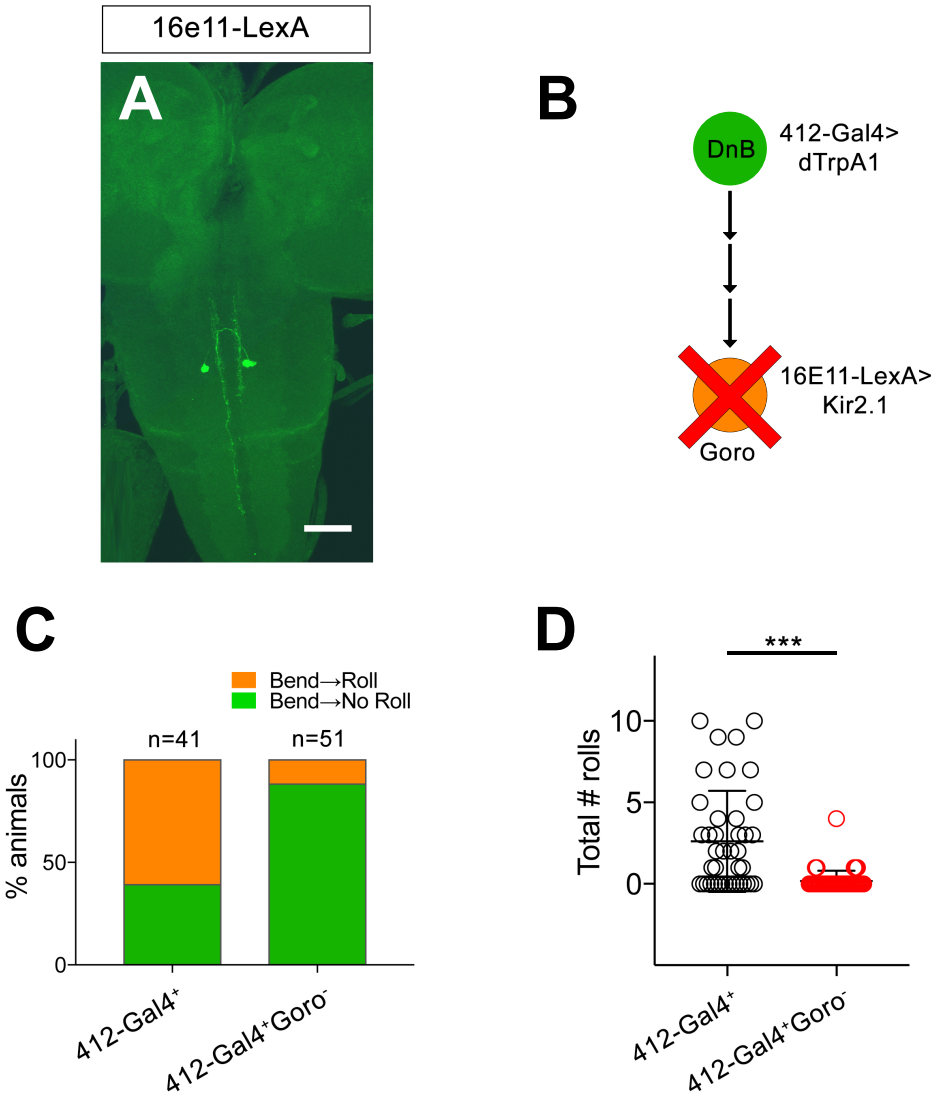

Figure 3.10: DnBs promote rolling, but not body bending, through Goro network

(A) Expression pattern of *16e11-LexA* labeling only Goro neurons

(B) Experimental setup for DnB thermogenetic activation and Goro silencing.

(C) Thermogenetic activation of *412-Gal4* neurons (*412-Gal4*$^{+}$) leads to dominant bend-roll nociceptive phenotype (bend→roll, orange). A minority of larvae show bending

without rolling responses (bend→ no roll, green). Coincident silencing of Goro neurons (*412-Gal4*$^{+}$*Goro*$^{-}$) subdues rolling responses but does not disrupt bending.
(D) Total number of rolls shown by control larvae (*412-Gal4* thermogenetic activation; black open circles) and upon Goro silencing (red open circles).

Scale bar: 40μm (A)

Genotypes: (A) *16e11-LexA/+;13xLexAop2-IVS-myr::GFP/+* (B) (i) *LexAop-Kir2.1/+;412-Gal4/UAS-dTrpA* (ii) *LexAop- Kir2.1/16e11-LexA;412-Gal4/UAS-dTrpA*

Scatter plot represents values for all animals tested with median (middle bar) and error bars representing standard deviation (SD). P values are indicated as ***p<0.0001, as determined by Mann Whitney test

Chapter IV:

Mechanosensory modulation of nociceptive behavior via Down-and-Back neurons

Abstract

Somatosensory circuits receive and integrate inputs to generate motor responses that are appropriate for combinations of stimuli. Nociception is the detection and avoidance of potentially harmful stimuli. The modulation of nociceptive input by additional somatosensory modalities remains incompletely understood. In *Drosophila* larvae, the class III (cIII) and class IV (cIV) dendritic arborization (da) neurons function as mechanosensors and nociceptors, respectively. Their axons project to specific locations in the neuropil, reminiscent of vertebrate dorsal horn organization. Here, I report that nociceptive interneurons, Down-and-Backs, also receive spatially segregated input from class III gentle touch-sensing neurons. Behavioral analyses suggest that the timing of cIII activation determines its effect on cIV induced nocifensive behavior. I show that low intensity co-activation of cIII and DnB neurons can enhance likelihood of displaying DnB-mediated C-shape bending. Finally, I present functional imaging techniques that can be used to probe somatosensory integration in DnB neurons. These results identify an anatomical locus for modulation of nocifensive behavior by input from gentle touch receptors.

Introduction

The combination of sensory cues detected by the nervous system gives rise to our multifaceted sensory experience. For instance, flavor results from the synergistic interactions between gustatory, olfactory, tactile, and even visual input (Yarmolinsky et al., 2009). Aside from enhancing our sensory experience, multisensory integration allows us to discriminate between different sensory events. These computations are particularly important in situations when multisensory information is weak, but could potentially signal danger (Stein and Stanford, 2008). Gaze orienting behaviors, allowing animals to turn towards the sound of a potential threat, combine visual, auditory, and somatosensory input, and have been well studied in the superior colliculus (SC) of cats. Visual and auditory stimuli presented in the same receptive field of an SC neuron, will yield an increase in firing pattern greater than when either stimulus is presented on its own (Alvarado et al., 2007). However, these studies often take place in higher order brain centers and less is known about integration during the first levels of sensory relay.

Recent work in the vertebrate spinal cord is beginning to reveal the degree of multisensory integration (sensory inputs converging onto a neural population) and cross-talk (sensory modalities influencing each other through local interneurons). The gate control theory posits that mechanosensory input can inhibit nociceptive transduction to the brain. Potential neural substrates for this theory were identified as C-fiber nociceptors and Aß mechanoreceptors converging on excitatory neurons marked by the somatostatin, that could be inhibited indirectly through Aß input via inhibitory dynactin positive neurons (Duan et al., 2014). In another study, activity of NPY-receptor 2 expressing A-fibres, mediating mechanical nociception, were inhibited by low-threshold mechanoreceptors (Arcourt et al., 2017). Low-threshold mechanoreceptors have also been shown to gate mechanically-evoked itch, potentially through inhibitory neurons in

the spinal cord (Bourane et al., 2015; Duan et al., 2017). Therefore, spinal circuits possess some degree of multisensory convergence onto common targets and cross-modal communication via local interneurons, yet without knowing the underlying neural connectivity, it is difficult to determine the extent of multisensory modulation, and its role on sensory-evoked behavior.

In the previous chapter, I used electron microscopic (EM) reconstruction to show that Down-and-back (DnB) interneurons in *Drosophila* larvae receive both nociceptive input, through class IV dendritic arborization neurons, and mechanosensory stimuli, mostly via class-III gentle-touch sensing neurons. The impact of gentle-touch and nociceptive integration at the first somatosensory relay, and its effect on nocifensive behavior (defensive withdrawal to noxious stimuli) has not been extensively studied.

Here, I show that a population of second-order somatosensory neurons, Down-and-Backs (DnBs), receive input from nociceptive sensory neurons and spatially-segregated terminals of touch receptive class III (cIII) da neurons, suggesting that they comprise a node for multimodal integration in the nociceptive circuit that may be analogous to that observed in mammals. This study provides evidence that mechanosensory input modulates nociceptive behavioral responses triggered by cIV nociceptors, and DnB neurons. These findings reveal a novel component of the nociceptive circuit and provide an entry point for studying the impact of nociception and tactile integration on generating nocifensive motor outputs.

Results

DnB neurons receive spatially segregated gentle-touch input

EM reconstruction of Down-and-Back upstream circuitry revealed that DnBs received input from mechanoreceptors (22%), including 15% from gentle-touch sensing class III (cIII) neurons. I co-labeled DnB neurons and cIII gentle-touch sensory axons to

visualize connectivity among these populations of neurons. cIII gentle-touch axons occupy a domain just lateral to cIV axon terminals (Figure 4.1A-A')(Grueber et al., 2007). Co-labeling with *412-Gal4* and the cIII/chordotonal marker *nompC-LexA* (Shearin et al., 2013) revealed overlap between cIII axons and the lateral region of DnB dendrites (Figure 4.1B-B''). Next, I used the synapse-restricted, activity dependent, GFP reconstitution across synaptic partners (GRASP) technique (Feinberg et al., 2008; Gordon and Scott, 2009; Macpherson et al., 2015) (Chapter II) to visualize connectivity between cIII sensory neurons and DnBs *in vivo*. Expression of n-syb-GFP$^{1-10}$ in cIII neurons using *nompC-QF* and CD4-GFP^{11} using *412-Gal4* produced GFP reconstitution (Figure 4.1D) in two parallel bands lateral to cIV axonal termination sites. *nompC-QF* also strongly labels chordotonal (chd) sensory neurons (Figure 4.1C), which synapse with nociceptive interneurons, Basins (Ohyama et al., 2015). Yet, I only observed reconstitution between DnBs and class III neurons (Figure 4.1D). No fluorescence was observed when expressing n-syb-GFP$^{1-10}$ alone (Figure 4.1E). These results support the EM reconstructed connectivity between DnB dendrites and cIII sensory neurons, and indicate that cIII targets a distinct non-overlapping region of the DnB dendritic arbor relative to cIV nociceptive axons.

Mechanosensory modulation of nociceptive escape behavior

To begin assessing the role of mechanosensory convergence onto DnB neurons, I asked whether DnB neurons were required for gentle-touch evoked behavior.
To test gentle-touch behavior, I scored responses to gentle-touch stimuli using the Kernan score system (Kernan et al., 1994) where 0= no response, 1=pause, 2= turn or anterior withdrawal, 3= single reverse contraction, and 4= multiple reverse contractions. Animals were tested four times, and cumulative scores were averaged per animal tested. Control animals, expressing an inactivated form of tetanus toxin (TNTi; Sweeney,

1995} in *412-Gal4* neurons, had a median Kernan score of 8, with high frequency of turning/anterior withdrawal behaviors (Figure 4.2) Silencing DnB neurons using *412-Gal4* to drive TNT (Sweeney et al., 1995) did not significantly disrupt median gentle-touch responses (Median Kernan score =7)(Figure 4.2A). However, animals did perform a wider range of behaviors with a higher frequency of non-responders (Score 0) and reverse locomotion (Score 3-4). Although I cannot eliminate the possibility that DnB neurons play a role in enhancing reliability of light-touch responses, our previous data indicate that across different activation intensities, DnB activity does not produce gentle-touch responses (Chapter II). Together, these data suggest that DnB neurons predominantly drive nocifensive behavior and raise the possibility that cIII mechanosensory input could be modulating nocifensive behavior.

First, I explored the potential role of class III gentle-touch modulation of nociceptive outputs. I co-activated cIII and cIV neurons by driving dTrpA1 using the cIV driver *ppk*$^{1.9}$*-Gal4* (Ainsley et al., 2003) and the cIII driver *R83B04-Gal4* (Figure 4.3A). I compared responses upon cIII/cIV co-activation to responses when only cIV neurons were activated (Figure 4.3B). cIII/cIV co-activation did not prevent rolling, nor did it affect time spent rolling compared to cIV activation alone (Figure 4.3C). However, I did find that during cIII/ cIV co-activation, animals showed a significantly longer latency to initiate rolling (Figure 4.3D). These data suggest that activation of cIII neurons can inhibit or delay the onset of nociceptive behavior induced by cIV activity. One caveat is that strongly co-activating cIII and cIV neurons might not recapitulate naturalistic integration of these circuits, and instead this inhibition of nociceptive behavior could be a result of competition for motor circuits between cIII and cIV downstream circuitry.

In parasitic wasp attacks, mechanical sensing of the predator would normally precede noxious oviposition-related stimuli. I therefore asked whether varying the timing of cIII input might enhance or reduce cIV-induced nocifensive behavior. I activated cIII

neurons using *R83B04-Gal4* (Jenett et al., 2012) to drive dTrpA for 10 seconds prior to activating cIV neurons optogenetically using *dTrpA-QF* to drive *QUAS-ReaChR*. First, I tested animals raised in the absence of ATR (co-factor required for channelrhodopsin function) to measure class III-induced behaviors, and observed characteristic gentle-touch responses: scrunching and backwards crawling (Figure 4.4A). Notably, cIII activated animals displayed some rolling during lights ON condition (10% of trial time, n=30), while scrunching was terminated, resulting either from the effect of blue light, or from low level activation of class IV neurons in the absence of ATR. Next, I assessed cIV optogenetically evoked behaviors by testing animals at 25˚C, which did not activate class III neurons thermogenetically. I found a modest increase in time spent rolling (Figure 4.4B) during optogenetic cIV activation, which increased when class III input was presented prior to cIV activation (Figure 4.4B). To characterize the enhancement of cIII input on nocifensive rolling, I compared the number of rolls elicited by cIII → cIV activation, compared to class III or IV activation alone, and found that rolling significantly increased when cIII neurons were activated before cIVs (cIV only, median=0; cIII only, median=0; cIII→cIV, median=1.5). Together, these data suggest that cIII inputs enhance nociceptive behavioral outputs if received prior to cIV activation.

If class III input has the potential to enhance class IV-induced rolling behavior, I asked whether co-silencing these populations would exacerbate deficits to noxious heat stimuli upon class IV silencing. When I silenced cIV neurons and tested responses to local noxious heat stimuli by applying a heat probe (~50 degrees) to the body wall, I found a reduction in rolling, and withdrawal behavior (where animals bend away from heat probe, but do not perform rolling). However, silencing cIII mechanosensory neurons did not affect rolling or withdrawal behavior. Co-silencing both cIV and cIII populations does not eliminate all responses to local noxious heat stimuli, and the proportion of responders is similar to that of class IV silencing alone. These data provide evidence

against a role for class III neurons in responses to local heat noxious stimuli. However, these results are not necessarily inconsistent with my previous sequential cIII → cIV activation data, as cIII input could have a selective modulatory effect on mechanical nociception.

Mechanosensory modulation of DnB mediated motor outputs

Since my data suggested that mechanosensory cIII input could enhance nocifensive responses if presented prior to cIV activation, I asked whether cIII modulation of nocifensive behavior could be acting, at least in part, through DnBs. I found that activation of cIII neurons strongly inhibited the robust rolling behavior observed upon *412-Gal4* activation (Figure 4.6A). These data are consistent with the delay in rolling behavior upon cIII/cIV co-activation. Again, I explored an alternative behavioral paradigm to elucidate the role of cIII input on DnB-mediated outputs. I asked whether subthreshold thermogenetic activation of DnBs (i.e. insufficient to elicit rolling) could be enhanced by co-activation with cIII mechanosensory neurons (Figure 4.6B). Coincident activation of cIII and DnB populations, using *83B04-Gal4* and *412-Gal4* to drive dTrpA, slightly increased the percent of time spent rolling, and number of rolls, but increased time spent engaging in bend-only behavior (Figure 4.6C-D). These data suggest that at low levels of activation, cIII input might enhance DnB activity and increase C-shape bending, which could lead to increased probability of rolling behavior.

Preliminary development of functional imaging techniques for probing nociceptive and mechanosensory integration

Behavioral analyses of nociceptive and mechanosensory integration suggested that cIII input can modulate nocifensive escape behavior, potentially through DnB neurons. Functional imaging would provide a physiological understanding for DnB integration of cIII and cIV inputs. I performed calcium imaging on dissected larval CNS

preparations, using *412-Gal4* to express GCaMP6m in DnB cell bodies. First, I established this protocol by using 70mM KCl to broadly depolarize neurons. I observed robust calcium transients in response to KCl application and not with saline application (Figure 4.7A-B). Since I could not precisely control the time of application with the initial set of experiments, I compare the initial frame (pre-stimulus) to the peak fluorescence (F_{max}) (Figure 4.7A). I detected a similar degree of increased fluorescence upon KCl application across animals (Figure 4.7C). Next, I expressed ATP-activated cation channel, P2X2 in class IV neurons using the *38A10-LexA* driver. Upon ATP application, I observed robust calcium transients in 1/3 somas monitored, and a slight increase in 1/3 somas (Figure 4.7D). When I used this method to activate cIII neurons using *83B04-LexA* (Galindo, unpublished), I observed an increase in GCaMP fluorescence in DnB neurons (1/1 soma) (Figure 4.7E). I also imaged from DnB dendrites and found increases in fluorescence following both cIII (1/1 animal) and cIV activation (5/5 animals) (Figure 4.7F). Unlike cell bodies which are easily detected with baseline GCaMP fluorescence, dendrites were difficult to identify, and were not analyzed because I could not determine a pre-stimulus region of interest. Finally, I co-activated cIII and cIV neurons and detected increases in 1/2 animals imaged (Figure 4.7G). My preliminary data suggests that cIV can directly activate DnB neurons, but the number of cells monitored was too small to draw conclusions regarding the effect of cIII input on DnB activity. Potential improvements could include leaving somatosensory neurons intact with the larval body wall, activating only a few somatosensory nerves at once (locally applied ATP), and labeling DnB anatomy for reference with a red fluorophore. Upon further adjustment, this setup can be used to determine how DnB neurons respond to concurrent activation of cIII and cIV vs. cIII or cIV activation alone. These functional data will allow us to probe integration between mechanosensory and nociceptive stimuli at the first relay of somatosensory processing.

Discussion

Addressing how somatosensory input is transmitted and integrated by central circuits in model organisms that show robust behaviors, yet relatively simple nervous systems, might illuminate conserved mechanisms for sensory-motor processing. Here, I provide insight into the behavioral implications of mechanosensory and nociceptive integration at the first relay element of somatosensation. I show that Down-and-Back interneurons receive spatially segregated input from class III (cIII) gentle-touch sensing and class IV (cIV) nociceptive sensory neurons. The behavioral data suggests that the timing and level of cIII activation determines its effect on nocifensive behavior. These findings provide a handle for understanding how input from multiple, functionally distinct, classes of somatosensory is integrated.

Mechanosensory and Nociceptive spatially segregated axonal targeting of DnB dendrites

Prior results identified spatial segregation of axonal terminals of cIII and cIV neurons, and proposed that this arrangement might underlie connectivity with distinct central targets (Grueber et al., 2007). While it is likely that at least some targets are distinct, these results here reveal a population of second-order neurons that span the cIII-cIV target area. Thus, in this instance, axon terminal segregation leads to synaptic connectivity on distinct regions of a common dendritic target. The locations of synaptic inputs along a dendritic arbor can have profound impacts on dendritic integration. For instance, if inputs from the same pathway cluster in similar regions of a dendrite then it is easier to activate or suppress their activity collectively, without greatly impacting pathways targeting distinct regions of the dendritic arbor (Kastellakis et al., 2015; Yang

et al., 2016). Future studies of DnB neurons might reveal the molecular underpinnings, and functional consequences of this laminar dendritic targeting of afferents.

Behavioral consequences of nociceptive and mechanosensory integration

Integration of sensory inputs improves behavioral selection by enhancing the salience of a sensory event. More specifically, sensory input convergence can increase (superadditive integration) or decrease (subadditive integration) neural activity, which could impact the activation of downstream motor patterns (Alvarado et al., 2007; Stein and Stanford, 2008). Sensory integration and cross-talk can take place across multiple levels of sensory processing (Ohyama et al., 2015; Prescott et al., 2014; Stein and Stanford, 2008). The anatomical and behavioral results I present suggest that DnBs represent a point of multimodal integration early in the nociceptive circuit for integration of cIII and cIV inputs. In response to touch stimuli larvae pause, recoil, turn, or reverse the direction of movement (Kernan et al., 1994; Yan et al., 2013), which is distinct from the rolling, body bending, and fast escape crawl characteristic of nocifensive behaviors. Silencing DnB neurons did not significantly alter gentle-touch responses, and gentle-touch behaviors were not observed during *412-Gal4* activation across various activation intensities, suggesting that DnB neurons do not play a prominent role in generating gentle-touch behaviors, but instead cIII input might modulate nocifensive behavior. Coincident activation of cIII and cIV neurons led to a slight delay in rolling onset. Surprisingly, however, coincident activation of cIII and DnBs led to a strong inhibition of rolling. One possible interpretation of these results is that activation of parallel roll-promoting circuitry upon cIII/cIV activation can eventually overcome competition with cIII activation. By contrast, if cIII neurons are co-activated with DnBs, DnB downstream circuitry might be insufficient to overcome this competition for motor circuits.

We also provide evidence that cIII input can enhance both cIV- and DnB-triggered nocifensive behavior. Presenting cIII input prior to cIV activation increased the number of evoked rolls. Co-silencing cIII and cIV input did not enhance behavioral deficits to noxious heat compared to cIV silencing alone. These results do not exclude the possibility that cIII input could be enhancing nocifensive responses to mechanical nociception. Indeed, a recent study found that cII and cIII mechanosensory input is required for mechanonocicepion (Hu et al., 2017). They also found that silencing cII-cIII activity, surprisingly, abolished nocifensive rolling induced by harsh mechanical stimuli, although the bending remained largely intact. These data suggest that not only are there divergent circuits for mechanical and thermal nociception, but that components of the mechanical noxious response (bending vs. rolling) might be under the control of different microcircuits. Studying DnB function and mechanosensory integration in the context mechanical nociception would be an interesting future direction. Moreover, thermogenetically co-activating cIII/DnB neurons at an intensity that did not induce rolling in *412-Gal4* activation alone, modestly increased likelihood of rolling, and increased likelihood of performing C-shape bends. Since DnB neurons also receive input from additional mechanosensory subtypes (Chapter III) (class II, and es cells), co-activating with these groups along with cIII neurons might further enhance nociceptive responses. Interestingly, co-activating low-threshold mechanosensory and A-fibre nociceptive afferents enhances motor coordination of nocifensive paw withdrawal, pointing to potential parallels between vertebrate and invertebrate models of nociception.

Mechanosensory enhancement of nociceptive stimuli is consistent with the implications of vibration sensing chordotonals and noxious integration. The concurrent activation of chordotonals and cIV neurons increases likelihood of rolling escape behavior (Ohyama et al., 2015). Mechanosensory and nociceptive convergence might

facilitate selection of escape behavior in threatening situations where there are weak multimodal inputs (Stein and Stanford, 2008).

Recent work has implicated cIII neurons in cold nociception (Turner et al., 2016), suggesting that my manipulations could also be affecting cold nociceptive circuitry. Turner *et al*., also monitored behavior during cIII/cIV optogenetic co-activation over shorter time intervals, which could explain why they exclusively observed cold induced contraction (CT) phenotypes without nocifensive behavior. Gentle-touch also elicits recoil behavior, which might be difficult to distinguish from CT upon cIII activation. As our knowledge of nociceptive larval circuits continues to expand, it is likely that DnB neurons are not the only microcircuits integrating cIII and cIV input, but their early position in somatosensory processing, convergence of multiple mechanosensory subtypes, and important role in nociception makes them an interesting model for investigating mechanosensory modulation of nocifensive behavior.

Vertebrate analogies for mechanosensory and nociceptive integration

One popular theory describing the impact of tactile information on nociceptive transduction is the gate control theory (Melzack and Wall, 1965), which stipulates that a theoretical “T” neuron, converging tactile and nociceptive inputs, transmits nociceptive signals to the brain, and can be gated by mechanosensory feedforward inhibition via “IN” neurons. Duan *et al*., identified circuits that fit this description, such that upon co-activation of C-fiber/A*∂* nociceptors and Aß mechanoreceptors, DYN interneurons in the spinal cord gate mechanical pain by inhibiting SOM interneurons from relaying noxious input to the brain (Duan et al., 2014). Ablating SOM neurons does not affect innocuous touch responses. However, the interplay between these circuit elements is thought to mediate allodynia (the perception of non-noxious stimuli as painful) and the ability of gentle-touch to attenuate perceptions of pain (Duan et al., 2014). Similar to SOM

interneurons, DnBs are also dually innervated by tactile and nociceptive afferents and are preferentially required for nocifensive behavior. Future work could reveal whether cIII neurons also provide indirect inhibitory input to DnB neurons, and whether manipulating the properties of this microcircuit could induce 'allodynia' type of responses where gentle-touch induces nocifensive behavior. Given the possible analogies to vertebrate pain circuits, it will be important to elucidate the cellular and molecular basis for modulation of nociception by touch in this *Drosophila* circuit.

Methods

Fly Stocks

(1) *PB[IT.Gal4]0412* (referred to in the text as *412-Gal4*; (Gohl et al., 2011)), (2) *UAS-mCD8-GFP* (Lee and Luo, 1999), (3) *QUAS-syb-spGFP*$^{1-10}$ (Macpherson et al., 2015), (4) *UAS-CD4-spGFP*^{11}(Feinberg et al., 2008; Gordon and Scott, 2009), (5) *nompC-QF* (Bloomington Stock Center), (6) *20X-UAS-IVS-GCaMP6m* (Chen et al., 2013), (7) *UAS-dTrpA1* (Hamada et al., 2008), (8) *UAS-ReaChR* (Lin et al., 2013) (9) *UAS-TNT* and (10) *UAS-TNTi* (Sweeney et al., 1995), (11) *R38A10-LexA* (Jenett et al., 2012)(12) *R83B04-Gal4* (Jenett et al., 2012) (13) *ppk*$^{1.9}$*-Gal4* (Ainsley et al., 2003), (14) *nompC-LexA, 10X-lexAop2-myr-GFP/TM6B* (Shearin et al., 2013), (11) *R83B04-LexA* (Galindo, unpublished) (12) *TrpA-QF* (Petersen and Stowers, 2011), (13) *5XQUAS-ReaChR*:*tdTomato*, (14) QUAS-TdTomato

Immunohistochemistry

Immunohistochemistry was performed essentially as described (Matthews et al., 2007). Third instar larvae were dissected in 1X PBS, fixed in 4% paraformaldehyde (Electron Microscopy Sciences) in 1X PBS for 15 minutes, rinsed three times in 1X PBS + 0.3% Triton X-100 (PBS-TX), and blocked for 1 hour at 4°C in normal donkey serum (Jackson Immunoresearch). Primary antibodies used were chicken anti-GFP (1:1000; Abcam) and rabbit anti-DsRed (1:250, Clontech). Animals were incubated overnight in primary antibodies at 4°C, rinsed repeatedly in PBS-TX, and incubated overnight at 4°C in species-specific, fluorophore-conjugated secondary antibodies (Jackson ImmunoResearch) at 1:200 in PBS-TX. Tissue was mounted on poly-L-lysine coated coverslips, dehydrated in ethanol series, cleared in xylenes, and mounted in DPX (Fluka).

For GRASP experiments, third instar larval brains were dissected in 1X PBS and fixed in fresh 4% paraformaldehyde (Electron Microscopy Sciences) for 15 minutes. Brains were mounted in Vectashield (Vector lab) on poly-L-lysine coated coverslips, and imaged for native reconstituted GFP signal.

Behavioral analysis

For behavioral analysis, flies were reared at 25˚C and tested as wandering third instar larvae. For each experiment, at least three trials, taken on separate days, were performed for each genotype. Larvae were only tested once unless otherwise noted.

Thermogenetic activation

Third instar larvae were rinsed briefly in double distilled water and placed on a 1% agarose gels with 0.6% black ink (Super Black India ink, Speedball) heated to either peltier device (CP-031, TE technology) and temperature controller (TC-36-25-RS232, TE

technology) to heat the gel to 29-29.9˚C or 32.5˚C, depending on experimental condition. Animals displaying 360˚ rotations were classified as 'rollers'. 'Bend-roll' was counted as coincident C-shape bending and 360˚ rotation, 'Bend-crawl' was counted when animals persistently bent as they crawled and did not perform straight forward crawling, and 'Bend-only' behavior, was counted when animals remained in a curved posture without rolling or crawling. Trachea were used as a reference for bending and rolling categorization. Animal behavior was recorded using a Leica M50 camera along with Leica FireCam software and QuickTime screen capture for 30 seconds. Videos were quantified offline with experimenter blind to condition.

Optogenetic activation

For optogenetic experiments, I tested animals in a photostimulation arena (de Vries and Clandinin, 2013). Flies were raised on molasses food with or without 100mM all-*trans*-retinal (ATR). Third instar larvae were rinsed briefly in double distilled water and placed on a 100 x 15mm petri dish containing double distilled water blended with yeast particles to facilitate nocifensive behavior (S. Mauthner, personal communication). Larvae were recorded using DALSA Falcon 4M30 4 megapixel digital camera and CamStudio screen capture software with 10 seconds blue light off-10 second blue light on (23500 Lux). A dim red light was on for the entirety of the experiment to illuminate larvae during lights off periods (300 Lux). Videos were quantified offline.

For sequential activation, peltier device was placed in photostimulation arena. Animals were placed on first placed on 1% agarose with 0.6% black ink, heated to 32.5˚C, for 10s, followed by 10s of lights ON of blue light (23500 Lux). Gentle-touch behaviors (scrunching, backward crawling, and head swinging) and nocifensive rolling were quantified.

Local Heat Assay

Local heat assay was performed as previously described (Tracey et al., 2003) with slight modifications. Soldering iron (SKU25337, Sinometer) was used as a noxious thermal probe and the temperature was set to 51.6-55.5˚C by adjusting voltage using a variac (3PN1010B, Staco Energy). Digital thermometer (51 II, Fluke) with thermocouple temperature sensor was used to measure the temperature of the thermal probe. Larvae were lightly touched with thermal probe at segments 4-6 for 5 seconds. Animals were characterized as 'responder' if they performed 360˚ roll within 5 seconds, and 'non-responder' if they did not. Animal behavior was recorded using Leica FireCam and QuickTime screen capture. Videos were quantified offline with experimenter blind to genotype.

Gentle Touch Assay

For the gentle touch assay, experiments were conducted as previously described (Kernan et al., 1994). Third instar larvae were rinsed off in double distilled water, then left to acclimate on 1% agar for 3 minutes. Animals were tested on 1% agar 100 x 15mm petri dish and assigned a Kernan score for each behavior 1: hesitate, 2: anterior withdraw or turn, 3: single reverse wave, 4: multiple reverse waves. Experimenter was blind to genotypes during testing.

DnB neurons calcium imaging

Protocol is modified from (Ohyama et al., 2015). Third instar larval CNS was dissected in saline solution (108 mM NaCl 5 mM KCl 5 mM Hepes 5 mM Trehalose/2H_2O 10mM Sucrose 1mM NaH_2PO_4 2mM $CaCl_2$) (Wang et al., 2003). Brains were mounted on poly-L-lysine coated coverslips dorsal side up for soma imaging, and ventral side up for

dendritic imaging. Coverslip was placed in sylgard dish with 2mL of saline solution. Imaging was performed on LSM 510 or LSM 700 with 40X water immersion objective. 1mL of freshly prepared ATP diluted in saline (3.3 mM for soma imaging, and 10mM for dendritic imaging) or KCl (70mM) was applied during imaging. Trials consisted of three dimensional time lapse imaging with XY dimensions and 3 slices 5.02μm thick centered around soma or dendritic scaffold at a scan speed of 9 under pseudocolor Rainbow2. Each scan cycle lasted ~2.6 seconds. Images were analyzed using MATLAB (Mathworks). Polygon was drawn around region of interest (soma) based on baseline fluorescence. The baseline (F_o) was set as the average of the first 8 frames, and ΔF was calculated as $F-F_0$, where F is the raw fluorescent intensity of a given frame.

Statistical Analysis

When comparing two groups of quantitative data (e.g. number of rolls), unpaired t-test was performed if data showed a normal distribution (determined using D'Agostino & Pearson omnibus normality test) and Mann-Whitney test if data distribution was non-normal. When comparing three or more groups, data were analyzed using One-way ANOVA (normal distribution data) or Kruskal-Wallis test (non-normal distribution data) with Dunn's correction for multiple testing, followed by post-hoc T-test to determine exact p-value.

Acknowledgments

We are grateful to Drs. Richard Axel and Charles Zuker for fly stocks. I thank Dr. Lindsey Macpherson for sharing reagents prior to publication. I thank Thomas Khan for writing a script for blinding video files. I thank Samantha Galindo for donating *R83B04-Gal4* and generating *R83B04-LexA* (Galindo, unpublished). I thank Sam C. Qian for providing MATLAB code for analyzing calcium imaging data, and providing useful input on calcium

imaging setup and analysis. This research was supported by an NSF graduate research fellowship DGE-11-44155 (AB), National Institutes of Health (NIH) Predoctoral Fellowship 1F31NS090909-01 (AB) and NIH NINDS R01 NS061908 (WBG).

Figure 4.1: Down-and-Back neurons receive spatially restricted class III mechanosensory input

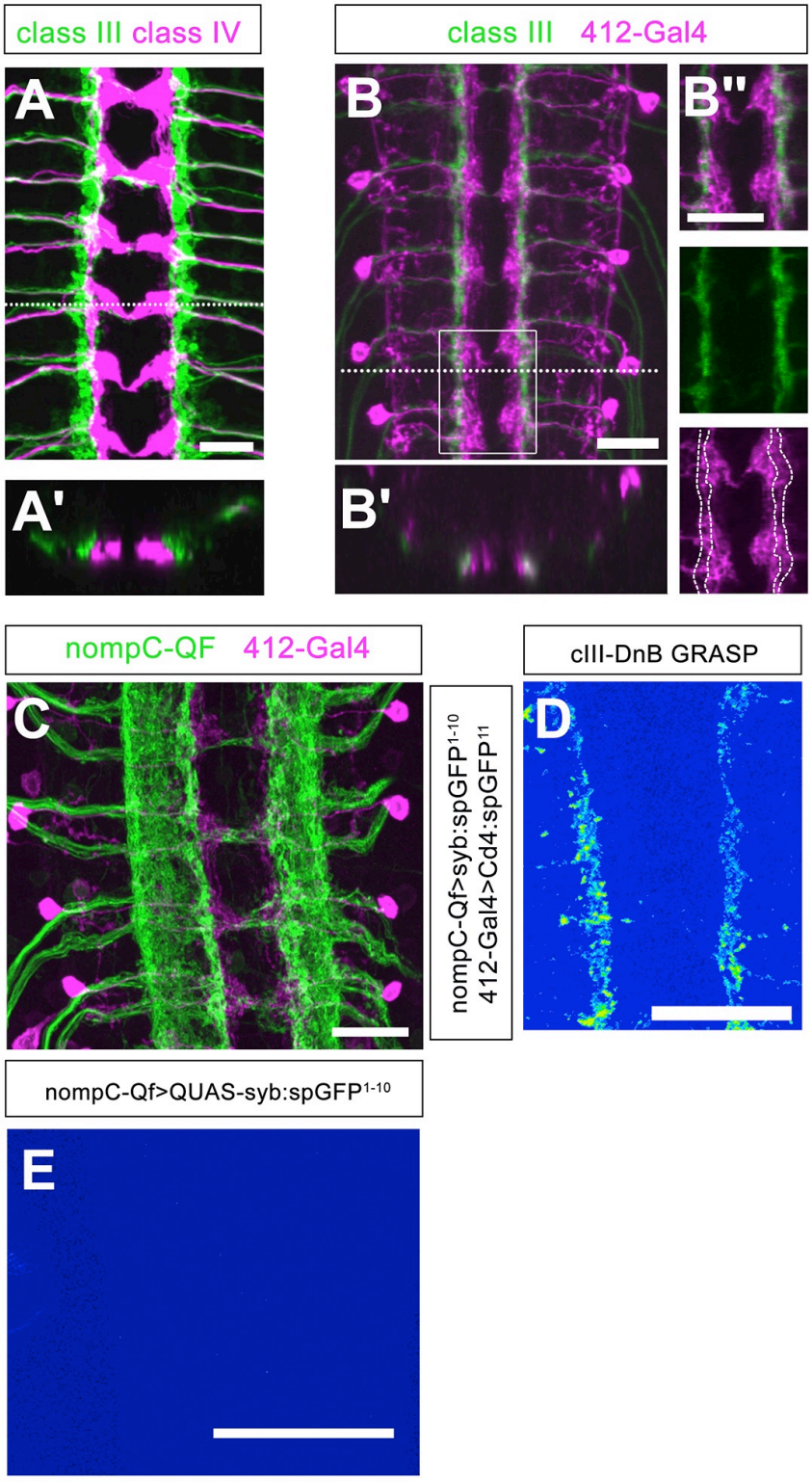

Figure 4.1: **Down-and-Back neurons receive spatially restricted class III mechanosensory input**

(A-A') Co-labeling cIII (anti-GFP, green) and cIV (anti-dsRed, magenta) axons in the CNS. Dotted line represents the location of the transverse section shown in (A').

(B-B'') Co-labeling of cIII axons (anti-GFP, green) and *412-Gal4* neurons (anti-dsRed, magenta). Dotted line represents transverse section shown in B'. Boxed region is shown as a single plane image in B''. Location of cIII axon terminals is outlined in the lower panel to show overlap with DnB dendrites.

(C) Co-labeling cIII and chordotonal (Chd) neurons (anti-dsRed, green) with nompC-QF and DnB neurons (anti-GFP, magenta) in the CNS.

(D) Reconstitution of GFP in cIII region when syb:spGFP$^{1-10}$ was driven in cIII and Chd neurons using *nompC-QF* and CD4:spGFP^{11} driven by *412-Gal4*. Image shows native reconstituted GFP in pseudocolor.

(E) No reconstitution of GFP observed with *nompC-QF* driving expression of QUAS-syb:spGFP1-10. Image shown in pseudocolor.

Scale bar: 15μm (A- B''), 20μm (C), 40μm (D), 50μm (E)

Genotypes: (A-A') *dTrpA1-QF/QUAS-mtdTom3XHA; nompC-LexA, 10X-LexAop2-myr-GFP/+* (B –B'') *nompC-LexA, 10XLexAop2-IVS-myr-GFP/412-Gal4, UAS-CD4-tdTom*

(C) *nompC-QF,QUAS-TdTomato/+; 412-Gal4, UAS-CD8-GFP/+*

(D) *nompC-QF/UAS-CD4-spGFP^{11}; 412-Gal4/QUAS-syb-spGFP$^{1-10}$* (E) *nompC-QF/UAS-CD4-SpGFP11; +/QUAS-syb:spGFP$^{1-1}$*

Figure 4.2: Silencing Down-and-Back neurons does not affect median gentle-touch responses

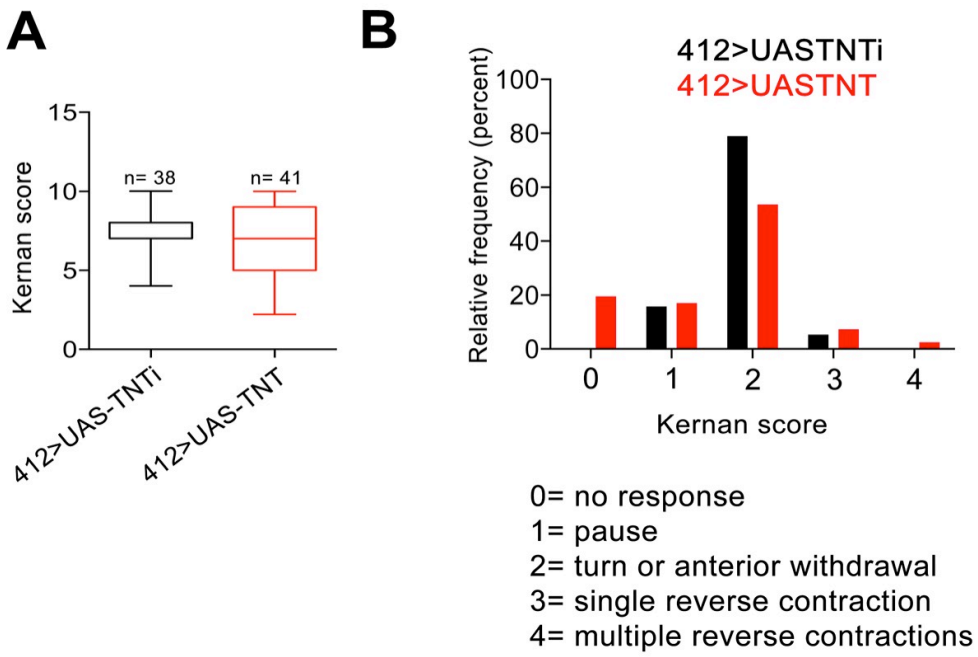

Figure 4.2: **Silencing Down-and-Back neurons does not affect median gentle-touch responses**

(A) Average cumulative Kernan score after 4 consecutive trials/animal.

(B) Relative frequency (percent) shown for each Kernan score, 0: no response, 1: hesitates, 2: withdraws anterior or turns, 3: single reverse backward movement, 4: multiple waves of reverse locomotion.

Genotypes: (A-B) (i) *UAS-TNTi/+;412-Gal4/+* (ii) *UAS-TNT/+;412-Gal4/+*

Box plots show median (middle line) and 25th to 75th percentiles with whiskers representing 10 to 90 percentiles

Figure 4.3: Gentle-touch and nociceptor co-activation delays rolling onset

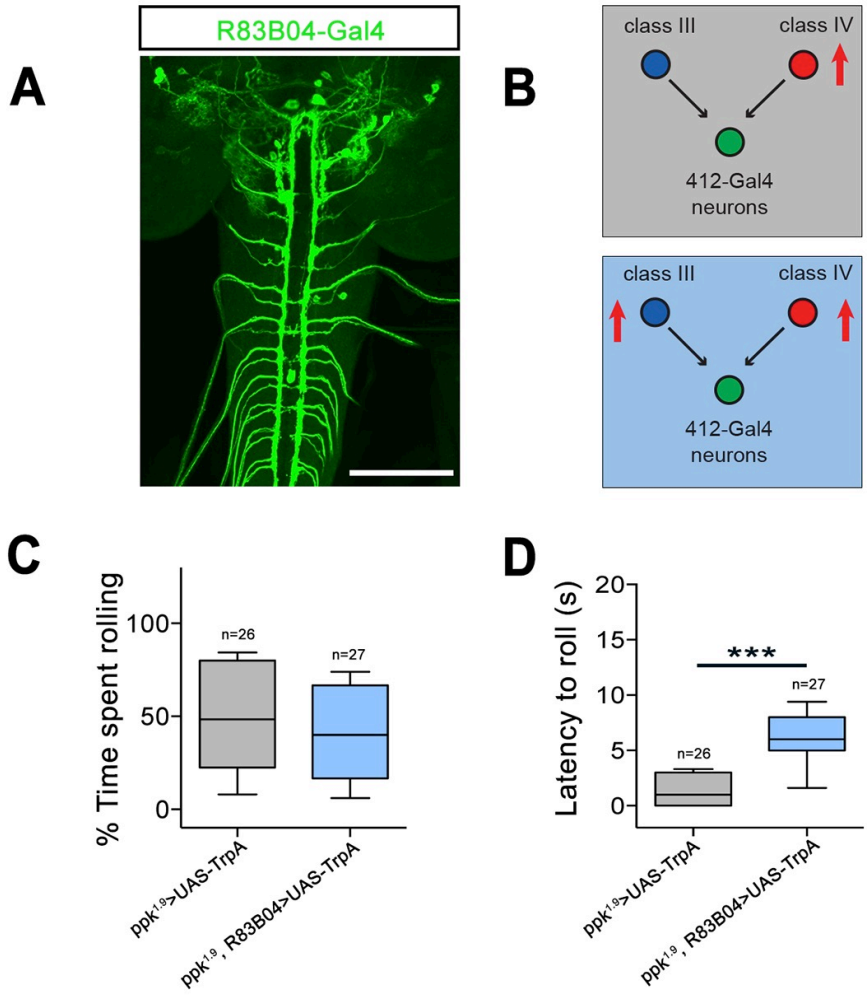

Figure 4.3: Gentle-touch and nociceptor co-activation delays rolling onset

(A) *R83B04-Gal4* driven mCD8:GFP labels cIII sensory axons in the CNS

(B) Schematic for activation of cIV vs. cIV and cIII neurons

(C-D) Co-activating class IV with *ppk*$^{1.9}$-*Gal4* and class III neurons with *R83B04-Gal4*, driving dTrpA, does not affect % of time spent rolling, but increases latency to roll compared to activating class IV neurons alone.

Genotypes: (A) *UAS-mCD8:GFP/+; R83B04-Gal4/+* (C-D) (i) *ppk$^{1.9}$-Gal4/+; UAS-dTrpA/+* (ii) *ppk$^{1.9}$-Gal4/+; UAS-dTrpA/R83B04-Gal4*

Box plots show median (middle line) and 25th to 75th percentiles with whiskers representing 10 to 90 percentiles. P values are indicated as ***p<0.001, as determined by Mann Whitney.

Figure 4.4: Sequential class III gentle touch, class IV nociceptive activation enhances rolling

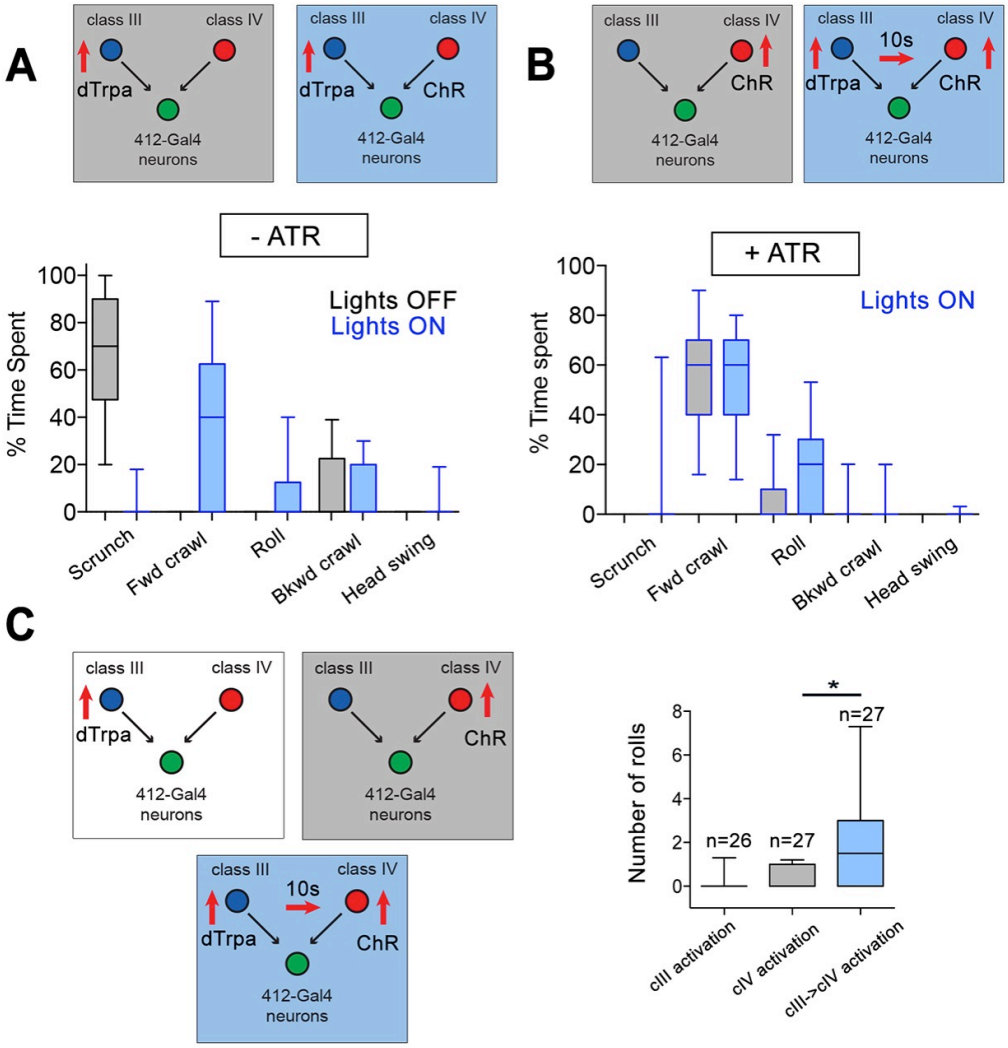

Figure 4.4: **Sequential class III gentle touch, class IV nociceptive activation enhances rolling**

(A) Schematic representation of experimental paradigm of activation. Class III neurons were activated with dTrpA for 10s with lightsOFF (grey) and then the same group of animals were tested for 10s with lightsON (blue). Animals were raised without ATR

(ATR-), which is a cofactor important for channel rhodopsin function. As a result, class IV neurons were not activated during lightsON. Percent of time spent engaging in gentle-touch like behaviors: scrunch, head swing, backward crawl, and in nociceptive behaviors: rolling.

(B) Schematic representation of experimental paradigm of activation. Two separate group of animals activated under different condition. The first group (grey) is activated for 10 s with optogenetic activation of class IVs, lightsON at 25˚C, which does not thermogenetically activate dTrpA expressing class III neurons. The second group (blue) is primed with 10s of class III thermogenetic activation before optogenetic activation of class IV neurons with LightsON.

(C) Increase in number of rolls observed when class III input is presented prior to class IV activation, compared to class III activation or class IV activation alone.

Genotypes: (A-B,D) *UAS-dTrpA1/ TrpA-QF,QUAS-ReaChR; R83B04-Gal4/+*

Box plots show median (middle line) and 25th to 75th percentiles with whiskers representing 10 to 90 percentiles. P values are indicated as *p=0.0102, as determined by Kruskal Wallis with posthoc Mann-Whitney test (C).

.

Figure 4.5: Co-silencing class III and IV does not further reduce response to local heat assay

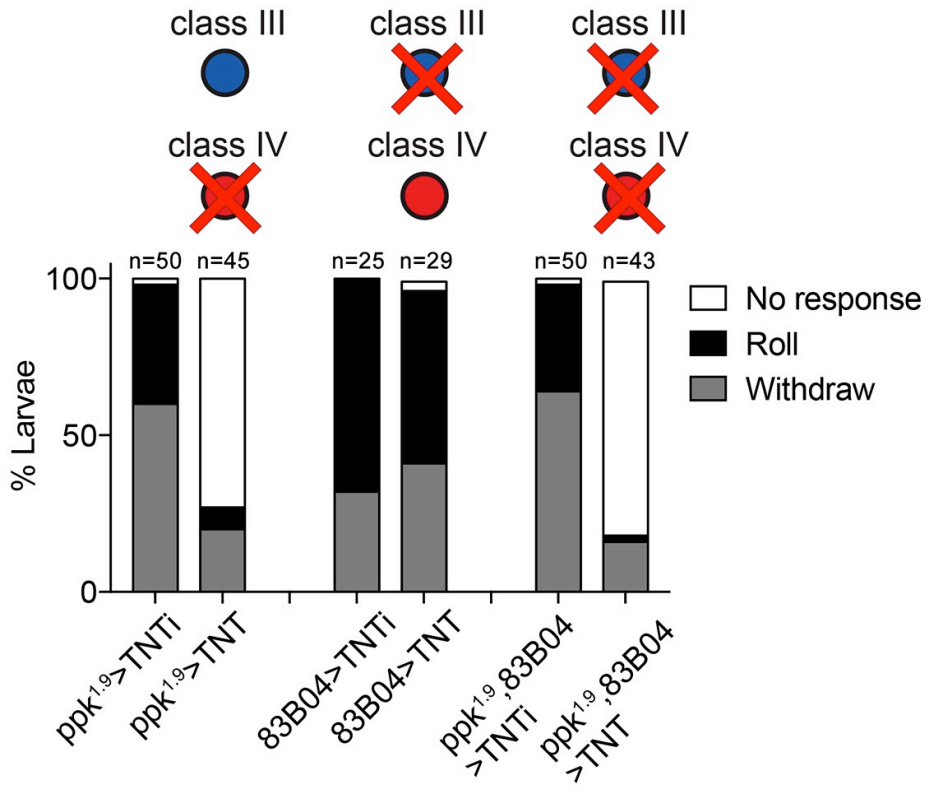

Figure 4.5: **Co-silencing class III and IV does not further reduce response to local heat assay**

Comparing percent of larvae responding to noxious local heat stimuli when class IV neurons are silenced, class III neurons are silenced, or both populations are silenced. Behaviors recorded: no response, withdrawal (bend away from stimulus, without roll), and rolling.

Genotypes: (i) *UAS-TNTi/PPK$^{1.9}$-Gal4* (ii) *UAS-TNT/ PPK$^{1.9}$-Gal4* (iii) *UAS-TNTi/+;83B04-Gal4/+* (iv) *UAS-TNT/+;83B04-Gal4/+* (v) *UAS-TNTi/ PPK$^{1.9}$-Gal4;83B04-Gal4/+* (vi) *UAS-TNT/ PPK$^{1.9}$-Gal4;83B04-Gal4/+*

Figure 4.6: Gentle-touch class III modulation of Down-and-Back mediated behavior

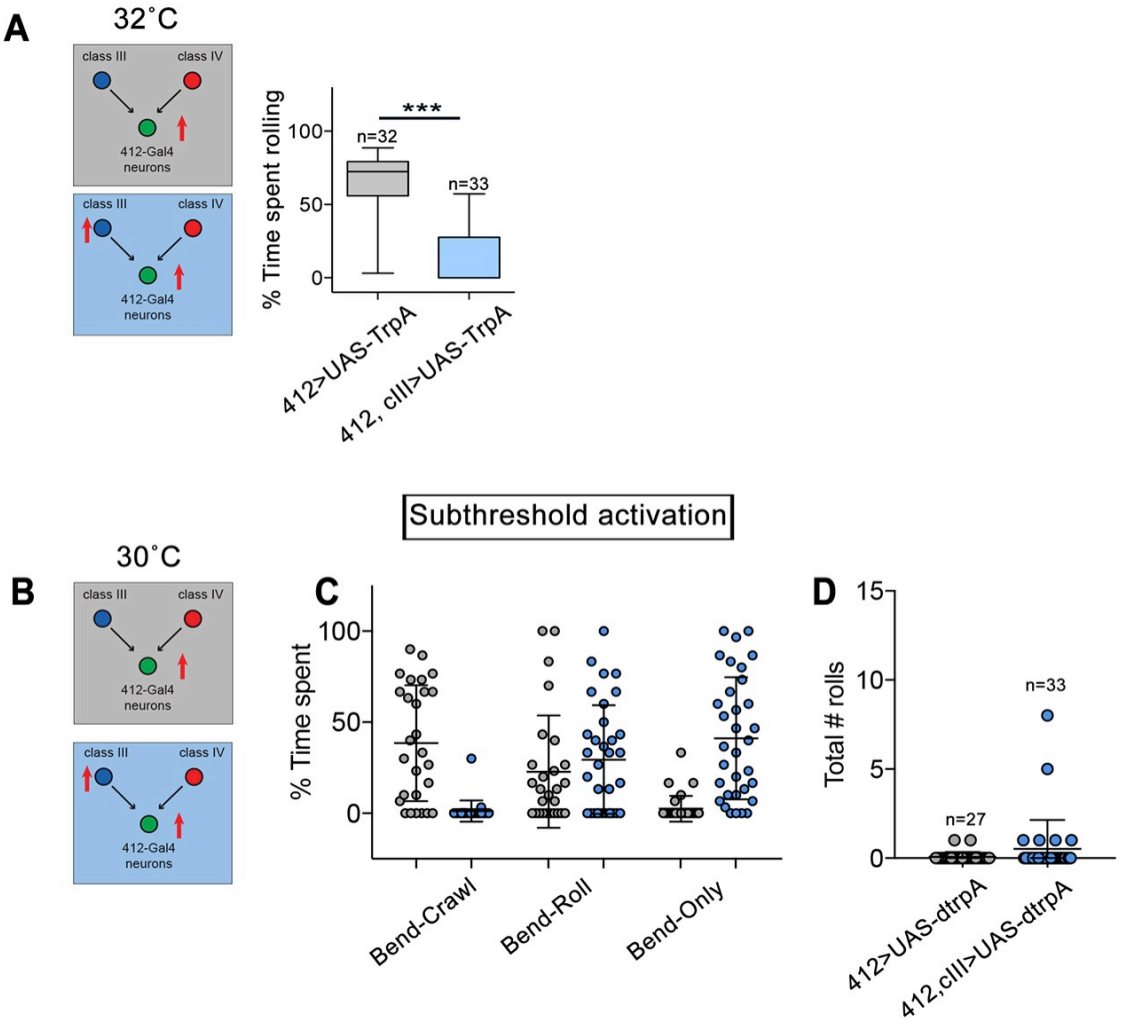

Figure 4.6: **Gentle-touch class III modulation of Down-and-Back mediated behavior**

(A) Co-activating *412-Gal4* neurons and class III neurons with *R83B04-Gal4*, driving dTrpA, reduces nocifensive rolling observed upon activating *412-Gal4* neurons alone. (B-D) Thermogenetic activation of *412-Gal4* at 30˚C does not induce rolling, but time spent bending is modestly increased upon class III co-activation (ns, Kruskal-Wallis)

Scatter plot represents values for all animals tested with mean (middle bar) and error bars representing standard deviation (SD). ***p<0.001, as determined by Mann-Whitney (A).

Genotypes: (A) (i) *UAS-dTrpA/+; 412-Gal4/+* (ii) *UAS-dTrpA/+; 412-Gal4/83B04-Gal4* (B) (i) *UAS-dTrpA/sp or CyonucGFP; 412-Gal4, 83B04-Gal4* (ii) *UAS-dTrpA/+; 412-Gal4, 83B04-Gal4*

Figure 4.7: Preliminary Down-and-Back functional imaging probing mechanosensory and nociceptive integration

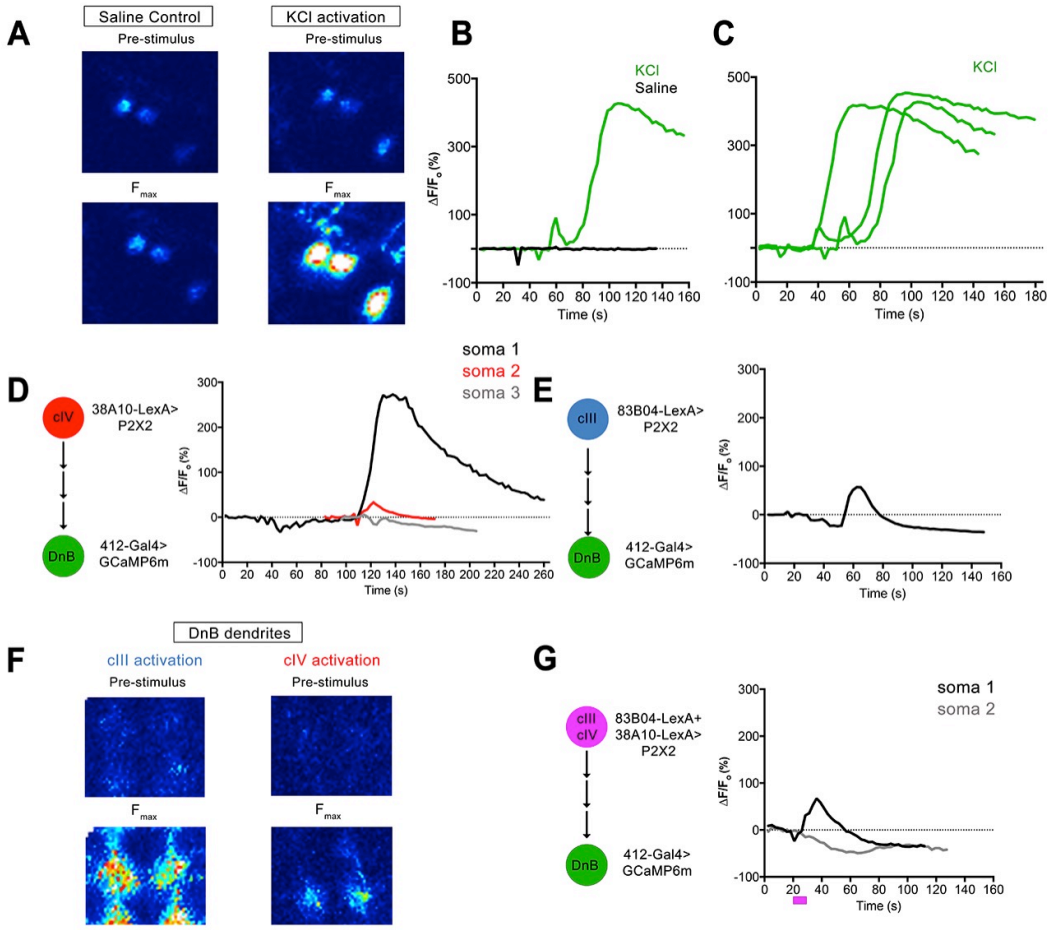

Figure 4.7: Preliminary Down-and-Back functional imaging probing mechanosensory and nociceptive integration

(A) Image of the same Down-and-Back neuron expressing GCaMP6m with *412-Gal4* during saline control vs. 70mM KCl application before stimulus, and at maximum fluorescence (F_{max})

(B) Change in fluorescence in DnB cell body during saline control and 70mM KCl application

(C) Change in fluorescence in DnB cell body after 70mM KCl application (n=3 animals)

(D) Change in fluorescence in DnB cell body after class IV> P2X2 activation with 3.3mM ATP (n=3 animals)

(E) Change in fluorescence in DnB cell body after class III> P2X2 activation with 3.3mM ATP (n=1 animal)

(F) Change in fluorescence in DnB dendrites before and at maximum fluorescence (F_{max}) after P2X2 activation of cIII or cIV neuron with 10mM ATP

(G) Change in fluorescence in DnB cell body after class III+class IV>P2X2 activation with 3.3mM ATP during ~20.8-26 seconds (n=2 animals)

Time estimated from scan cycle length, each cycle= ~2.6 seconds.

Genotypes: (A-C) *20X-UAS-GCaMP6m; 412-Gal4* (D) *20X-UAS-GCaMP6m/38A10-LexA;412-Gal4/LexAop-P2X2* (E) *20X-UAS-GCaMP6m/+;412-Gal4,83B04-LexA/LexAop-P2X2*

(F) (i) *20X-UAS-GCaMP6m/+;412-Gal4, 38A10-LexA/LexAop-P2X2* (ii) *20X-UAS-GCaMP6m/38A10-LexA;412-Gal4/LexAop-P2X2* (G) *20X-UAS-GCaMP6m/38A10-LexA;412-Gal4,83B04-LexA/LexAop-P2X2*

Chapter V:

Conclusions and Future Direction

"More highly evolved organisms generally derive their superior qualities not so much from novel mechanisms at the cellular level as from a richer complexity in the orchestration of basic designs that they share with simpler organisms."

-- Walter Heiligenberg, neuroethologist

How sensory information is combined and transformed into behavioral outputs remains a key question in neuroscience (Adolphs, 2015). Even 'simple' brains can combine sensory stimuli to enhance motor outputs, such as the integration of visual and mechanosensory integration required for *Drosophila* to climb over gap crossings (Huston and Jayaraman, 2011; Niven, 2010; Triphan et al., 2010). Therefore, general mechanisms of sensorimotor integration can potentially be gained from studying a simple nervous system. *Drosophila* larvae, in particular, have served as useful model for studying the development, dendritic patterning, and transduction mechanisms of somatosensory neurons. The larval somatosensory system is comprised of dendritic arborization (da) neurons (Bodmer and Jan, 1987; Grueber et al., 2002) that detect distinct stimuli. The da axon terminals sort out into modality specific locations in the nerve cord (Grueber et al., 2007; Merritt and Whitington, 1995). The characterization of this somatosensory system makes it suitable for studying sensory transduction and integration, and neural circuitry underlying sensory-evoked behavior.

Drosophila larvae perform a stereotypic sequential escape behavior (bend→roll→escape crawl) in response to noxious stimuli, such as harsh touch, or high temperature >39˚C. The work I have presented here characterizes a novel microcircuit underlying the initial bend stage of the escape sequence. I provide evidence that the identified population of neurons, the Down-and-Backs (DnBs), coordinate sequential motor outputs in the escape response (bend→roll) by targeting distinct motor pathways. The key experiments supporting these findings are summarized in Figure 5.1. Moreover, DnB neurons receive mechanosensory and nociceptive input, which might serve to enhance nocifensive responses. This work has combined anatomical analyses, neural circuit EM reconstruction, functional imaging, and detailed behavioral analyses to

demonstrate how Down-and-Back neurons organize modular motor pathways to drive nociceptive escape behavior (Figure 5.1).

Modular microcircuits driving sequential behavior

'Behavior' is often comprised of motor modules acting in concert or rapid succession, prominent examples including feeding, mating and escape motor programs. The work laid out in Chapter II and III provides anatomical, functional, and behavioral evidence that Down-and-Back interneurons receive input from mechanosensory and nociceptive inputs, and promote the bend → rolling escape sequence. Activation and silencing of DnB neurons revealed modularity in the rolling response, such that the initial C-shape bend could be initiated separately, without rolling (Figure 5.1A-C). Previous studies investigating nocifensive escape had not recognized this separation of motor programs (Hwang et al., 2007; Ohyama et al., 2013; Ohyama et al., 2015). I utilized EM neural reconstruction to show that DnB neurons primarily target premotor circuits, and indirectly connect to Goro, rolling command-like neurons. We hypothesized that this circuit divergence could underlie DnB activation of both bending and rolling modules, independently. Indeed, silencing Goro during DnB activation triggered bending, without rolling (Figure 5.1D). This modular organization of nocifensive escape raises the question about whether these modules are recruited during additional behavioral outputs, similar to the C-bend in goldfish that is triggered in escape responses, but also during feeding and prey capture (Korn and Faber, 2005). A C-shape-like bend is also a component of the self-righting response, where an animal that is dorsal side down will flip itself 180˚ to orient itself ventral side down. In fact, DnB neurons target motor neurons innervating LT1 muscles, which have been shown to be involved in self-righting (Picao-Osorio et al., 2015). An appealing hypothesis is that DnB-bending motor

pathways are recruited along with other motor circuits promoting 180˚, rather than the 360˚ turns which occur during rolling. Combining modules in response to different sensory stimuli might be an effective strategy for expanding the repertoire of motor outputs without the need for additional circuitry.

Crawling is slightly increased during DnB-silencing, but otherwise coordinated and intact. This raises the question of how overlapping groups of premotor neurons can generate both forward and lateral locomotion. One possibility is that DnB neurons are recruited along with other circuit elements, such as central pattern generators (CPGs), to orchestrate this shift to lateral movement. Another possibility is that peptidergic modulation might reconfigure the circuit to generate different forms of locomotion (see next section). So far, nothing is known about the CPGs activated during rolling, or the muscle activity underlying these behaviors. Moreover, The final stage of nocifensive escape is increased crawling (escape crawl), which prompts interesting questions about sequence transitions from rolling to crawling. A potential strategy might include inhibiting bending circuitry to rapidly terminate rolling, and straighten out the animal to permit escape crawl. One potential candidate could be the only non-sensory input to DnB neurons, Handle-A inhibitory neurons. Identifying reagents to manipulate Handle-A activity would be important to test its role in nocifensive sequence progression.

The prevailing theories for sequence generation propose that sequential behavior arises either from synaptic chaining, where one module activates the next module in the series, or by parallel activation, where competing circuits are activated at once and inhibitory interactions between modules establishes a sequence (Lashley, 1951). The Down-and-Back circuitry suggests that circuits activated in parallel can also act cooperatively to generate sequences, such that bending is activated first in order to facilitate rolling behavior. It is not currently known how the timing of bending and rolling is established. One potential scenario is that Down-and-Back neurons are activated

before Goro, so that bending can be triggered before rolling. Electrophysiological approaches might be useful in detecting millisecond differences between Goro and DnB activity upon cIV activation. It is also conceivable that proprioceptive input could facilitate rolling motor patterns once the bend is achieved. Silencing Class I neurons, which function as proprioceptors (Hughes and Thomas, 2007) slightly, but significantly reduces rolling efficiency (Hwang et al., 2007; Ohyama et al., 2013). Future work could reveal the contribution of proprioception on nocifensive escape locomotion. Another possibility, which could be complementary to circuit control bend→roll, is that rolling is physically constrained by bending. A high degree of curvature might be important for an animal to translate the force of contraction along a lateral vector.

Potential for peptidergic modulation of nocifensive behavior

Wiring diagrams can provide potential routes for information flow, but overlying the entire connectome is an invisible neuromodulatory map. Neuromodulators can recruit or exclude neural microcircuits both locally and far away from its release site, thus expanding the flexibility of behavioral outputs beyond the confines of synaptic connectivity. EM sections showed many dense-core vesicles at Down-and-Back axons suggesting peptidergic or aminergic release. Recent work has implicated neuropeptides in larval mechanical nociception (Hu et al., 2017), so the use of neuromodulators might be extensive in this circuit. In vertebrate nociception, neuropeptides are widespread, and can contribute to central sensitization to noxious stimuli. For instance, two well-studied neuropeptides CGRP and SP are expressed by primary afferents and bind to receptors on spinal cord neurons to increase excitability (Seybold, 2009). Both CGRP and SP production is increased during inflammation, which can cause enhanced response to noxious stimuli (hyperalgesia). However, most studies have focused on the role of

peripheral nociceptors in neuromodulation, and less is known about neuromodulation by central circuits and how they impact motor networks. Some evidence from invertebrate work suggests that oxytocin/vasopressin peptides in *C.elegans* can coordinate the stages of reproductive motor patterns (Garrison et al., 2012). Moreover, the exoskeleton shedding at the end of each molt (ecdysis) is a prominent example of neuropeptide control of sequential behavior. (Ewer, 2005). For instance, the transition from 2nd to 3rd instar consists of sequential anterior-posterior contractions, squeezing waves, and forward to backward thrusts to shed the old cuticle (Park et al., 2002). The initiation of these motor patterns is coordinated by a cascade of neuropeptides including eclosion hormone (EH) induction of eclosion triggering hormone (ETH), and CCAP, which terminates pre-ecdysis behaviors, and initiates the ecdysis motor pattern (Ewer, 2005; Truman and Riddiford, 1970). Thus, identifying the neuromodulator released by Down-and-Back neurons could reveal insight into the transduction of nociception and/or the coordination of sequential motor programs.

Spatial organization of Down-and-Back inputs and outputs

A general theme in the initial relay of sensory information to the CNS is the convergence of similar inputs (i.e. detecting the same modality or stimulus feature) onto the same region in the CNS, forming sensory maps (Grueber et al., 2007; Todd, 2010; Vosshall and Stocker, 2007). Such modality-specific organization would facilitate communication with postsynaptic partners. Here, I provide evidence that sensory axons can preserve their laminar organization onto the dendritic field of a common post-synaptic target. EM reconstruction, and GRASP visualization of synaptic sites, revealed that DnBs receive spatially segregated input along their dendritic arbor from mechanosensory class III, and nociceptive class IV neurons. Consistent with the laminar

lateral to medial organization of cIII and cIV afferents across the nerve cord, cIII synaptic input were restricted to the lateral region of the DnB dendrite, while cIV synapses were found exclusively in the medial region of the dendritic arbor. Synaptic clustering has been observed in hippocampal pyramidal neurons, where they are thought to play a role in memory storage (Kastellakis et al., 2015). Studies have also suggested that neurons involved in the same pathway might cluster on a dendritic branch, to facilitate modulation by top-down signals, without necessarily impacting pathways targeting apposing branches (Yang et al., 2016). DnB neurons also receive minor mechanosensory inputs through external sensory (es) and class II neurons on postsynaptic sites on the lateral DnB processes. Collateral branches of cII neurons were previously proposed to provide additional sites of output, expanding the circuits targeted by cII neurons (Grueber et al., 2007). Since cII and es input is not located on the DnB dendrite it is likely not contributing to dendritic integration, and could have role in presynaptic modulation.

The spatially restricted cIII-cIV targeting raises interesting development questions about the mechanisms underlying axon sorting and synapse formation onto common postsynaptic partners. In line with previous descriptions (Grueber et al., 2007), co-labeling cIII and cIV afferents shows that they target adjacent non-overlapping regions of the neuropil (Chapter IV). The mechanisms that give rise to this laminar organization are currently under investigation in our lab, but one possibility is that the presence of cIV axons in the medial region precludes the growth of cIII axons into that region, which could impact cIII synapse targeting onto DnB dendrites. One precedent for axon-axon interactions underlying 'biased' wiring onto common targets comes from the visual system. Type 6 and Type 7 bipolar cells (BCs) provide major and minor input to retinal ganglion cells (RGCs), respectively (Okawa et al., 2014a; Okawa et al., 2014b). In the absence of Type 6 BCs, Type 7 BCs will increase its connectivity with RGCs. Such axon-axon imposed restriction on synapse formation have also been studied in *C.*

elegans, where motor neurons use Plexin-Semaphorin signaling to restrict targeting to non-overlapping regions of the muscle domain (Mizumoto and Shen, 2013).

Another observation is that class IV neurons overlap extensively with their targets (Ohyama et al., 2015) (Gerhard, unpublished), yet only form a large number of synapses with a select few cell types, namely DnBs, and Basins-2,4 (Gerhard, unpublished). Varying levels of cell-adhesion molecules or receptor expression by target neurons, either facilitating or restricting synapse number might underlie this selectivity (Sanes and Yamagata, 2009; Wills et al., 2012; Yogev and Shen, 2014).

Down-and-Back neurons primarily target two pathways, premotor-circuitry, and 'nociceptive integrators', which provide links to Goro rolling command neurons, and integrate input from cIV neurons, and other nociceptive interneurons. My data supports a divergent role in bending and rolling for premotor, and Goro circuits, respectively. Interestingly, this divergence is also reflected in the location of DnB presynaptic sites targeting these pathways. Premotor neurons form synapses with DnB axons, on the lateral region of the neuron, whereas nociceptive integrators form connections with presynaptic sites on the DnB dendrite. This localization could potentially facilitate spatial and temporal summation of excitatory postsynaptic potentials (EPSP) on nociceptive integrators during coincident class IV and DnB activation (Spruston et al., 2008).

Integration between touch and nociception

There are several theories proposed for somatosensory neural coding. The three most prevalent include: 1) specificity theory, where central circuits receive input from one sensory modality, 2) pattern theory, which states that central circuits receive input from many sensory modalities and pattern of activation dictates coding, and 3) population, or

combinatorial theory, which is a combination of both, asserting that there is some degree of specificity in central circuits, but they converge multiple sensory inputs (Prescott et al., 2014). Duan *et al.*, identified neural substrates for the 'gate control theory' (Melzack and Wall, 1965) which describes mechanosensory gating of nociceptive signaling. This theory is an example of pattern theory. However, the somatostatin (SOM) expressing neurons that converge tactile and nociceptive input are not involved in transducing thermal, touch, or cold stimuli (Duan et al., 2014), indicating is a degree of selectivity in these interneurons that is in line with a combinatorial coding of sensory stimuli. Down-and-Back neurons are, so far, more consistent with a combinatorial theory of sensory coding. DnBs are dually innervated by mechanosensory and nociception, yet DnBs receive a higher percentage of input from nociceptors compared to gentle-touch sensing neurons (45.5% v. 15%, respectively). This preferential input from cIV is reflected in DnB mediated behavior, as both activation and silencing experiments suggest that DnBs are required for robust nocifensive responses, but mostly dispensable for gentle-touch behavior. Thus, these observations are in line with the combinatorial theory of coding stating that central circuits may have preferred inputs, yet still integrate multiple sensory stimuli (Ma, 2012).

My work provides evidence that cIII input could potentially enhance class IV nocifensive outputs when presented before cIV stimulation, or at low activation levels. Future experiments could look at the effect of cIII mechanosensory input on cIV outputs over a range of activation intensities to understand the nature of cIII modulation. Particularly, since superadditive integration (multisensory response exceeds sum of unimodal sensory responses) is proportionally larger during weakly presented stimuli (Stein and Stanford, 2008). Thus, the effect of cIII input on DnB outputs might be most significant during weak activation.

The work presented here reveals how a relatively simple nervous system can provide insight into how sensory information is transformed into sequential motor outputs. Hopefully, these findings can be extended to uncover neural mechanisms controlling sequence progression, peptidergic modulation of nociception, and developmental mechanisms underlying afferent sorting onto common targets.

Figure 5.1: Summary model for DnB neurons controlling nocifensive escape

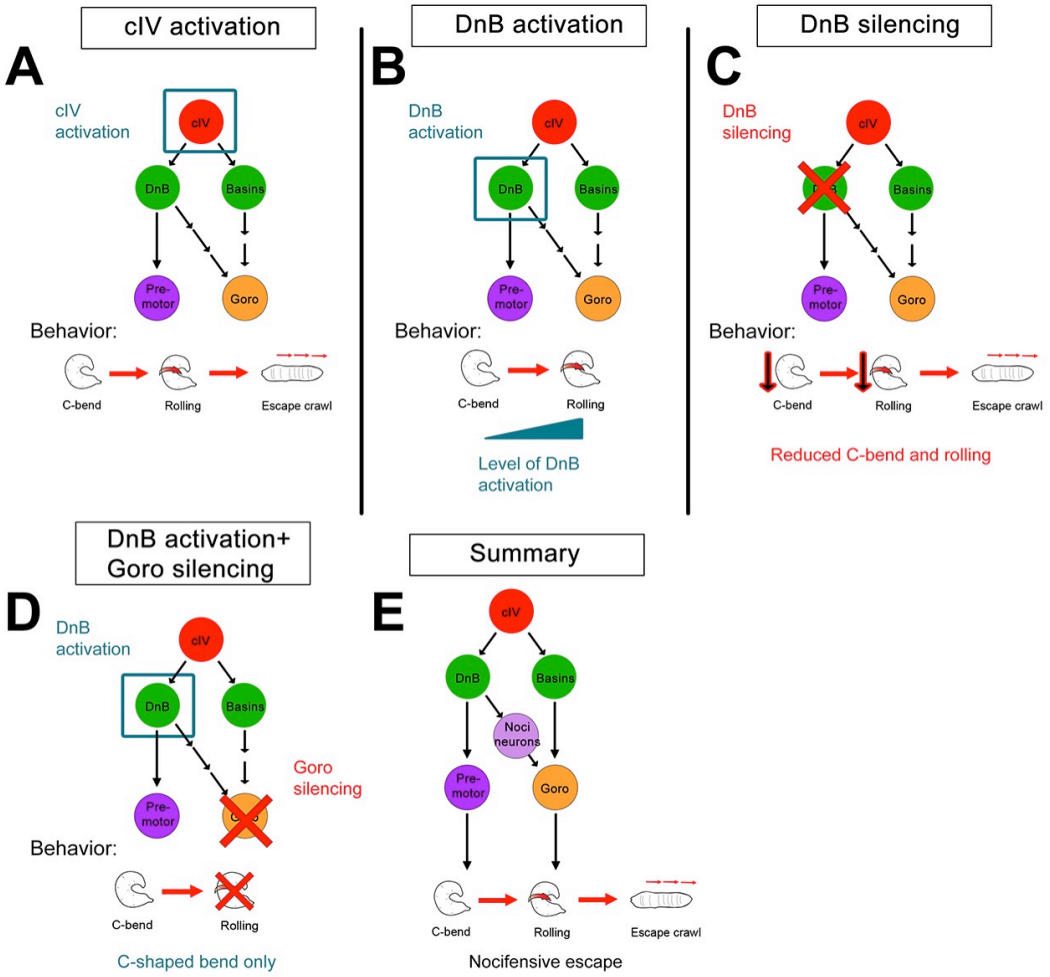

Figure 5.1: Summary model for DnB neurons controlling nocifensive escape

A) Activation of cIV neurons triggers the nocifensive response: C-bend→Rolling→Escape crawl

B) Activation of DnB neurons triggers C-bend and Rolling in an intensity-depending manner

C) Silencing DnB neurons reduces C-bend curvature and rolling

D) Activation of DnB neurons, while silencing Goro rolling command-like neurons reduces rolling, while leaving bending intact

E) Summary model: DnB neurons promote sequential nocifensive escape behavior via co-activation of downstream premotor circuits and command-like Goro neurons.

References

Adolfsen, B., Saraswati, S., Yoshihara, M., and Littleton, J.T. (2004). Synaptotagmins are trafficked to distinct subcellular domains including the postsynaptic compartment. The Journal of cell biology *166*, 249-260.

Adolphs, R. (2015). The unsolved problems of neuroscience. Trends in cognitive sciences *19*, 173-175.

Ainsley, J.A., Pettus, J.M., Bosenko, D., Gerstein, C.E., Zinkevich, N., Anderson, M.G., Adams, C.M., Welsh, M.J., and Johnson, W.A. (2003). Enhanced locomotion caused by loss of the Drosophila DEG/ENaC protein Pickpocket1. Curr Biol *13*, 1557-1563.

Alekseyenko, O.V., Lee, C., and Kravitz, E.A. (2010). Targeted manipulation of serotonergic neurotransmission affects the escalation of aggression in adult male Drosophila melanogaster. PLoS One *5*, e10806.

Alexandre, C., Lecourtois, M., and Vincent, J. (1999). Wingless and Hedgehog pattern Drosophila denticle belts by regulating the production of short-range signals. Development *126*, 5689-5698.

Alvarado, J.C., Vaughan, J.W., Stanford, T.R., and Stein, B.E. (2007). Multisensory versus unisensory integration: contrasting modes in the superior colliculus. Journal of neurophysiology *97*, 3193-3205.

Arcourt, A., Gorham, L., Dhandapani, R., Prato, V., Taberner, F.J., Wende, H., Gangadharan, V., Birchmeier, C., Heppenstall, P.A., and Lechner, S.G. (2017). Touch Receptor-Derived Sensory Information Alleviates Acute Pain Signaling and Fine-Tunes Nociceptive Reflex Coordination. Neuron *93*, 179-193.

Babcock, D.T., Landry, C., and Galko, M.J. (2009). Cytokine signaling mediates UV-induced nociceptive sensitization in Drosophila larvae. Curr Biol *19*, 799-806.

Babcock, D.T., Shi, S., Jo, J., Shaw, M., Gutstein, H.B., and Galko, M.J. (2011). Hedgehog signaling regulates nociceptive sensitization. Curr Biol *21*, 1525-1533.

Baines, R.A., Uhler, J.P., Thompson, A., Sweeney, S.T., and Bate, M. (2001). Altered electrical properties in Drosophila neurons developing without synaptic transmission. J Neurosci *21*, 1523-1531.

Basler, K., and Struhl, G. (1994). Compartment boundaries and the control of Drosophila limb pattern by hedgehog protein. Nature *368*, 208-214.

Bellen, H.J., Tong, C., and Tsuda, H. (2010). 100 years of Drosophila research and its impact on vertebrate neuroscience: a history lesson for the future. Nat Rev Neurosci *11*, 514-522.

Bels, V.L., Aerts, P., Chardon, M., Vandewalle, P., Berkhoudt, H., Crompton, A.W., Vree, d.F., Dullemeijer, P., Ewert, J.P., and Frazzetta, T.H. (2012). Biomechanics of feeding in vertebrates, Vol 18 (Springer Science & Business Media).

Blivis, D., Haspel, G., Mannes, P.Z., O'Donovan, M.J., and Iadarola, M.J. (2017). Identification of a novel spinal nociceptive-motor gate control for Adelta pain stimuli in rats. eLife *6*.

Bodmer, R., and Jan, Y.N. (1987). Morphological differentiation of the embryonic peripheral neurons in Drosophila. Roux's archives of developmental biology : the official organ of the EDBO *196*, 69-77.

Bourane, S., Duan, B., Koch, S.C., Dalet, A., Britz, O., Garcia-Campmany, L., Kim, E., Cheng, L., Ghosh, A., Ma, Q.*, et al.* (2015). Gate control of mechanical itch by a subpopulation of spinal cord interneurons. Science *350*, 550-554.

Brand, A.H., and Perrimon, N. (1993). Targeted gene expression as a means of altering cell fates and generating dominant phenotypes. Development *118*, 401-415.

Braz, J., Solorzano, C., Wang, X., and Basbaum, A.I. (2014). Transmitting pain and itch messages: a contemporary view of the spinal cord circuits that generate gate control. Neuron *82*, 522-536.
Card, G.M. (2012). Escape behaviors in insects. Current opinion in neurobiology *22*, 180-186.
Chalfie, M., Sulston, J.E., White, J.G., Southgate, E., Thomson, J.N., and Brenner, S. (1985). The neural circuit for touch sensitivity in Caenorhabditis elegans. J Neurosci *5*, 956-964.
Chen, T.W., Wardill, T.J., Sun, Y., Pulver, S.R., Renninger, S.L., Baohan, A., Schreiter, E.R., Kerr, R.A., Orger, M.B., Jayaraman, V.*, et al.* (2013). Ultrasensitive fluorescent proteins for imaging neuronal activity. Nature *499*, 295-300.
Clowney, E.J., Iguchi, S., Bussell, J.J., Scheer, E., and Ruta, V. (2015). Multimodal Chemosensory Circuits Controlling Male Courtship in Drosophila. Neuron *87*, 1036-1049.
Craig, A.D., and Bushnell, M.C. (1994). The thermal grill illusion: unmasking the burn of cold pain. Science *265*, 252-255.
Daniels, R.W., Collins, C.A., Gelfand, M.V., Dant, J., Brooks, E.S., Krantz, D.E., and DiAntonio, A. (2004). Increased expression of the Drosophila vesicular glutamate transporter leads to excess glutamate release and a compensatory decrease in quantal content. J Neurosci *24*, 10466-10474.
de Vries, S.E., and Clandinin, T. (2013). Optogenetic stimulation of escape behavior in Drosophila melanogaster. J Vis Exp.
Domenici, P., Booth, D., Blagburn, J.M., and Bacon, J.P. (2008). Cockroaches keep predators guessing by using preferred escape trajectories. Curr Biol *18*, 1792-1796.
Driscoll, M.K., Fourkas, J.T., and Losert, W. (2011). Local and global measures of shape dynamics. Phys Biol *8*, 055001.
Driscoll, M.K., McCann, C., Kopace, R., Homan, T., Fourkas, J.T., Parent, C., and Losert, W. (2012). Cell shape dynamics: from waves to migration. PLoS Comput Biol *8*, e1002392.
Duan, B., Cheng, L., Bourane, S., Britz, O., Padilla, C., Garcia-Campmany, L., Krashes, M., Knowlton, W., Velasquez, T., Ren, X.*, et al.* (2014). Identification of spinal circuits transmitting and gating mechanical pain. Cell *159*, 1417-1432.
Duan, B., Cheng, L., and Ma, Q. (2017). Spinal Circuits Transmitting Mechanical Pain and Itch. Neuroscience bulletin.
Dudai, Y., Jan, Y.N., Byers, D., Quinn, W.G., and Benzer, S. (1976). dunce, a mutant of Drosophila deficient in learning. Proc Natl Acad Sci U S A *73*, 1684-1688.
Eaton, R.C., and Hackett, J.T. (1984). The role of the Mauthner cell in fast-starts involving escape in teleost fishes (Springer).
Ebrahim, S.A., Dweck, H.K., Stokl, J., Hofferberth, J.E., Trona, F., Weniger, K., Rybak, J., Seki, Y., Stensmyr, M.C., Sachse, S.*, et al.* (2015). Drosophila Avoids Parasitoids by Sensing Their Semiochemicals via a Dedicated Olfactory Circuit. PLoS biology *13*, e1002318.
Ewer, J. (2005). Behavioral actions of neuropeptides in invertebrates: insights from Drosophila. Hormones and behavior *48*, 418-429.
Fan, R.J., Kung, J.C., Olausson, B.A., and Shyu, B.C. (2009). Nocifensive behaviors components evoked by brief laser pulses are mediated by C fibers. Physiology & behavior *98*, 108-117.
Fan, R.J., Shyu, B.C., and Hsiao, S. (1995). Analysis of nocifensive behavior induced in rats by CO2 laser pulse stimulation. Physiology & behavior *57*, 1131-1137.

Faris, P.L., Komisaruk, B.R., Watkins, L.R., and Mayer, D.J. (1983). Evidence for the neuropeptide cholecystokinin as an antagonist of opiate analgesia. Science *219*, 310-312.
Feinberg, E.H., Vanhoven, M.K., Bendesky, A., Wang, G., Fetter, R.D., Shen, K., and Bargmann, C.I. (2008). GFP Reconstitution Across Synaptic Partners (GRASP) defines cell contacts and synapses in living nervous systems. Neuron *57*, 353-363.
Feng, K., Palfreyman, M.T., Hasemeyer, M., Talsma, A., and Dickson, B.J. (2014). Ascending SAG neurons control sexual receptivity of Drosophila females. Neuron *83*, 135-148.
Flourens, P. (1842). Recherches expérimentales sur les propriétés et les fonctions du système nerveux dans les animaux vertébrés (Ballière).
Frank, D.D., Jouandet, G.C., Kearney, P.J., Macpherson, L.J., and Gallio, M. (2015). Temperature representation in the Drosophila brain. Nature *519*, 358-361.
Frings, H. (1945). The reception of mechanical and thermal stimuli by caterpillars. Journal of Experimental Zoology Part A: Ecological ….
Fushiki, A., Zwart, M.F., Kohsaka, H., Fetter, R.D., Cardona, A., and Nose, A. (2016). A circuit mechanism for the propagation of waves of muscle contraction in Drosophila. eLife *5*.
Garrison, J.L., Macosko, E.Z., Bernstein, S., Pokala, N., Albrecht, D.R., and Bargmann, C.I. (2012). Oxytocin/vasopressin-related peptides have an ancient role in reproductive behavior. Science *338*, 540-543.
Gohl, D.M., Silies, M.A., Gao, X.J., Bhalerao, S., Luongo, F.J., Lin, C.-C., Potter, C.J., and Clandinin, T.R. (2011). A versatile in vivo system for directed dissection of gene expression patterns. Nature Methods *8*, 231-237.
Gordon, M.D., and Scott, K. (2009). Motor control in a Drosophila taste circuit. Neuron *61*, 373-384.
Grueber, W.B., Graubard, K., and Truman, J.W. (2001). Tiling of the body wall by multidendritic sensory neurons in Manduca sexta. The Journal of comparative neurology *440*, 271-283.
Grueber, W.B., Jan, L.Y., and Jan, Y.N. (2002). Tiling of the Drosophila epidermis by multidendritic sensory neurons. Development *129*, 2867-2878.
Grueber, W.B., Jan, L.Y., and Jan, Y.N. (2003). Different levels of the homeodomain protein cut regulate distinct dendrite branching patterns of Drosophila multidendritic neurons. Cell *112*, 805-818.
Grueber, W.B., Ye, B., Yang, C.H., Younger, S., Borden, K., Jan, L.Y., and Jan, Y.N. (2007). Projections of Drosophila multidendritic neurons in the central nervous system: links with peripheral dendrite morphology. Development *134*, 55-64.
Hall, D.H., and Treinin, M. (2011). How does morphology relate to function in sensory arbors? Trends Neurosci *34*, 443-451.
Hamada, F.N., Rosenzweig, M., Kang, K., Pulver, S.R., Ghezzi, A., Jegla, T.J., and Garrity, P.A. (2008). An internal thermal sensor controlling temperature preference in Drosophila. Nature *454*, 217-220.
Han, C., Jan, L.Y., and Jan, Y.-N.N. (2011). Enhancer-driven membrane markers for analysis of nonautonomous mechanisms reveal neuron-glia interactions in Drosophila. Proceedings of the National Academy of Sciences of the United States of America *108*, 9673-9678.
Helmstaedter, M., Briggman, K.L., and Denk, W. (2011). High-accuracy neurite reconstruction for high-throughput neuroanatomy. Nat Neurosci *14*, 1081-1088.
Hewes, R.S., Park, D., Gauthier, S.A., Schaefer, A.M., and Taghert, P.H. (2003). The bHLH protein Dimmed controls neuroendocrine cell differentiation in Drosophila. Development *130*, 1771-1781.

Hodgkin, A.L., and Katz, B. (1949). The effect of sodium ions on the electrical activity of giant axon of the squid. The Journal of physiology *108*, 37-77.
Honjo, K., Mauthner, S.E., Wang, Y., Skene, J.H., and Tracey, W.D., Jr. (2016). Nociceptor-Enriched Genes Required for Normal Thermal Nociception. Cell Rep *16*, 295-303.
Hu, C., Petersen, M., Hoyer, N., Spitzweck, B., Tenedini, F., Wang, D., Gruschka, A., Burchardt, L.S., Szpotowicz, E., Schweizer, M.*, et al.* (2017). Sensory integration and neuromodulatory feedback facilitate Drosophila mechanonociceptive behavior. Nat Neurosci.
Hughes, C.L., and Thomas, J.B. (2007). A sensory feedback circuit coordinates muscle activity in Drosophila. Molecular and cellular neurosciences *35*, 383-396.
Huser, A., Rohwedder, A., Apostolopoulou, A.A., Widmann, A., Pfitzenmaier, J.E., Maiolo, E.M., Selcho, M., Pauls, D., von Essen, A., Gupta, T.*, et al.* (2012). The serotonergic central nervous system of the Drosophila larva: anatomy and behavioral function. PLoS One *7*, e47518.
Huston, S.J., and Jayaraman, V. (2011). Studying sensorimotor integration in insects. Current opinion in neurobiology *21*, 527-534.
Hwang, R.Y., Zhong, L., Xu, Y., Johnson, T., Zhang, F., Deisseroth, K., and Tracey, W.D. (2007). Nociceptive neurons protect Drosophila larvae from parasitoid wasps. Curr Biol *17*, 2105-2116.
Im, S.H., Takle, K., Jo, J., Babcock, D.T., Ma, Z., Xiang, Y., and Galko, M.J. (2015). Tachykinin acts upstream of autocrine Hedgehog signaling during nociceptive sensitization in Drosophila. eLife *4*, e10735.
Inui, A. (2003). Neuropeptide gene polymorphisms and human behavioural disorders. Nature reviews Drug discovery *2*, 986-998.
Jenett, A., Rubin, G.M., Ngo, T.T., Shepherd, D., Murphy, C., Dionne, H., Pfeiffer, B.D., Cavallaro, A., Hall, D., Jeter, J.*, et al.* (2012). A GAL4-driver line resource for Drosophila neurobiology. Cell Rep *2*, 991-1001.
Jovanic, T., Schneider-Mizell, C.M., Shao, M., Masson, J.B., Denisov, G., Fetter, R.D., Mensh, B.D., Truman, J.W., Cardona, A., and Zlatic, M. (2016). Competitive Disinhibition Mediates Behavioral Choice and Sequences in Drosophila. Cell *167*, 858-870 e819.
Kahsai, L., and Zars, T. (2011). Learning and memory in Drosophila: behavior, genetics, and neural systems. International review of neurobiology *99*, 139-167.
Kaneko, M., and Hall, J.C. (2000). Neuroanatomy of cells expressing clock genes in Drosophila: transgenic manipulation of the period and timeless genes to mark the perikarya of circadian pacemaker neurons and their projections. The Journal of comparative neurology *422*, 66-94.
Karuppudurai, T., Lin, T.Y., Ting, C.Y., Pursley, R., Melnattur, K.V., Diao, F., White, B.H., Macpherson, L.J., Gallio, M., Pohida, T.*, et al.* (2014). A hard-wired glutamatergic circuit pools and relays UV signals to mediate spectral preference in Drosophila. Neuron *81*, 603-615.
Kastellakis, G., Cai, D.J., Mednick, S.C., Silva, A.J., and Poirazi, P. (2015). Synaptic clustering within dendrites: an emerging theory of memory formation. Progress in neurobiology *126*, 19-35.
Kernan, M., Cowan, D., and Zuker, C. (1994). Genetic dissection of mechanosensory transduction: mechanoreception-defective mutations of Drosophila. Neuron *12*, 1195-1206.
Kitamoto, T. (2002). Conditional disruption of synaptic transmission induces male-male courtship behavior in Drosophila. Proc Natl Acad Sci U S A *99*, 13232-13237.
Klapoetke, N.C., Murata, Y., Kim, S.S., Pulver, S.R., Birdsey-Benson, A., Cho, Y.K., Morimoto, T.K., Chuong, A.S., Carpenter, E.J., Tian, Z.*, et al.* (2014). Independent optical excitation of distinct neural populations. Nat Methods *11*, 338-346.

Kohsaka, H., Guertin, P.A., and Nose, A. (2016). Neural circuits underlying fly larval locomotion. Current pharmaceutical design.
Kohsaka, H., Takasu, E., Morimoto, T., and Nose, A. (2014). A group of segmental premotor interneurons regulates the speed of axial locomotion in Drosophila larvae. Curr Biol *24*, 2632-2642.
Konopka, R.J., and Benzer, S. (1971). Clock mutants of Drosophila melanogaster. Proc Natl Acad Sci U S A *68*, 2112-2116.
Korn, H., and Faber, D.S. (2005). The Mauthner cell half a century later: a neurobiological model for decision-making? Neuron *47*, 13-28.
Kuner, R. (2010). Central mechanisms of pathological pain. Nature medicine *16*, 1258-1266.
Lacin, H., and Truman, J.W. (2016). Lineage mapping identifies molecular and architectural similarities between the larval and adult Drosophila central nervous system. eLife *5*, e13399.
Lai, S.L., and Lee, T. (2006). Genetic mosaic with dual binary transcriptional systems in Drosophila. Nat Neurosci *9*, 703-709.
Lashley, K. (1951). The problem of serial order in behavior (Wiley, New York: L.A. Jeffress (Ed.), Cerebral mechanisms in behavior).
Lee, T., and Luo, L. (1999). Mosaic analysis with a repressible cell marker for studies of gene function in neuronal morphogenesis. Neuron *22*, 451-461.
Li, H.H., Kroll, J.R., Lennox, S.M., Ogundeyi, O., Jeter, J., Depasquale, G., and Truman, J.W. (2014). A GAL4 driver resource for developmental and behavioral studies on the larval CNS of Drosophila. Cell Rep *8*, 897-908.
Lin, J.Y., Knutsen, P.M., Muller, A., Kleinfeld, D., and Tsien, R.Y. (2013). ReaChR: a red-shifted variant of channelrhodopsin enables deep transcranial optogenetic excitation. Nat Neurosci *16*, 1499-1508.
Long, M.A., Jin, D.Z., and Fee, M.S. (2010). Support for a synaptic chain model of neuronal sequence generation. Nature *468*, 394-399.
Lumpkin, E.A., and Caterina, M.J. (2007). Mechanisms of sensory transduction in the skin. Nature *445*, 858-865.
Ma, Q. (2012). Population coding of somatic sensations. Neuroscience bulletin *28*, 91-99.
Macpherson, L.J., Zaharieva, E.E., Kearney, P.J., Alpert, M.H., Lin, T.Y., Turan, Z., Lee, C.H., and Gallio, M. (2015). Dynamic labelling of neural connections in multiple colours by trans-synaptic fluorescence complementation. Nature communications *6*, 10024.
Mantyh, P.W., Rogers, S.D., Honore, P., Allen, B.J., Ghilardi, J.R., Li, J., Daughters, R.S., Lappi, D.A., Wiley, R.G., and Simone, D.A. (1997). Inhibition of hyperalgesia by ablation of lamina I spinal neurons expressing the substance P receptor. Science *278*, 275-279.
Marder, E. (2012). Neuromodulation of neuronal circuits: back to the future. Neuron *76*, 1-11.
Marley, R., and Baines, R.A. (2011). Whole-cell patch recording from Drosophila larval neurons. Cold Spring Harbor protocols *2011*.
Matthews, B.J., Kim, M.E., Flanagan, J.J., Hattori, D., Clemens, J.C., Zipursky, S.L., and Grueber, W.B. (2007). Dendrite self-avoidance is controlled by Dscam. Cell *129*, 593-604.
Mellert, D.J., and Truman, J.W. (2012). Transvection is common throughout the Drosophila genome. Genetics *191*, 1129-1141.
Melzack, R., and Wall, P.D. (1965). Pain mechanisms: a new theory. Science *150*, 971-979.
Merritt, D.J., and Whitington, P.M. (1995). Central projections of sensory neurons in the Drosophila embryo correlate with sensory modality, soma position, and proneural gene function. J Neurosci *15*, 1755-1767.
Mizumoto, K., and Shen, K. (2013). Interaxonal interaction defines tiled presynaptic innervation in C. elegans. Neuron *77*, 655-666.

Nagarkar-Jaiswal, S., Lee, P.T., Campbell, M.E., Chen, K., Anguiano-Zarate, S., Gutierrez, M.C., Busby, T., Lin, W.W., He, Y., Schulze, K.L.*, et al.* (2015). A library of MiMICs allows tagging of genes and reversible, spatial and temporal knockdown of proteins in Drosophila. eLife *4*.

Nicolai, L.J., Ramaekers, A., Raemaekers, T., Drozdzecki, A., Mauss, A.S., Yan, J., Landgraf, M., Annaert, W., and Hassan, B.A. (2010). Genetically encoded dendritic marker sheds light on neuronal connectivity in Drosophila. Proc Natl Acad Sci U S A *107*, 20553-20558.

Niven, J.E. (2010). Visuomotor control: Drosophila bridges the gap. Curr Biol *20*, R309-311.

Norman, W.W. (1900). Do the reactions of the lower animals against injury indicate pain sensations? American Journal of Physiology--Legacy ….

Ohyama, T., Jovanic, T., Denisov, G., Dang, T.C., Hoffmann, D., Kerr, R.A., and Zlatic, M. (2013). High-throughput analysis of stimulus-evoked behaviors in Drosophila larva reveals multiple modality-specific escape strategies. PLoS One *8*, e71706.

Ohyama, T., Schneider-Mizell, C.M., Fetter, R.D., Aleman, J.V., Franconville, R., Rivera-Alba, M., Mensh, B.D., Branson, K.M., Simpson, J.H., Truman, J.W.*, et al.* (2015). A multilevel multimodal circuit enhances action selection in Drosophila. Nature *520*, 633-639.

Okawa, H., Della Santina, L., Schwartz, G.W., Rieke, F., and Wong, R.O. (2014a). Interplay of cell-autonomous and nonautonomous mechanisms tailors synaptic connectivity of converging axons in vivo. Neuron *82*, 125-137.

Okawa, H., Hoon, M., Yoshimatsu, T., Della Santina, L., and Wong, R.O. (2014b). Illuminating the multifaceted roles of neurotransmission in shaping neuronal circuitry. Neuron *83*, 1303-1318.

Okusawa, S., Kohsaka, H., and Nose, A. (2014). Serotonin and downstream leucokinin neurons modulate larval turning behavior in Drosophila. J Neurosci *34*, 2544-2558.

Park, D., Li, P., Dani, A., and Taghert, P.H. (2014). Peptidergic cell-specific synaptotagmins in Drosophila: localization to dense-core granules and regulation by the bHLH protein DIMMED. J Neurosci *34*, 13195-13207.

Park, Y., Filippov, V., Gill, S.S., and Adams, M.E. (2002). Deletion of the ecdysis-triggering hormone gene leads to lethal ecdysis deficiency. Development *129*, 493-503.

Petersen, L.K., and Stowers, R.S. (2011). A Gateway MultiSite recombination cloning toolkit. PLoS One *6*, e24531.

Picao-Osorio, J., Johnston, J., Landgraf, M., Berni, J., and Alonso, C.R. (2015). MicroRNA-encoded behavior in Drosophila. Science *350*, 815-820.

Pirri, J.K., and Alkema, M.J. (2012). The neuroethology of C. elegans escape. Current opinion in neurobiology *22*, 187-193.

Pirri, J.K., McPherson, A.D., Donnelly, J.L., Francis, M.M., and Alkema, M.J. (2009). A tyramine-gated chloride channel coordinates distinct motor programs of a Caenorhabditis elegans escape response. Neuron *62*, 526-538.

Potter, C.J., Tasic, B., Russler, E.V., Liang, L., and Luo, L. (2010). The Q system: a repressible binary system for transgene expression, lineage tracing, and mosaic analysis. Cell *141*, 536-548.

Prescott, S.A., Ma, Q., and De Koninck, Y. (2014). Normal and abnormal coding of somatosensory stimuli causing pain. Nat Neurosci *17*, 183-191.

Pulver, S.R., Bayley, T.G., Taylor, A.L., Berni, J., Bate, M., and Hedwig, B. (2015). Imaging fictive locomotor patterns in larval Drosophila. Journal of neurophysiology *114*, 2564-2577.

Rao, S., Lang, C., Levitan, E.S., and Deitcher, D.L. (2001). Visualization of neuropeptide expression, transport, and exocytosis in Drosophila melanogaster. Journal of neurobiology *49*, 159-172.

Ribeiro-da-Silva, A., and De Koninck, Y. (2008). Morphological and neurochemical organization of the spinal dorsal horn. The Science of Pain, 279-310.
Risse, B., Thomas, S., Otto, N., Lopmeier, T., Valkov, D., Jiang, X., and Klambt, C. (2013). FIM, a novel FTIR-based imaging method for high throughput locomotion analysis. PLoS One *8*, e53963.
Robertson, J.L., Tsubouchi, A., and Tracey, W.D. (2013). Larval defense against attack from parasitoid wasps requires nociceptive neurons. PLoS One *8*, e78704.
Saalfeld, S., Cardona, A., Hartenstein, V., and Tomancak, P. (2009). CATMAID: collaborative annotation toolkit for massive amounts of image data. Bioinformatics *25*, 1984-1986.
Sakai, T., Kasuya, J., Kitamoto, T., and Aigaki, T. (2009). The Drosophila TRPA channel, Painless, regulates sexual receptivity in virgin females. Genes, brain, and behavior *8*, 546-557.
Sanes, J.R., and Yamagata, M. (2009). Many paths to synaptic specificity. Annual review of cell and developmental biology *25*, 161-195.
Sanes, J.R., and Zipursky, S.L. (2010). Design principles of insect and vertebrate visual systems. Neuron *66*, 15-36.
Schlegel, P., Texada, M.J., Miroschnikow, A., Schoofs, A., Huckesfeld, S., Peters, M., Schneider-Mizell, C.M., Lacin, H., Li, F., Fetter, R.D*., et al.* (2016). Synaptic transmission parallels neuromodulation in a central food-intake circuit. eLife *5*.
Schmid, A., Hallermann, S., Kittel, R.J., Khorramshahi, O., Frolich, A.M., Quentin, C., Rasse, T.M., Mertel, S., Heckmann, M., and Sigrist, S.J. (2008). Activity-dependent site-specific changes of glutamate receptor composition in vivo. Nat Neurosci *11*, 659-666.
Schneider-Mizell, C.M., Gerhard, S., Longair, M., Kazimiers, T., Li, F., Zwart, M.F., Champion, A., Midgley, F.M., Fetter, R.D., Saalfeld, S*., et al.* (2016). Quantitative neuroanatomy for connectomics in Drosophila. eLife *5*.
Seeds, A.M., Ravbar, P., Chung, P., Hampel, S., Midgley, F.M., Jr., Mensh, B.D., and Simpson, J.H. (2014). A suppression hierarchy among competing motor programs drives sequential grooming in Drosophila. eLife *3*, e02951.
Selverston, A. (1999). What invertebrate circuits have taught us about the brain. Brain research bulletin *50*, 439-440.
Seybold, V.S. (2009). The role of peptides in central sensitization. Handbook of experimental pharmacology, 451-491.
Shearin, H.K., Dvarishkis, A.R., Kozeluh, C.D., and Stowers, R.S. (2013). Expansion of the gateway multisite recombination cloning toolkit. PLoS One *8*, e77724.
Shirangi, T.R., Stern, D.L., and Truman, J.W. (2013). Motor control of Drosophila courtship song. Cell Rep *5*, 678-686.
Sillar, K.T. (2009). Mauthner cells. Curr Biol *19*, R353-355.
Simmons, P.J., Rind, F.C., and Santer, R.D. (2010). Escapes with and without preparation: the neuroethology of visual startle in locusts. Journal of insect physiology *56*, 876-883.
Spruston, N., Stuart, G., and Hausser, M. (2008). Dendritic integration. In Dendrites, G. Stuart, N. Spruston, and M. Hausser, eds. (UK: Oxford University Press).
Stein, B.E., and Stanford, T.R. (2008). Multisensory integration: current issues from the perspective of the single neuron. Nat Rev Neurosci *9*, 255-266.
Sun, R.Q., Tu, Y.J., Lawand, N.B., Yan, J.Y., Lin, Q., and Willis, W.D. (2004). Calcitonin gene-related peptide receptor activation produces PKA- and PKC-dependent mechanical hyperalgesia and central sensitization. Journal of neurophysiology *92*, 2859-2866.
Sweeney, S.T., Broadie, K., Keane, J., Niemann, H., and O'Kane, C.J. (1995). Targeted expression of tetanus toxin light chain in Drosophila specifically eliminates synaptic transmission and causes behavioral defects. Neuron *14*, 341-351.

Swierczek, N.A., Giles, A.C., Rankin, C.H., and Kerr, R.A. (2011). High-throughput behavioral analysis in C. elegans. Nat Methods *8*, 592-598.
Takemura, S.Y. (2015). Connectome of the fly visual circuitry. Microscopy *64*, 37-44.
Terada, S., Matsubara, D., Onodera, K., Matsuzaki, M., Uemura, T., and Usui, T. (2016). Neuronal processing of noxious thermal stimuli mediated by dendritic Ca(2+) influx in Drosophila somatosensory neurons. eLife *5*.
Todd, A.J. (2010). Neuronal circuitry for pain processing in the dorsal horn. Nat Rev Neurosci *11*, 823-836.
Tracey, W.D., Jr., Wilson, R.I., Laurent, G., and Benzer, S. (2003). painless, a Drosophila gene essential for nociception. Cell *113*, 261-273.
Triphan, T., Poeck, B., Neuser, K., and Strauss, R. (2010). Visual targeting of motor actions in climbing Drosophila. Curr Biol *20*, 663-668.
Truman, J.W., and Riddiford, L.M. (1970). Neuroendocrine control of ecdysis in silkmoths. Science *167*, 1624-1626.
Tsubouchi, A., Caldwell, J.C., and Tracey, W.D. (2012). Dendritic filopodia, Ripped Pocket, NOMPC, and NMDARs contribute to the sense of touch in Drosophila larvae. Curr Biol *22*, 2124-2134.
Turner, H.N., Armengol, K., Patel, A.A., Himmel, N.J., Sullivan, L., Iyer, S.C., Bhattacharya, S., Iyer, E.P., Landry, C., Galko, M.J.*, et al.* (2016). The TRP Channels Pkd2, NompC, and Trpm Act in Cold-Sensing Neurons to Mediate Unique Aversive Behaviors to Noxious Cold in Drosophila. Curr Biol *26*, 3116-3128.
Vanegas, H., and Schaible, H.G. (2004). Descending control of persistent pain: inhibitory or facilitatory? Brain research Brain research reviews *46*, 295-309.
Vosshall, L.B., and Stocker, R.F. (2007). Molecular architecture of smell and taste in Drosophila. Annual review of neuroscience *30*, 505-533.
Walters, E.T., Illich, P.A., Weeks, J.C., and Lewin, M.R. (2001). Defensive responses of larval Manduca sexta and their sensitization by noxious stimuli in the laboratory and field. The Journal of experimental biology *204*, 457-469.
Wang, J.W., Wong, A.M., Flores, J., Vosshall, L.B., and Axel, R. (2003). Two-photon calcium imaging reveals an odor-evoked map of activity in the fly brain. Cell *112*, 271-282.
White, J.G., Southgate, E., Thomson, J.N., and Brenner, S. (1986). The structure of the nervous system of the nematode Caenorhabditis elegans. Philosophical transactions of the Royal Society of London Series B, Biological sciences *314*, 1-340.
Wills, Z.P., Mandel-Brehm, C., Mardinly, A.R., McCord, A.E., Giger, R.J., and Greenberg, M.E. (2012). The nogo receptor family restricts synapse number in the developing hippocampus. Neuron *73*, 466-481.
Wilson, D.M. (1959). Function of Giant Mauthner's Neurons in the Lungfish. Science *129*, 841-842.
Wilson, D.M., and Wyman, R.J. (1965). Motor Output Patterns during Random and Rhythmic Stimulation of Locust Thoracic Ganglia. Biophysical journal *5*, 121-143.
Wong, A.M., Wang, J.W., and Axel, R. (2002). Spatial representation of the glomerular map in the Drosophila protocerebrum. Cell *109*, 229-241.
Wreden, C.C., Meng, J.L., Feng, W., Chi, W., Marshall, Z.D., and Heckscher, E.S. (2017). Temporal Cohorts of Lineage-Related Neurons Perform Analogous Functions in Distinct Sensorimotor Circuits. Curr Biol *27*, 1521-1528 e1524.
Xiang, Y., Yuan, Q., Vogt, N., Looger, L.L., Jan, L.Y., and Jan, Y.N. (2010). Light-avoidance-mediating photoreceptors tile the Drosophila larval body wall. Nature *468*, 921-926.
Yamamoto, D., and Koganezawa, M. (2013). Genes and circuits of courtship behaviour in Drosophila males. Nat Rev Neurosci *14*, 681-692.

Yan, Z., Zhang, W., He, Y., Gorczyca, D., Xiang, Y., Cheng, L.E., Meltzer, S., Jan, L.Y., and Jan, Y.N. (2013). Drosophila NOMPC is a mechanotransduction channel subunit for gentle-touch sensation. Nature *493*, 221-225.

Yang, G.R., Murray, J.D., and Wang, X.J. (2016). A dendritic disinhibitory circuit mechanism for pathway-specific gating. Nature communications *7*, 12815.

Yang, P., Shaver, S.A., Hilliker, A.J., and Sokolowski, M.B. (2000). Abnormal turning behavior in Drosophila larvae. Identification and molecular analysis of scribbler (sbb). Genetics *155*, 1161-1174.

Yarmolinsky, D.A., Zuker, C.S., and Ryba, N.J. (2009). Common sense about taste: from mammals to insects. Cell *139*, 234-244.

Yau, J.M., DeAngelis, G.C., and Angelaki, D.E. (2015). Dissecting neural circuits for multisensory integration and crossmodal processing. Philosophical transactions of the Royal Society of London Series B, Biological sciences *370*, 20140203.

Yogev, S., and Shen, K. (2014). Cellular and molecular mechanisms of synaptic specificity. Annual review of cell and developmental biology *30*, 417-437.

Zhong, L., Bellemer, A., Yan, H., Ken, H., Jessica, R., Hwang, R.Y., Pitt, G.S., and Tracey, W.D. (2012). Thermosensory and nonthermosensory isoforms of Drosophila melanogaster TRPA1 reveal heat-sensor domains of a thermoTRP Channel. Cell Rep *1*, 43-55.

Zhu, P.C., Thureson-Klein, A., and Klein, R.L. (1986). Exocytosis from large dense cored vesicles outside the active synaptic zones of terminals within the trigeminal subnucleus caudalis: a possible mechanism for neuropeptide release. Neuroscience *19*, 43-54.

Zwart, M.F., Pulver, S.R., Truman, J.W., Fushiki, A., Fetter, R.D., Cardona, A., and Landgraf, M. (2016). Selective Inhibition Mediates the Sequential Recruitment of Motor Pools. Neuron *91*, 944.